

Characterization of Retinal Ganglion Cell Responses to Electrical Stimulation Using White Noise

Dissertation

zur Erlangung des Grades eines
Doktors der Naturwissenschaften

der Mathematisch-Naturwissenschaftlichen Fakultät
und
der Medizinischen Fakultät
der Eberhard-Karls-Universität Tübingen

vorgelegt

von

[Sudarshan Sekhar](#)
aus Neu-Delhi, Indien

November - 2017

Tag der mündlichen Prüfung:

Dekan der Math.-Nat. Fakultät: Prof. Dr. W. Rosenstiel

Dekan der Medizinischen Fakultät: Prof. Dr. I. B. Autenrieth

1. Berichterstatter: Prof. Dr. Eberhart Zrenner

2. Berichterstatter: Prof. Dr. Thomas Euler

Prüfungskommission: Prof. Dr. Eberhart Zrenner

Prof. Dr. Thomas Euler

Prof. Dr. Jakob Macke

Prof. Dr. Frank Schaeffel

Erklärung / Declaration:

Ich erkläre, dass ich die zur Promotion eingereichte Arbeit mit dem Titel: **“Characterization of Retinal Ganglion Cell Responses to Electrical Stimulation Using White Noise”**, selbständig verfasst, nur die angegebenen Quellen und Hilfsmittel benutzt und wörtlich oder inhaltlich übernommene Stellen als solche gekennzeichnet habe. Ich versichere an Eides statt, dass diese Angaben wahr sind und dass ich nichts verschwiegen habe. Mir ist bekannt, dass die falsche Abgabe einer Versicherung an Eides statt mit Freiheitsstrafe bis zu drei Jahren oder mit Geldstrafe bestraft wird.

*I hereby declare that I have produced the work entitled **“Characterization of Retinal Ganglion Cell Responses to Electrical Stimulation Using White Noise”**, submitted for the award of a doctorate, on my own (without external help), have used only the sources and aids indicated and have marked passages included from other works, whether verbatim or in content, as such. I swear upon oath that these statements are true and that I have not concealed anything. I am aware that making a false declaration under oath is punishable by a term of imprisonment of up to three years or by a fine.*

Tübingen, den

.....

Datum / Date

Unterschrift /Signature

*dedicated
to*

அம்மா & அப்பா

Contents

Abbreviations	7
Abstract	8
Introduction.....	9
Basic Anatomy of the Human Eye	10
Cellular Components of the Retina	11
Retinal Pigment Epithelium	12
Photoreceptors.....	12
Horizontal Cells.....	12
Bipolar Cells.....	13
Amacrine Cells	13
Retinal Ganglion Cells.....	14
Müller Cells.....	14
Retinal Diseases.....	15
Cataracts.....	16
Glaucoma.....	17
Age-Related Macular Degeneration and Retinitis Pigmentosa	17
Treatment Options	20
Gene Therapy	21
Stem Cell-Based Approaches.....	22
Optogenetics and Photopharmacology.....	24
Retinal Prosthesis	25
Summary of Retinal Implants	31
Overview of Thesis Work.....	32
Methods	35
Retinal Preparation	36
Spike Sorting.....	36
Cell Validation.....	37
Systems Identification	37
White Noise Stimulation and Analysis	38
Spike-Triggered Average	40
Linear Nonlinear Poisson Models.....	42
Generalized Linear Models.....	44
Summary of Results.....	46
Tickling the retina: integration of subthreshold electrical pulses can activate retinal neurons.....	46

Correspondence between visual and electrical input filters of ON and OFF mouse retinal ganglion cells.....	49
Characterizing retinal responses to electrical stimulation using generalized linear models	51
Discussion	53
References.....	59
Appendix 1.....	72
Electrical STAs at alternate stimulus conditions	72
Appendix 2.....	75
Manuscript 1: Tickling the retina: integration of subthreshold electrical pulses can activate retinal neurons.....	75
Appendix 3.....	85
Manuscript 2: Correspondence between visual and electrical input filters of ON and OFF mouse retinal ganglion cells.....	85
Appendix 4.....	103
Manuscript 3: Characterizing retinal responses to electrical stimulation using generalized linear models	103
Summary	125
Curriculum Vitae.....	126
Acknowledgments.....	128

Abbreviations

ACSF	Artificial Cerebrospinal Fluid
AMD	Age-Related Macular Degeneration
ESC	Embryonic Stem Cells
GC	Ganglion Cell Layer
GLM	Generalized Linear Model
INL	Inner Nuclear Layer
IPL	Inner Plexiform Layer
iPSC	Induced Pluripotency Stem Cells
IS	Inner Segment
ISI	Inter-Spike Interval
LNP	Linear Nonlinear Poisson
MAP	Maximum a Posterior
MEA	Microelectrode Array
MLE	Maximum Likelihood Estimation
MPM	Model Performance Measure
mV	Millivolt
ONL	Outer Nuclear Layer
OPL	Outer Plexiform Layer
OS	Outer Segment
PSTH	Peristimulus Time Histogram
RGC	Retinal Ganglion Cell
RP	Retinitis Pigmentosa
RPE	Retinal Pigment Epithelium
SD	Standard Deviation
STA	Spike-Triggered Average

Abstract

Retinitis pigmentosa and age-related macular degeneration are two leading causes of degenerative blindness. While there is still not a definitive course of treatment for either of these diseases, there is currently the world over, many different treatment strategies being explored. Of these various strategies, one of the most successful has been retinal implants. Retinal implants are microelectrode or photodiode arrays, that are implanted in the eye of a patient, to electrically stimulate the degenerating retina. Clinical trials have shown that many patients implanted with such a device, are able to regain a certain degree of functional vision. However, while the results of these ongoing clinical trials have been promising, there are still many technical challenges that need to be overcome. One of the biggest challenges facing present implants is the inability to preferentially stimulate different retinal pathways. This is because retinal implants use large-amplitude current or voltage pulses. This in turn leads to the indiscriminate activation of multiple classes of retinal ganglion cells (RGCs), and therefore, an overall reduction in the restored visual acuity. To tackle this issue, we decided to explore a novel stimulus paradigm, in which we present to the retina, a stream of smaller-amplitude subthreshold voltage pulses. By then correlating the retinal spikes to the stimuli preceding them, we calculate temporal input filters for various classes of RGCs, using a technique called spike-triggered averaging (STA). In doing this, we found that ON and OFF RGCs have electrical filters, which are very distinct from each other. This finding creates the possibility for the selective activation of the retina through the use of STA-based waveforms. Finally, using statistical models, we verify how well these temporal filters can predict RGC responses to novel electrical stimuli. In a broad sense, our work represents the successful application of systems engineering tools to retinal prosthetics, in an attempt to answer one of the field's most difficult questions, namely selective stimulation of the retina.

Introduction

We navigate our world by processing and responding to the inputs from our five senses. Of these five senses, it can be argued that vision is one of the most important. Therefore, visual impairment or worse, blindness is extremely debilitating from both an economic and psychosocial perspective. It has been shown that patients with age-related macular degeneration (AMD) or retinitis pigmentosa (RP) are at a higher risk of developing depression in comparison to their peers who do not have any sensory dysfunction. The risk of developing depression in these cases also increases with the age of the patient **(Casten & Rovner, 2008; Moschos et al., 2015)**. The correlations between depression and visual disability are also seen across various other eye diseases such as glaucoma and refractive errors **(Moschos et al., 2015; Owsley et al., 2007; Skalicky & Goldberg, 2008)**. Moreover, even when controlled for visual acuity, AMD/RP patients who develop depression can experience worse subjective vision-related functions than those AMD/RP patients who do not **(Hahm et al., 2008; Rovner & Casten, 2001)**. Additionally, in the U.S.A. alone the annual economic impact of blindness is 5.5 billion dollars, and more than 209,000 quality-adjusted life years **(Frick et al., 2007)**. Factoring in the ever-increasing life expectancy rates, the number of cases of eye diseases such as AMD is projected to increase in the future **(Owen et al., 2012; Rudnicka et al., 2015)**. For these reasons, much effort has been made over the years in finding cures, or at least treatments for the diseases mentioned above. This effort has in turn given rise to effective treatment options for cataracts and glaucoma, the two leading causes of blindness world over **(World Health Organization, 2010)**. Though treatment options such as stem cell therapy, photopharmacology, optogenetics and retinal prosthetics do exist for RP and AMD, the third most common cause of blindness **(Lorach et al., 2013)**, these strategies are still in their nascent stage with much room for improvement. Of these varied strategies, retinal prosthetics have to date had the best restored visual acuity. Therefore, the main focus of this thesis is the characterization of a novel prosthetic stimulation strategy that has applications to the treatment of patients with RP and AMD. In this chapter, the reader will find an introduction to the anatomy of the eye and the retinal circuitry. This is followed by a brief description of some eye diseases namely cataracts, glaucoma, AMD, and RP. Finally, the various treatment options for RP and AMD are discussed with particular emphasis placed on prosthetic based approaches.

Basic Anatomy of the Human Eye

The eye is the organ of sight (**Figure 1.1**). Light reaches the retina through the **pupil**, the circular opening at the front of our eye (**Litzinger & Rio-Tsonis, 2002**). The size of the pupil determines the amount of light reaching the retina and is controlled by the **iris**, the coloured part of the eye surrounding the pupil. The highly pigmented iris ensures that incoming light only enters the eye through the pupil and not the iris itself. The iris, in turn, is surrounded by the **sclera**, which is a white, opaque, fibrous structure that forms a protective outer layer for the eye (**Litzinger & Rio-Tsonis, 2002**).

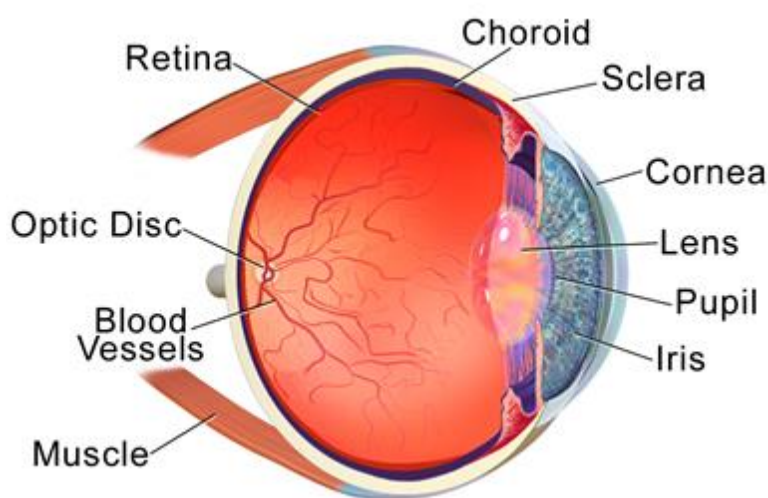


Figure 1.1: Anatomy of the eye. Images reaching the eye are focused onto the retina by the cornea and lens. The photons impinging the retina are subsequently converted to electrochemical signals, which are then sent to the visual cortex for higher processing. From Blausen.com staff (2014) "Medical gallery of Blausen Medical 2014". WikiJournal of Medicine 1 (2). doi:10.15347/wjm/2014.010. ISSN 2002-4436. Used according to Creative Commons Attribution 3.0 Unreported license.

To have clear vision, light has to be focused onto the retina. This is done jointly by the **cornea** and the **lens**. Light reaching the eye first passes through the cornea, a transparent circular layer present at the front of the eye which is responsible for the majority of the refraction (refractive power ~ 43 diopters) (**Olsen, 1986**). The lens which is behind the pupil focuses the already refracted light onto the retina by dynamically changing its curvature. This dynamic change in curvature is what enables us to shift our focus from near to far objects and vice versa and is in turn controlled by the ciliary **muscle**. When relaxed, the lens flattens and focusses on long-range objects. Conversely, when the ciliary muscle contracts, the lens becomes more spherical and focuses on close-range objects. This ability of the lens to change its shape and therefore, the range of focus is called accommodation. Between the retina and

the sclera lies the **choroid layer (Litzinger & Rio-Tsonis, 2002)**. The choroid layer is made up of connective tissue and is highly vascular. It, therefore, provides nourishment and oxygen to the outer layers of the retina. The retina is light-sensitive tissue that transduces incoming photons into electrochemical signals before projecting to the visual cortex through the **optic disc** via retinal ganglion cell axons. The optic disc also corresponds to the blind spot of the eye. The major **blood vessels** that supply the retina enter the eye via the optic disc (**Litzinger & Rio-Tsonis, 2002**).

Cellular Components of the Retina

The retinal circuitry consists of several different layers containing different cell types (**Figure 1.2**). The primary retinal cell types are photoreceptors, horizontal cells, bipolar cells, amacrine cells and retinal ganglion cells (RGC). Other important components are the retinal pigment epithelium (RPE) and Müller cells.

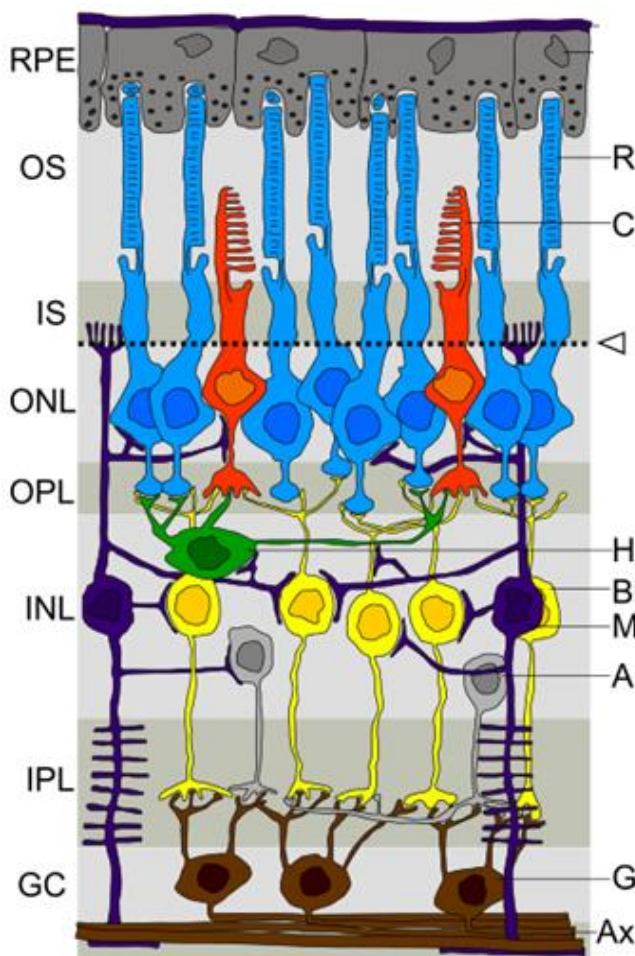


Figure 1.2: Components of the Retina. The retina consists of many different cell types. Each of these cell types has various subclasses, with specific functions, anatomical structures and layers of differentiation. Source location of image is https://commons.wikimedia.org/wiki/File:Retina_layers.svg. Created by Peter Hartmann, on 13th July 2013. Used according to Creative Commons Attribution-Share Alike 3.0 Unreported license

Retinal Pigment Epithelium

The retinal pigment epithelium (RPE) is a pigmented cell layer which lies between the choroid and the photoreceptors (**Litzinger & Rio-Tsonis, 2002**). It serves many important functions such as regulating the level of immune activity in the eye by secretion of immunosuppressive factors, phagocytosis of the photoreceptor outer segments (OS), improving visual quality by absorption of scattered light, reducing oxidative stress, and regeneration of photopigments (**Litzinger & Rio-Tsonis, 2002; Strauss, 2005**).

Photoreceptors

As the human eye is inverted, incoming photons traverse the entire retinal network before reaching the photoreceptors lining the back of the eye. Photoreceptors represent the first functional layer of the retina and transduce visual information (in the form of photons) to graded electrochemical signals. These signals are in turn relayed to the visual cortex through action potentials. Photoreceptors are further classified into rods (R) and cones (C). Rods are highly sensitive to light and can even detect single photons (**Baylor et al., 1979; Hecht et al., 1942**). They are therefore recruited for vision during low luminance (scotopic) conditions (10^{-6} to 10^{-3} cd/m²). As luminance increases, rod activity starts to saturate, and cones start to become active. The region where both rods and cones are active is called mesopic (luminance level 10^{-3} to $10^{0.5}$ cd/m²). As luminance levels further increase cones are primarily active. This region is called photopic (luminance level 10 to 10^8 cd/m²). Colour vision is primarily based on cone activation. This recruitment of the different cell types for different luminance conditions is what allows humans to see over a wide dynamic range (from scotopic to photopic/high luminance). Photoreceptors consist of both an outer segment (OS) and an inner segment (IS). The OS is responsible for the absorption of photons. The membrane potential of the OS is reset after photon absorption through Na⁺/K⁺ pump activity. These pumps get their energy (ATP) from the mitochondria present in the IS (**Baker & Kerov, 2013**). The cell bodies of the photoreceptors are found in the outer nuclear layer (ONL).

Horizontal Cells

Photoreceptor activity is modulated by a group of cells known as horizontal (H) cells through integration and inhibition. Horizontal cells integrate the response of numerous photoreceptors and synapse back onto them, thereby providing surround inhibition. They are also thought to provide inhibition to the dendrites of bipolar cells (**Demb & Singer, 2015; Masland, 2012**). This activity of horizontal cells helps to regulate photoreceptor output and is

furthermore believed to contribute to local gain control and edge detection (**Masland, 2012; Szikra & Križaj, 2006**). The synaptic connections between inner segments of photoreceptors and dendrites of horizontal cells are located in the outer plexiform layer (OPL).

Bipolar Cells

Photoreceptors synapse onto bipolar (Bi) cells. There are at least ten different classes of bipolar cells (**Euler et al., 2014**). These various classes form parallel image processing channels that dissect complex visual input into subcomponents such as temporal information, contrast, colour, and luminance. Depending on the type of photoreceptor they synapse with, bipolar cells can be classified as rod or cone bipolar cells. In contrast to other bipolar cells, rod bipolar cells are unique because they do not directly connect to retinal ganglion cells (RGCs). Instead, they first synapse onto A-II amacrine cells which then, in turn, excite ON cone bipolar cells (via gap junctions) and inhibit OFF cone bipolar (via glycinergic synapses). These ON cone bipolar cells then contact RGCs. Therefore, rod bipolar cells can be thought to override the cone pathway of the retina during low luminance conditions. They do not have an OFF pathway (**Euler et al., 2014; Kolb & Famiglietti, 1974; Lamb, 2016**). The above mentioned ON bipolar cells respond to the presence of light while OFF bipolar cells respond to the absence. Alternatively, differentiation can also be done based on the shape and layer of stratification of the bipolar cell axonal processes, or morphology of their dendrites. All these different classification schemes show that bipolar cells are not simple relay systems, but instead complex image processing units, which are fundamental to making sense of visual information (**Euler et al., 2014**). The activity of the bipolar cells is modulated by amacrine cells. Bipolar cell bodies are found in the inner nuclear layer (INL).

Amacrine Cells

Amacrine (A) cells modulate the synaptic activity between bipolar and retinal ganglion cells at the inner plexiform layer (IPL). Amacrine cells are highly diversified with regards to factors such as their dendritic shape, the dendritic layer of stratification within the IPL, and coverage width (**MacNeil & Masland, 1998**). There are at least thirty different classes of amacrine cells with a very even distribution across them. Like bipolar cells, these differences in amacrine cells are tied into their functional roles. For example, A-II amacrine cells connect the rod bipolar cells to the cone pathway and multiplex signals from ON bipolar cells to both ON and OFF retinal ganglion cells. Starburst amacrine cells are important for direction selectivity of motion amongst retinal ganglion cells (**Famiglietti, 1987; Vaney et al., 2001**). A17 amacrine cells,

which connect almost exclusively to thousands of rod bipolar cells, are responsible for the amplification of signals coming from the rod pathways under scotopic conditions (**Menger & Wässle, 2000; Vaney, 1986**). These different classes of amacrine cells form microcircuits within the retina that help to further refine input coming from the bipolar cells through various synaptic mechanisms.

Retinal Ganglion Cells

Retinal ganglion cells (commonly abbreviated to RGC, but represented in **figure 2** as G) are the final output cells of the retina. They receive inputs from the bipolar cells and send their axonal (Ax) projections via the optic nerve to higher brain regions such as the lateral geniculate nucleus (LGN), pretectal nuclei, superior colliculus and suprachiasmatic nucleus. Like bipolar cells and amacrine cells, there are many different types of RGCs. The difference between these cells is based on factors such as genetic, anatomical, and response type. Recent research has shown that there are at least thirty types of RGCs in the mouse retina (**Baden et al., 2016**). In very broad terms, RGCs can be classified as ON, OFF, or ON-OFF, based upon their response to light. ON RGCs respond primarily to the presence of light, OFF RGCs respond primarily to its absence, while ON-OFF cells respond strongly to both. This broad classification scheme can be further divided based on the response to direction of motion, the presence of edges, global or local features, contrast, or frequency, as well as the type of responses, such as sustained or transient (**Baden et al., 2016**). These different RGC types are, therefore part of a parallel and distributed retinal network that breaks down complex visual scenery into many unique features. These features are then further processed by the visual cortex in order to comprehend and act upon the high dimensional visual input. RGCs are found in the ganglion cell layer (GC).

Müller Cells

Müller (M) cells, which span across the entire retinal thickness are the most common type of retinal glial cells. They perform many important functions such as regulation of extracellular K⁺ concentration, mechanical support to the retina, removal of debris, and neurotransmitter uptake. For example, photoreceptors have very large rates of oxidative metabolism which in turn leads to a high demand for glucose and oxygen. A by-product of this high glucose metabolism is the production of carbon dioxide and water. This metabolic waste is removed from the retina and sent to the bloodstream and vitreous by Müller cells. By doing so, the pH of the retina is maintained. During neuronal signaling, the size of different parts of the retinal

tissue changes constantly. When glutamate neurotransmitters bind to AMPA/kainate receptors, Na⁺ ions and water enter the cell. This causes swelling of the cell and shrinkage of extracellular space. During this process, Müller cells constantly adapt their morphology to the swelling of the activated retinal neurons, therefore maintaining mechanical stability in the retina. Müller cells are also capable of detecting mechanical stress in the retina via calcium-dependent mechanisms. Upon detection of mechanical stress, Müller cells can intervene to mitigate the damage by the release of neuroprotective factors. Additionally, they serve as optical guides, by carrying incoming photons to the photoreceptors through the retinal layers. It has been shown, that the presence of Müller cells helps drastically to reduce light scatter. In summation, Müller cells, play an important role in maintaining a healthy function of the retina **(Reichenbach & Bringmann, 2013)**.

As shown above, the eye is a complex organ consisting of many different components such as the lens, pigment epithelium, and the retina with its various classes of different retinal cell types. Even if only one of these components ceases to function properly, it can lead to visual impairment or even blindness. In the next section, we characterize some of the leading causes of blindness.

Retinal Diseases

According to the WHO, the two leading causes of blindness are cataracts and glaucoma **(Figure 1.3)**. However, though they both cause major vision loss, there are many effective treatment options for them. In contrast, RP and AMD, the third most common cause of blindness, are incurable. While RP and AMD are different diseases, they share many similarities such as progressive vision loss through photoreceptor degeneration. They also share similar treatment options. Below is a summary of these four diseases.

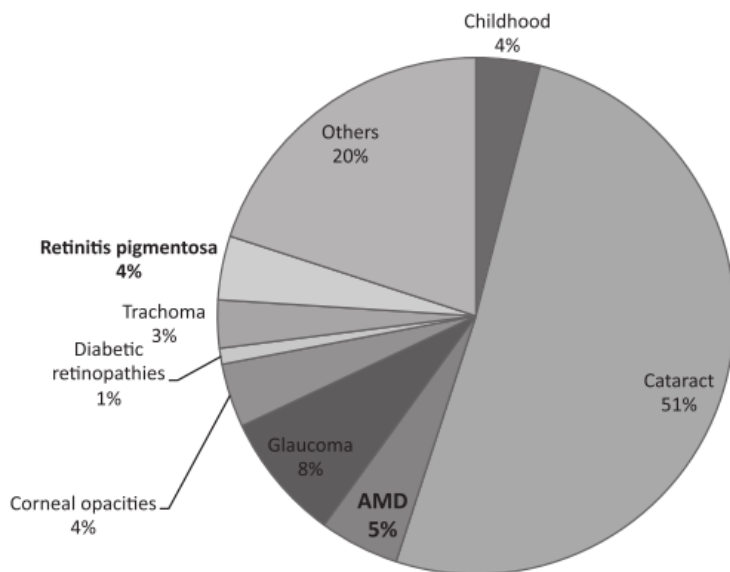


Figure 1.3 Leading causes of blindness world over. Data provided by the World Health Organization. Figure reprinted from *J Physiol Paris*, 107(5), Lorach et al. 2013, *Neural stimulation for visual rehabilitation: Advances and challenges*, 421-431, 2013, with permission from Elsevier.

Cataracts

The leading cause of blindness worldwide is cataracts (**Figure 1.4**). The lens along with the cornea, focusses incoming light onto the retina, to provide clear vision. The lens is made of mostly proteins. Cataracts occur when the proteins in the lens start to clump together, causing opacity and light scattering, therefore preventing light from being focused onto the retina. Factors affecting cataracts include age, use of certain therapeutic drugs, severe and chronic dehydration, prolonged exposure to Ultra-Violet light, sunlight, and improper nutrition. The prevalence of cataracts also varies with demographics.

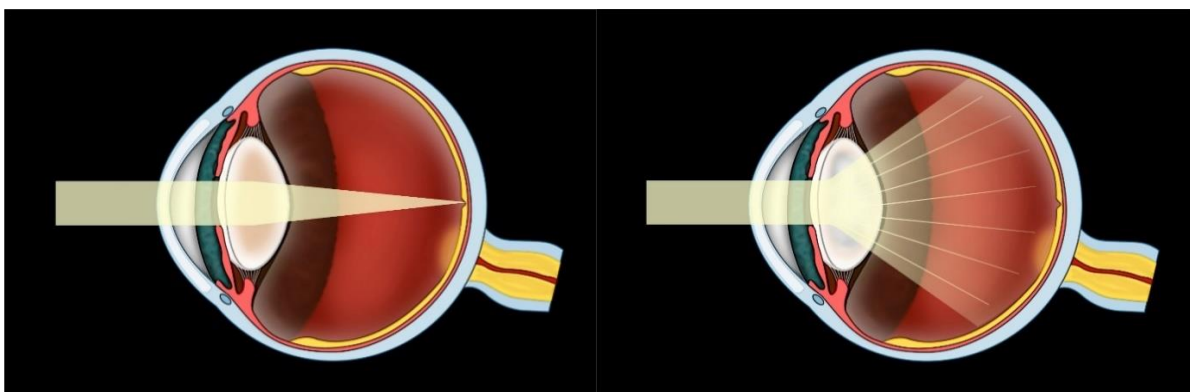


Figure 1.4: Cataracts. Cataracts are the primary cause of blindness world over (51%)(Lorach et al., 2013). Cataracts are caused by clumping together of the proteins inside the lens, therefore causing blurring of vision. On the left is an illustration of how light enters a healthy eye, and on the right is when light enters an eye with cataracts. Images courtesy R. Ebenhoch, University of Tuebingen.

It has been found that occurrence of cataracts is much higher amongst developing countries than in developed countries. Though cataracts are the leading cause of blindness, it is often

surgically treatable. In these surgeries, the opaque lens is replaced with an artificial lens (Livingston et al., 1995).

Glaucoma

The second major cause of blindness is glaucoma (Figure 1.5). The two main types of glaucoma are open-angled and close-angled glaucoma. In both cases, there is damage to the optic nerve of the eye leading to irreversible vision loss. While the exact cause of this disease is still a topic of research, in both cases, there is usually a large increase in intraocular pressure.

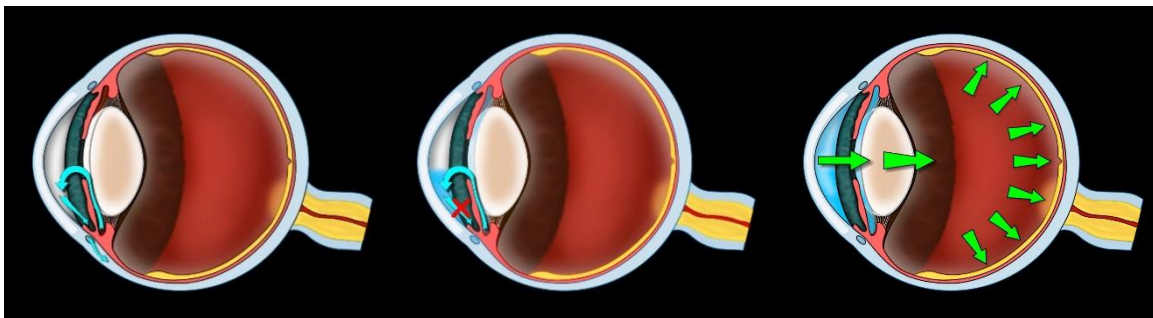


Figure 1.5: Development of Glaucoma. Left) The flow of aqueous humour through draining canal in the healthy eye. Middle) Buildup of fluid when trabecular meshwork is blocked. Right) Increase in eye pressure due to the fluid buildup, causes optic nerve damage. Images courtesy R. Ebenhoch, University of Tuebingen.

The rise in intraocular pressure is due to the inability of the eye to properly drain the aqueous humor. This is due to a blockage of the trabecular meshwork, caused either due to clogging (open-angle) or due to the forward projection of the iris (closed-angle). The main course of treatment is eye drops, used to reduce the intraocular pressure. If these are ineffective, laser therapy or surgery can also be tried (Mantravadi & Vadhar, 2015). The prevalence and type of glaucoma are affected by factors such as race, gender, family history of glaucoma, age, central corneal thickness and intraocular pressure (Wilson & Gallardo, 2010). Finally, there is mounting evidence that the vascular system plays a major role in glaucoma. It has been found that there are strong correlations between glaucoma occurrence/progression and blood pressure. Patients with glaucoma tend to have lower blood pressure (hypotension) and less ocular blood flow (Caprioli & Coleman, 2010; Flammer & Orgül, 1998; Nakazawa, 2016).

Age-Related Macular Degeneration and Retinitis Pigmentosa

AMD is the third most common cause of blindness (Figure 1.3). This disease occurs most frequently in the developed world amongst older people and involves a loss of central vision, which then proceeds to the periphery (Figure 1.6). Though it does not always result in total blindness, the loss of central vision is extremely debilitating as it hinders many day to day

activities such as face recognition, reading and driving. AMD is associated with a disturbance in RPE pigmentation, basal laminar deposits, thickening of the Bruch's membrane and an accumulation of drusen (Young, 1987). Drusen are protein and lipid deposits, most likely generated due to an incomplete degradation of waste cellular components by the RPE (Figure 1.7).



Figure 1.6: Left) Normal Vision. Right) The vision of someone with AMD. Due to the loss of photoreceptors in the fovea, people with AMD develop a blind spot in the very center of their vision. Images adapted from National Eye Institute, National Institute of Health. Images retrieved from <https://www.flickr.com/photos/nationaleyeminstitute/7544734596/> and <https://www.flickr.com/photos/nationaleyeminstitute/7544733860/>

It should be noted that the factors mentioned above, such as drusen deposits and thickening of Bruch's membrane, are common even in the eyes of healthy elderly people and are therefore, not always associated with AMD. A person is at risk of AMD only when drusen are present in large numbers (Young, 1987). There are two types of AMD, namely dry AMD, and its progression wet AMD. Dry AMD is believed to be caused by drusen deposits, which when present in large numbers have been associated with RPE atrophy and subsequent photoreceptor death.



Figure 1.7: Fundus Images. Left) Normal Retina. Right) Retina with AMD. The retina on the right has many yellow spots (drusen deposits) and appears thinner (due to the loss of the photoreceptor layer). Images from National Eye Institute, National Institute of Health. Images retrieved from <https://www.flickr.com/photos/nationaleyeinstitute/7544656150/> and <https://www.flickr.com/photos/nationaleyeinstitute/7543920284/>

In some cases, dry AMD triggers the release of the growth factor VEGF, which leads to abnormal neovascularization in the choroid, in turn giving rise to retinal scarring and hemorrhaging of the abnormal vessels. This then causes photoreceptor death and vision loss and is known as wet AMD (Sunness, 1999; Young, 1987).

Another disease involving photoreceptor death is retinitis pigmentosa. Though in itself a rare disease, retinitis pigmentosa is one of the most commonly inherited retinal degenerative diseases. Due to faulty genetic mutations, people suffering from RP first start to lose their rods, before losing their cones as well. Owing to the distribution of rods and cones in the retina, the visual field loss starts at the periphery, before proceeding to the fovea leading to tunnel vision (Figure 1.8). Early symptoms of this disease are difficulties in seeing under dim-light conditions, night blindness, problems differentiating colour, and a reduction of the visual field (Hamel, 2006).



Figure 1.8: Left) Normal Vision. Right) The vision of someone with retinitis pigmentosa. Retinitis pigmentosa usually leads to loss of rods before being followed by cones. Therefore; vision loss begins in the periphery, proceeding to the fovea resulting in tubular vision. Images adapted from National Eye Institute, National Institute of Health. Images retrieved from <https://www.flickr.com/photos/nationaleyeinstitute/7544734596/> and <https://www.flickr.com/photos/nationaleyeinstitute/7544734708/>

There are three patterns of inheritance, which can lead to RP, namely autosomal recessive, autosomal dominant and X-linked inheritance (**Hartong et al., 2006**). While the effects of RP are usually confined to the eye, it can also be associated with other diseases such as Usher's disease, which is connected with hearing loss or Bardet-Biedl syndrome, in which RP is associated with obesity, cognitive impairment, polydactyly, hypogenitalism, and renal disease (**Hartong et al., 2006**).

In total, there are around 4 million people around the world suffering from RP or AMD, with a global prevalence rate of 1 in 4000 for either of these diseases (**Hamel, 2006; Hartong et al., 2006; Pascolini & Mariotti, 2012; Resnikoff et al., 2004**)

Treatment Options

While for cataract and glaucoma over time well-established treatment regimes were developed, there is still much room for improvement with regards to the treatment options used for RP or AMD. The major areas of research for RP and AMD are in stem cells, photopharmacology, gene therapy, optogenetics, neuroprotection, and prosthetics. Each of these different strategies has had varying degrees of success in restoring vision already lost due to photoreceptor death. Provided below is an overview of some of these techniques.

Gene Therapy

In gene therapy, DNA is introduced into the patient usually by using a viral vector. The function of the newly introduced gene varies depending on the disease. In the case of retinitis pigmentosa, the goal is to replace the mutated gene responsible for photoreceptor death.

There are two primary methods of introducing the viral vector into the eye for treating retinal diseases. One is through subretinal injections, where the vector is introduced into the regions adjacent to the RPE and photoreceptors, causing a temporary retinal elevation, called bleb. This method has a very high efficacy for the gene transfer but is technically challenging. The second method is through intravitreal injections. Though these are technically much simpler, their efficiency at reaching the outer retina is low due to barriers, such as the inner limiting membrane (ILM), that blocks the passage of the vector. Intravitreal injections are therefore useful for targeting retinal ganglion cells or Müller glial cells for diseases such as Leber's hereditary optic neuropathy (LHON) or for certain optogenetic based therapies (**Acland et al., 2001; Dalkara et al., 2009; Martin et al., 2002**). In contrast, for diseases involving photoreceptors such as RP, subretinal injections are the preferred method of introducing viral vectors. However, a complication of gene therapy for RP is that there are over forty possible mutations that could cause the disease (**Daiger et al., 2007**). Therefore, gene therapy is highly individualized and could vary from patient to patient, requiring personalized treatments. This, in turn, raises the costs for developing such treatments. Moreover, the side effects of gene therapy, are not yet fully known and may be potentially deadly. When administering a gene, it is crucial that it targets only the intended cell type, and not alters the functionality of any other cell type. Furthermore, the introduction of viral vectors can at times trigger an immune response which can harm the patient. For these reasons, it is essential to have animal models that resemble as closely as possible the disease in humans. In the case of retinitis pigmentosa, to date the best animal models are primates due to their similarities to humans with regards to their eye structure and size, the thickness of nerve fiber layer and inner limiting membrane, and the configuration of the high acuity part of the fovea (**Yin et al., 2011**). However, developing the appropriate transgenic primate models of RP-based blindness is expensive. Moreover, when one factors in the multiple genetic mutations that can cause this disease (**Daiger et al., 2007**), developing a primate model for every single mutation further amplifies the costs. Recognizing these issues to be serious confounds in the development of gene-based treatment for rare diseases like RP, government organizations such as the EU (European

Union) have provided financial incentives to pharmaceutical companies working on such projects (**European Medicines Agency, 2014**). These incentives include market exclusivity for a given period of time, and tax credits on clinical research.

Nevertheless, despite the difficulties detailed above, gene therapy has shown much promise in the past in the treatment of retinal diseases. For example in **Maclaren et al., 2014**, a viral vector encoding for the REP1 protein was introduced into the eye using subfoveal injections for treatment of choroideremia. All six patients involved in this clinical trial found improvements in visual acuity post-treatment. This improvement is believed to be due to improvements in rod-cone function.

Stem Cell-Based Approaches

Stem cells are undifferentiated cells, which can either produce more stem cells or differentiate into varied types of specialized cells. There are broadly speaking two types of stem cells in the mammalian species, namely induced pluripotency stem cells (iPSC) and embryonic stem cells (ESC). Induced pluripotency stem cells are created from adult cells while embryonic stem cells are created from the inner cell mass of a blastocyst.

They are an area of active research, in treating neurodegenerative diseases, spinal cord injury, and even blindness. Diseases such as AMD or RP, where the death of RPE or the photoreceptors leads to vision loss are good candidates for the application of stem cell-based therapies. Detailed below are some stem cell-based approaches to treating AMD and RP.

Stem Cell Approach for AMD using Transplanted RPE

Since RPE atrophy is associated with AMD, researchers have transplanted RPE cells, derived from stem cells, in animal models either through subretinal injections of disassociated cells or through RPE cells with structural support in the form of scaffoldings (**Lu et al., 2012; Stanzel et al., 2014**). Both these methods come with their own set of advantages and drawbacks. While dissociated cell injections allow for a greater area of coverage, there is a higher chance of breaching the blood-brain barrier, thereby triggering an immune response. Moreover, survival of transplanted cells is lower due to the damaged Bruch's membrane. Finally, creating the polarized, monolayer RPE structure with disassociated cells is much more complicated (**Alexander et al., 2015; Binder, 2011**). On the other hand, while delivering cells with mechanical support do not face issues such as the formation of the correct RPE structure, the area of coverage is smaller. Despite these technical challenges, there have already been stem

cell-based trials with fairly promising results in both animals and humans. For example in **Kamao et al., 2014**, human induced pluripotent stem cell-derived RPE (hiPSC-RPE) cell sheets without any scaffolding were generated. This hiPSC-derived RPE displayed characteristics such as tight junctions with the polarized secretion of growth factors, phagocytotic capabilities, and gene expression patterns similar to RPE. Following this iPSCs-RPE derived from monkey somatic cells (miPSC-RPE) were introduced into the eyes of four monkeys (three as allografts and one as an autograft) without any immunosuppression. Follow-up analysis showed no signs of immune rejection or tumors for the autograft recipient alone. Moreover in **Schwartz et al., 2012** two patients were transplanted with human embryonic stem cell-derived RPE (hESC-RPE). One patient suffered from Stargardt's macular dystrophy and the other from dry age-related macular degeneration. Both patients showed signs of improvement in visual function following treatment. Importantly, the transplanted cells did not show any signs of hyperproliferation, tumorigenicity, ectopic tissue formation, or apparent rejection even after four months. The results of these two studies add to evidence that stem cell-derived RPE can be transplanted safely into humans to treat AMD.

Stem Cell Approach for RP using Transplanted Photoreceptors

In diseases such as RP, where there is a degeneration of rod photoreceptors followed by cones, transplantation of photoreceptors, obtained from stem cells, is a promising approach. There are multiple strategies involving transplantation of photoreceptors, one of which is to transplant intact, partial, or whole retinal sheets. However, research in animal models shows that such sheets do not always integrate well with the recipient circuitry (**Ghosh et al., 1999; Ghosh et al., 2004**). Another strategy is the transplantation of dissociated cells. However, to date transplantation of photoreceptor precursor cells has met with the most success (**Lakowski et al., 2010; MacLaren et al., 2006**). This success is measured by the transplanted precursor cell's ability to differentiate and express the morphological features characteristic of a fully-developed photoreceptor cell (**Eberle et al., 2012; Warre-Cornish et al., 2014**). **Pearson et al., 2012** show that rod-based vision and behaviour improves after the transplantation of photoreceptor precursor cells in an adult mouse model of congenital stationary night blindness. Currently, this strategy is being refined further, based on a number of factors, such as survival rates of transplanted cells and their ability to integrate with the host circuitry.

Optogenetics and Photopharmacology

In optogenetics and photopharmacology, molecules capable of detecting light are introduced into the retina, with the aim to compensate for the loss of photoreceptors. These light detecting molecules can be introduced either in the form of light-sensitive proteins that embed themselves into the surface of the target retinal cell (cone cell body, bipolar cells or retinal ganglion cells) (**Boyden et al., 2005; Nagel et al., 2003**), or as molecules that attach themselves to an existing ion channel, thereby making them light sensitive and acting as a switch (photoswitches). Some of the most commonly used optogenetic proteins for depolarization and hyperpolarization are from the channelrhodopsin family (**Nagel et al., 2003**) and halorhodopsin family (**Han & Boyden, 2007**), respectively.

There are various advantages and drawbacks to both, the optogenetic and photopharmacology approach. The genetic approach of embedding light-sensitive molecules into a cell membrane is a long-term approach, which has been shown to establish visual function and responses in mouse models of blindness (**Buskamp et al., 2010; Doroudchi et al., 2011**). However, since it is long lasting, if there are adverse effects such as a strong immune response, it would be very hard to control. Moreover, if a better treatment method is developed in the future, patients who underwent an optogenetic treatment will not be eligible for it. In the case of the photopharmacology approach, the molecule which attaches itself to existing ion channels degrades over time. Therefore, this approach does not have the drawbacks associated with optogenetics as it is temporary. On the other hand, due to its temporary nature, the photopharmacology approach requires multiple intravitreal injections to introduce the photoswitches to the retina. Intravitreal injections, though not uncommon, require a certain level of expertise to perform.

Another important question in such approaches (optogenetic or photopharmacology), is the target site for the molecule. If RGCs are targeted for inducing light sensitivity, it skips the existing retinal circuitry of bipolar cells and amacrine cells and their associated image processing. This, therefore, might be a suitable option for late-stage degenerate patients where the retina is known to undergo significant rewiring (**Jones et al., 2016; Marc et al., 2003**). Conversely, for early-stage degeneration, bipolar cells might be a more appropriate target, as this enables the use of existing retinal circuitry when the rewiring is still minimal. Nevertheless, even if the bipolar cells are successfully targeted in a retina which has not undergone major rewiring, there is some image processing that must be compensated for due

to the loss of photoreceptors (**Marc et al., 2003**). It has been proposed that the use of goggles, which project a pre-processed visual scene (that compensates for the photoreceptor loss) to the retina, could help overcome this issue (**Nirenberg & Pandarinath, 2012**). Finally, the amplification of the individual photonic signals is also a crucial concern. While isolated photons falling on a rod are detected and amplified through the high-density packing of the visual pigments and the associated biochemical cascade, this is not the case with artificially introduced light sensitivity through optogenetics or photopharmacology. The amount of current produced by a single light-sensitive protein or photoswitch is small. Therefore, a high concentration of these molecules is required. However, a large concentration of light-sensitive molecules could trigger an immune response (**Vinores et al., 1995**), as some diseases such as RP are known to breach the blood-brain barrier compromising the immune-privilege of the eye. Hence, to amplify signals coming from single photons, one could also engineer these molecules to have longer closing times, thereby allowing more current into the bipolar or retinal ganglion cells. This approach would, however, suffer from temporal smearing. Despite these many hurdles, there have been some promising studies, demonstrating that optogenetics can re-introduce light perception in the diseased retina. For example, in (**Lagali et al., 2008**) channelrhodopsin-2 was introduced into the ON bipolar cells of the rd1 mouse. The ON bipolar cells, so targeted, became photosensitive and could in turn drive light-induced activity in the downstream RGCs. Effects of this light-induced activity were seen at both, cortical and behavioral level, through the successful performance of optomotor tasks. In addition to this, the photopharmacology approach has also shown promise, by being able to restore visual responses in a mouse model of blindness (**Polosukhina et al., 2012**). Such studies, therefore, demonstrate the viability of an optogenetic- or photopharmacology-based approach in treating degenerative retinal diseases.

Retinal Prosthesis

The most successful approach to vision restoration for RP to date has been with retinal implants. In general, retinal implants aim to replace the lost photoreceptors through the activation of the RGCs either directly or indirectly via the retinal network, using current or voltage pulses. This activation of RGCs in turn elicits visual percepts in patients (**Zrenner, 2002**). Based on the site of implantation, retinal devices can be broadly classified as subretinal, epiretinal, or suprachoroidal (**Zrenner, 2013**)(**Figure 1.9**). In this section, these three implant strategies are discussed, including a detailed description of the first subretinal and epiretinal

devices to obtain regulatory approval for commercial sale. Though suprachoroidal implants have not yet been commercialized, the results of the most recent clinical trials with such devices are also discussed.

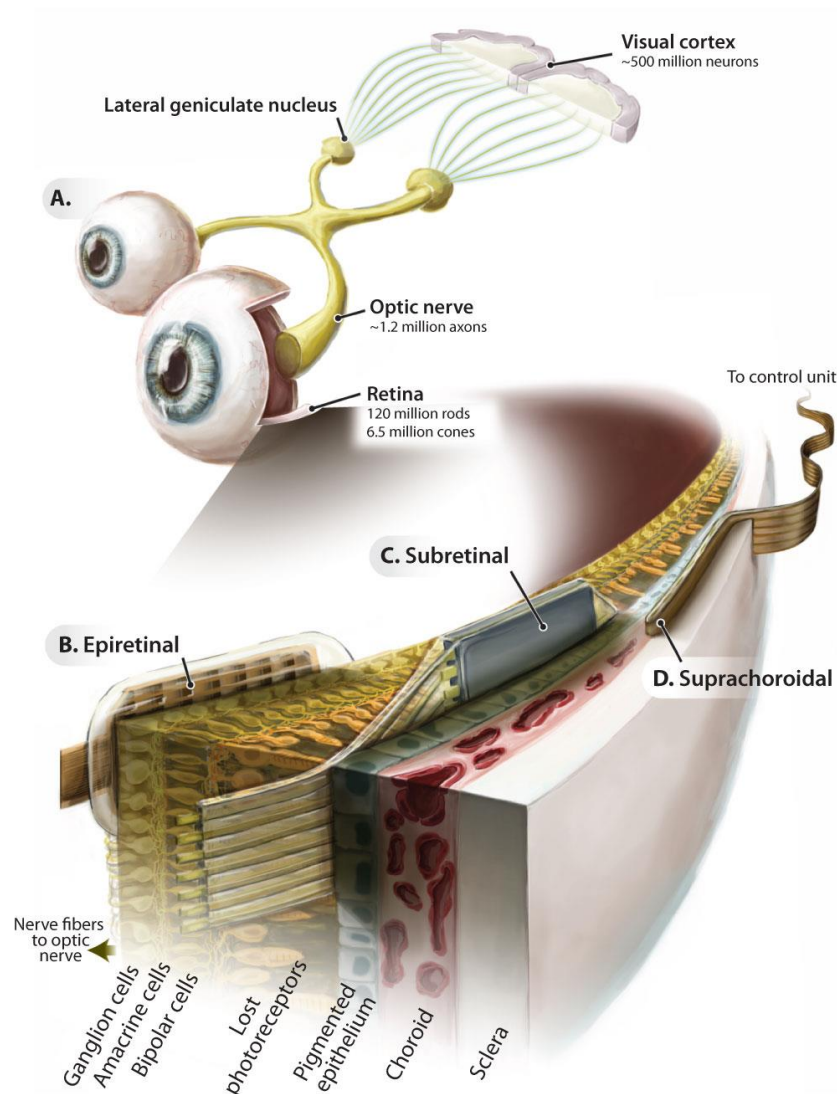


Figure 1.9: Different Implant Strategies based on site of implantation. Subretinal devices are implanted in the subretinal space between the RPE and bipolar cells. Epiretinal devices are tacked onto the RGCs. Suprachoroidal devices are implanted on the outer side of the choroid. Figure from (Zrenner, 2013). Reprinted with permission from AAAS.

Subretinal Implants

The Tuebingen retinal implant is the first subretinal device to obtain approval for commercial sale. This device is implanted in the region where the degenerate photoreceptors used to be. This strategy aims to activate still-intact bipolar cells. By doing so, the Tuebingen implant makes use of the native image processing, present in the remnant IPL circuitry (Zrenner, 2013). However, it also contends with the retinal rewiring associated with RP and AMD (Jones

et al., 2016). This retinal rewiring has a detrimental effect on the natural image processing done by the remnant IPL. The extent to which the rewiring affects the natural image processing is believed to depend on the extent of rewiring.

The current Tuebingen implant (Retinal Implant Alpha- IMS) consists of a micro-photodiode array with 1500 stimulating electrodes (Stingl et al., 2015). It is 3.0 x 3.0 mm in size with an inter-photodiode distance of 70 µm. The shape of the implant corresponds to a square visual field with 15 degrees visual angle diagonally (Stingl et al., 2015). A prototype of the device had to be powered with a subdermal cable that connected the subretinal implant to an external power source, through an opening behind the ear (Zrenner et al., 2011). Later versions are powered using a transmitter coil that allows for an inductive power transfer. Below is a schematic drawing of such an implant as well as the position in the eye (Stingl et al., 2015) (Figure 1.10).

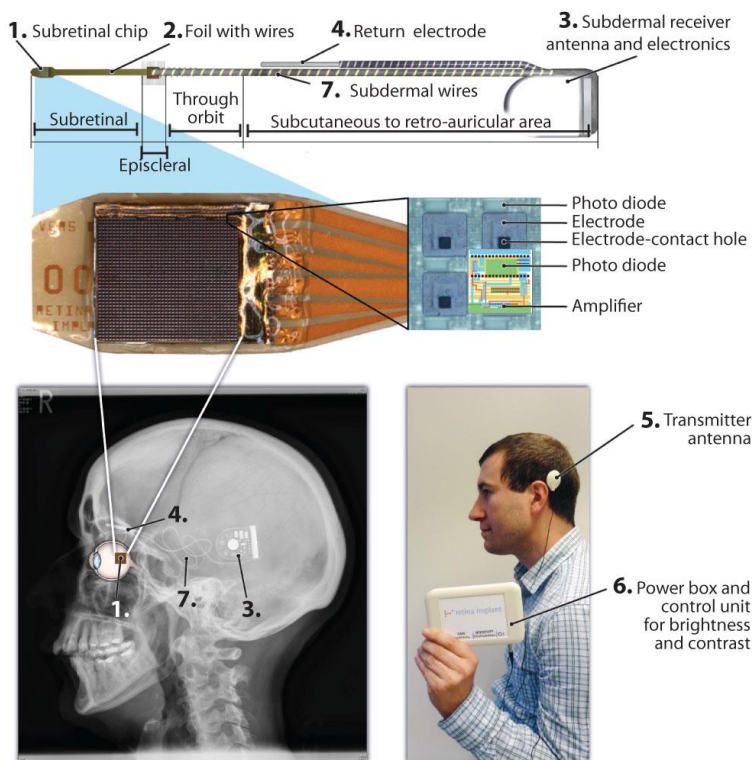


Figure 1.10: Tuebingen subretinal implant. The (1) subretinal implant is placed in the region where the photoreceptors used to be. The implant is connected via a (2) subretinal foil with gold wires and a (7) subdermal cable to a (3) subdermal receiver antenna. The subdermal receiver antenna is in turn connected via wireless transfer to an (6) external power box through an (5) external transmitter antenna, placed behind the ear. The (6) power box also contains hardware that enables the patient to change the settings of the chip in order to adjust to different brightness and contrasts of the environment. Figure from Zrenner, 2013. Reprinted with permission from AAAS.

Due to the site of implantation, subretinal implants are easier to position and to fix in comparison to epiretinal devices (Zrenner, 2002). Since the Tuebingen implant makes use of the remnant native image processing of the retina, there is no external visual processing unit. There is, however, an external device under the control of the patient to used adjust the global gain and sensitivity of the photodiodes. This helps the device operate within its dynamic range at different luminance conditions. However, since the gain and sensitivity control are global, local luminance adaptation is not possible (unlike in the healthy retina). Below (Figure 1.11) is a figure showing how the charge output by the photodiodes varies with luminance at different gain and sensitivity settings (Zrenner et al., 2011).

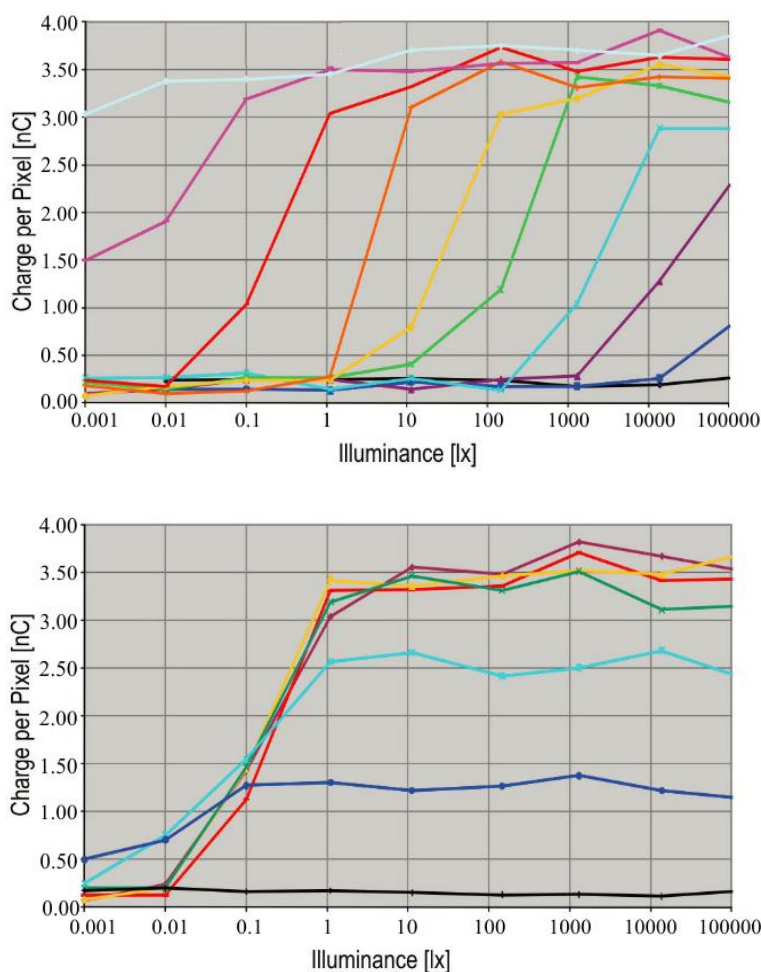


Figure 1.11: Sensitivity and gain settings of the implant. Top) The illuminance-charge output curves on the far-left and far-right of the figure correspond to the highest and lowest sensitivity of the photodiodes respectively. Bottom) The illuminance-charge output curves that saturate at bottom and top of the figure correspond to the lowest and highest gain settings of the photodiodes respectively. Figure adapted from Zrenner et al., 2011 and reused with permission according to CC-BY version 4.0 license

To date, the highest restored visual acuity in humans (20/546) has been with the Tuebingen subretinal implant (Stingl et al., 2015).

Epiretinal Implants

The first epiretinal implant to obtain approval for commercial sale is the Argus-II implant. This device is implanted on the ganglion cell side of the retina with an aim to directly activate the

RGCs (output cells of the retina). In doing so, it can more easily bypass abnormalities brought on by retinal rewiring. The epiretinal device is held in place either with cellular contacts, microtacks, or through mechanical pressure (**Zrenner, 2002**). Epiretinal devices tend to activate ganglion cell axons, in addition to the target ganglion cell bodies. Axonal stimulation leads to a smearing of visual percepts, contributing to a reduction in restored visual acuity (**Weiland & Humayun, 2014; Zrenner, 2002**). To compensate for the bypassed image processing of the IPL retinal network, epiretinal implants require an external camera and an external visual processing unit (VPU). An advantage of using an external VPU is, that improvements in image processing algorithms, can be more easily provided to the patients (**da Cruz et al., 2016; Humayun et al., 2012; Zrenner, 2002**). The Argus-II implant consists of camera-mounted glasses connected to the VPU. On the side of the glass frame is a transmitter coil. The camera captures the visual scenery directly in front of the patient's head and relays it to the VPU (**Figure 1.12**).

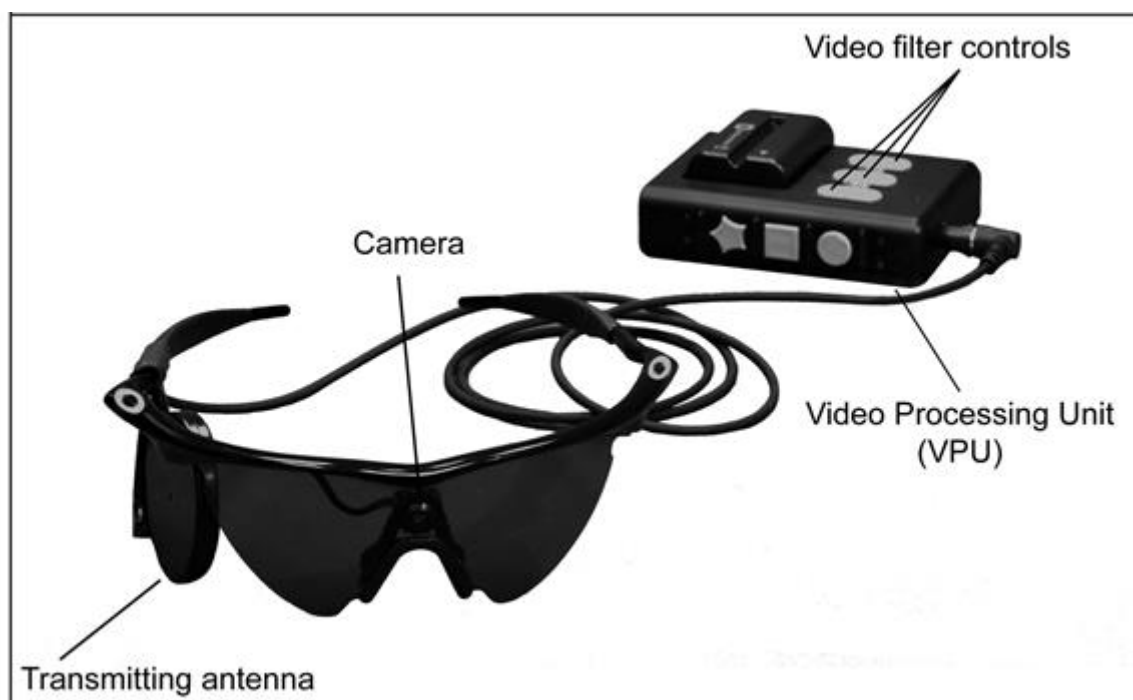


Figure 1.12 Camera-mounted glasses with the external visual processing unit for the Epiretinal implant. Since epiretinal devices are placed on ganglion cell side, they bypass the intrinsic image processing done by the retina. Therefore, an external visual processing unit is required to compensate for the image processing of the retina. Figure adapted from da Cruz et al., 2016 and reused with permission under CC BY-NC-ND 4.0 license

The VPU processes the image and then uses the coil to instruct the implant on the spatiotemporal pattern of electrical stimuli that must be delivered to the retina. The Argus-II

epiretinal device consists of 60 stimulating electrodes (**da Cruz et al., 2016; Humayun et al., 2012**). To date, the best-restored visual acuity with an epiretinal device is about 20/1260 (**Humayun et al., 2012**). Another epiretinal device which has received regulatory approval (in 2016) is Pixium Vision's Iris II implant. It consists of 150 electrodes and (like the Argus device) an external camera and image processing unit. Clinical trials with the device are currently underway.

Suprachoroidal Implants

A third category of implants are suprachoroidal implants. These devices are implanted in the space between the choroid and sclera (**Zrenner, 2013**). Since these devices also target bipolar cells (like subretinal implants) they benefit from the natural image processing done by the IPL network, too. Moreover, in comparison to the subretinal implants, the surgical procedure associated with the device is much simpler as it does not require penetrating through multiple layers of the eye to implant the device. It also has the ability to maintain stable contact with the neural tissue (**Fujikado et al., 2011; Shepherd et al., 2013; Shivdasani et al., 2014**). However, since thresholds depend on the retinal-electrode distance, suprachoroidal implants tend to have higher thresholds for retinal activation (**Shepherd et al., 2013**). This has the disadvantage of reducing the overall range of discrete stimulation levels available for encoding the visual scene. The larger distance also increases the spatial spread of the voltage/current pulses, thereby reducing the resolution and, therefore, the visual acuity that can be achieved (**Fujikado et al., 2011; Shepherd et al., 2013; Shivdasani et al., 2014; Zrenner, 2013**). To date, one of the major proponents of this device is the bionic vision group in Australia. A prototype of their device, consisting of 33 platinum stimulating electrodes, was implanted in 3 patients as a part of their clinical trials. **Figure 1.13** shows the implant in more detail.

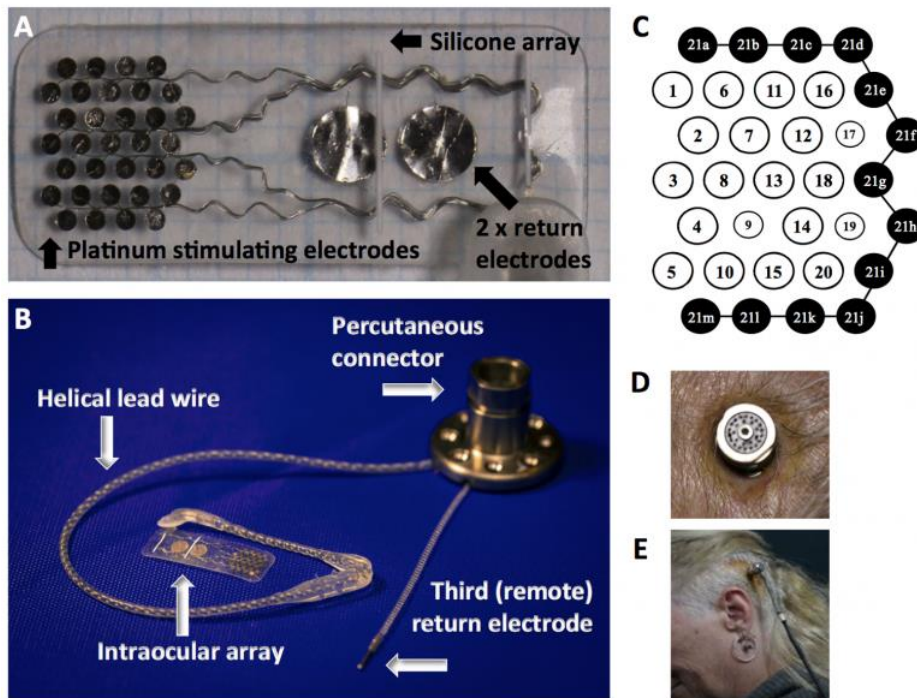


Figure 1.13 *The Australian suprachoroidal implant. A) Arrangement of platinum stimulating electrodes B) Intraocular array is linked to a percutaneous connector via a helical lead wire consisting of platinum/iridium wires C) Of the 33 electrodes, only 20 electrodes stimulate independently. D) Connector is implanted percutaneously behind the ear E) External Wires connect the implant via the percutaneous connector to an external power supply. Figure adapted from Ayton et al., 2014, and reused with permission according to CC-BY version 4.0 license.*

The implant is powered directly from a power source external to the body using platinum/iridium wires and a percutaneous connector. Visual function testing showed that all 3 subjects performed significantly better when the device was turned on (Ayton et al., 2014).

Summary of Retinal Implants

With hundreds of patients implanted worldwide, retinal prosthetics have come a long way from their conceptualization in the early-/mid-nineties. Three prosthetic companies, namely Second Sight, Retina Implant AG, and Pixium Vision, have received regulatory approval for their respective devices. Results of ongoing clinical trials are promising, with some of the implanted patients being able to distinguish different cutlery, make out shapes, read letters, words, localize objects, and navigate their environment (Ayton et al., 2014; Fujikado et al., 2011; Humayun et al., 2012; Zrenner et al., 2011).

Despite such encouraging results, restored visual acuity tends to fall below the theoretical limit that can be achieved with an implanted device (Stett et al., 2000). Moreover, there are also many patients with virtually no real improvement in their vision. This is because there are

still many technical issues that must be overcome. For example, one of the major problems facing retinal implants is the fading of visual percepts. Fading refers to diminishing visual percepts in patients when provided with constant amplitude stimulation above a certain frequency. The frequency at which fading sets in varies from patient to patient (**Pérez Fornos et al., 2012; Stingl et al., 2015**). Fading places, a biological limit on the temporal acuity that can be restored. Other major problems facing retinal implants are high stimulation thresholds, spatial spread of stimulation and indiscriminate retinal activation (**Shepherd et al., 2013; Weiland & Humayun, 2014; Zrenner, 2013**).

However, with clinical trials underway world over, the various retinal prosthetic strategies provide an ever-increasing cohort of implanted patients and in turn a basis for understanding how effective these devices can be in their present form, and to inform on future avenues of research within the field of retinal stimulation. Potential areas for improvement are a lower cost of manufacturing, less risky surgical procedures, and improved spatial and temporal acuity.

For a more detailed overview of all these different treatment options, the reader is referred to the report, **Restoring Vision to the Blind**, by the **Lasker/IRRF Initiative for Innovation in Vision Science**.

[Overview of Thesis Work](#)

Even though retinal implants have enjoyed considerable success in comparison to the other treatment options for RP/AMD, there are still many open issues, as detailed above. The bulk of basic research in retinal prosthetics has to date focused on these issues through exploration of different stimulation parameters such as pulse-width and its effect on activation thresholds, effect of electrode designs and spatial configurations with respect to spread of electrical stimulation, differential activation of RGCs using different waveforms like sine waves or sawtooths, biophysical modeling of retinal responses to electrical stimulation, characterizing desensitization (a possible retinal correlate of fading) to repetitive pulse stimulation, and comparison of anodic versus cathodic stimulation on activation thresholds (**Boinagrov et al., 2014; Im & Fried, 2015; Jensen & Rizzo, 2007; Jensen et al., 2005; Khalili Moghadam et al., 2013; Guo et al., 2014; Twyford & Fried, 2016**). Though these studies have helped make progress in our understanding of prosthetic activation of RGCs, there is still a gap between a systems level comprehension and the experimental data. For example, while there have been

attempts to explore different waveforms for preferential activation of the retina, the choice of these waveforms has been ad hoc and not grounded in any thorough, systematic exploration of the stimulus space of the various classes of RGCs. Therefore, in this thesis, we decided to bridge this gap by exploring a novel linear systems approach to characterize electrically driven RGC responses, recorded using microelectrode arrays. Using white noise stimulation and reverse correlation, we build black-box models of the retina for visual and electrical stimulation (**Figure 1.14**).

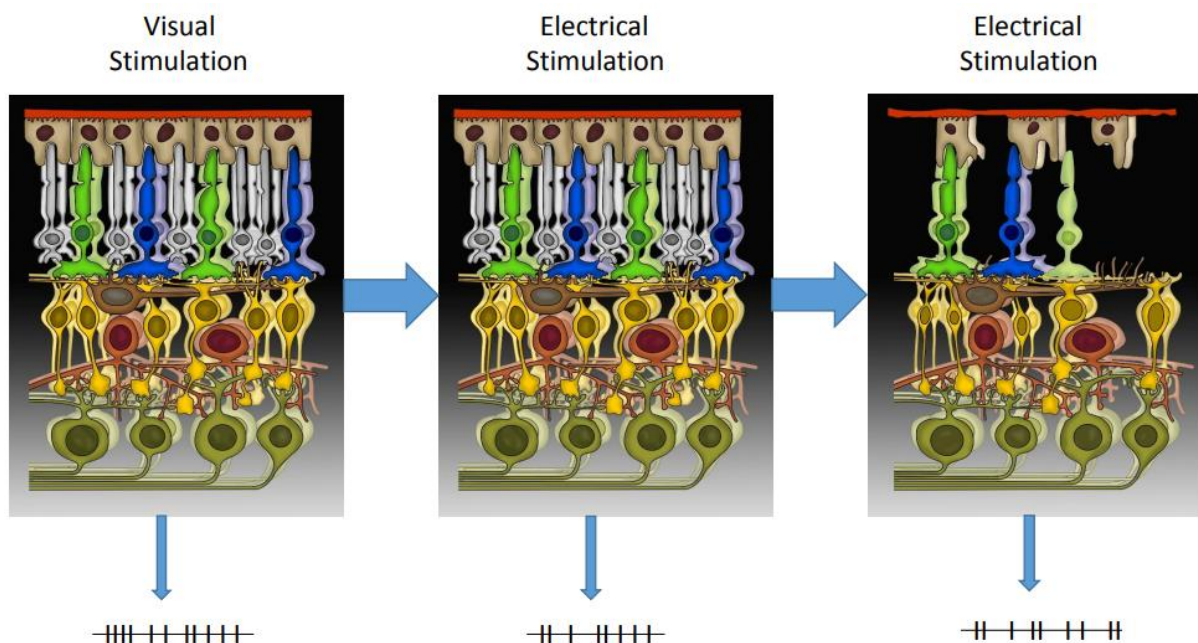


Figure 1.14: *Left) The wild type retina is visually stimulated in order to classify cell type and to characterize its visual input filters. Middle) The same retina is also provided with electrical stimulation in order to determine its electrical input filters. Right) Finally, the same electrical stimulus is given to the rd10 retina in order to understand how the functionality of the retinal circuit changes with photoreceptor loss and retinal rewiring. Using this approach, we hope to comprehend, in a systematic manner, the differences in spiking patterns (bottom of image) between visually- and electrically-driven retina (wild type and degenerate).*

In designing our stimuli, we aimed to minimize indiscriminate RGC activation brought about by large-amplitude suprathreshold pulses, by using smaller-amplitude subthreshold pulses instead. By using these smaller pulses, the retina is forced to integrate across time to reach activation threshold. This in turn allows us to search for correlations between RGC spikes, and the temporal stimuli preceding them. The details of the design of the electrical noise stimulus and linear filter estimation techniques are found in the **summary of results** section and **Sekhar et al., 2016 (Appendix 2)**. The visual and electrical black-box models for each cell, are compared, in order to find possible correlations between visually and electrically driven

responses for various cell types. Subsequently, these electrical noise methods were also extended to the *rd10* retina (a mouse model of RP) at late stage degeneration. This shed light on how the functionality of the retina changes with photoreceptor loss and retinal rewiring. The results of this analysis are also found in the **summary of results** section and **Sekhar et al., 2017 (Appendix 3)**. In a final step, statistical models, namely generalized linear models (GLM), are used to quantify how effective linear filters are at capturing the response dynamics of RGCs and if the response patterns of different cell types deviate significantly from linearity. This is an on-going study. The results so far, are detailed in the **summary of results** section and **Appendix 4**. In the section below, a brief primer is given on MEA-based data collection techniques and the theoretical foundations of reverse correlation and generalized linear modeling.

Methods

All data in this thesis was obtained using microelectrode arrays (MEAs) to record from explanted retinas. MEAs deploy a large number of electrodes to record from a given biological tissue at different spatial locations. The tissue that is being recorded, can range from cardiac to neural. Spiking activity of the tissue manifests as large and sudden decreases in the extracellular potential. Due to the use of numerous electrodes, MEAs can collect large amounts of data relatively quickly. Moreover, the activity of a population of cells to a given stimulus can also be studied (Meister et al., 1994). However, unlike in a single-electrode setup, it is more difficult to choose the cell type that is being recorded. Therefore, the recorded spikes need to go through a rigorous sorting procedure before being assigned to specific cells. Establishing a good contact between tissue and electrode is also crucial for the data collection process. Therefore, Teflon inserts are placed on the retinas once they are mounted onto the MEAs (Figure 1.15).

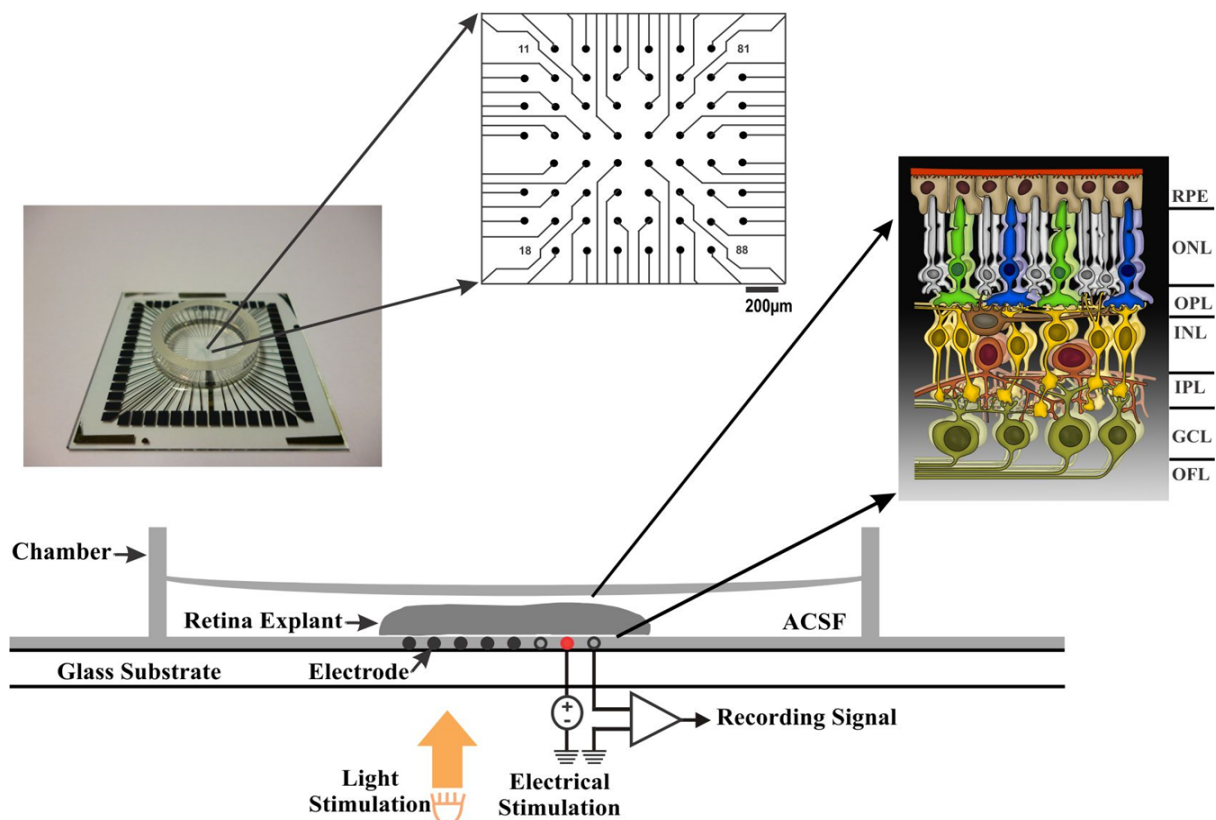


Figure 1.15: Experimental Setup. The retina is mounted on the MEA, which is then recessed in the MEA chamber. A Teflon insert is placed on the retina to press it onto the MEA and ensure good tissue-electrode contact. The retina is constantly perfused with ACSF at 33° C at a pH of 7.4. Signals from the electrodes are sent to the amplifier before being sampled at 50kHz/channel by the digitizer. Figure from Jalligampala et al., 2017, reused with permission

Once the retina is in the chamber, it is constantly perfused with artificial cerebrospinal fluid (ACSF) at 33° C to keep it alive and healthy. The temperature is maintained using both a heating plate for the MEA chamber and a heated perfusion cannula. The Teflon insert has a semipermeable dialysis membrane which allows essential nutrients from the ACSF to reach the retina. The ACSF is continuously bubbled with carbogen (95% O₂, 5% CO₂) in order to maintain a pH of 7.4. The MEA used is a standard 60 electrode array made of TiN (Titanium Nitride) electrodes arranged in an 8x8 manner with an inter-electrode distance of 200 micrometers (Multi Channel Systems MCS GmbH Reutlingen, Germany). One of these 60 electrodes, serves as the reference electrode, whereas the other 59 are recording electrodes. The diameter of an electrode is 30 micrometers. The MEA electrodes are planar and rest on a glass substrate.

Retinal Preparation

The mouse is asphyxiated with CO₂ inhalation before cervical dislocation and decapitation. A heat pen is used to make a small fiducial marking on the corneas of both eyes of the mouse. After pulling out the eyes using sharply curved forceps, the cornea is removed by cutting around it, using scissors.

The point of entry of the scissors is the corneal mark made by the heat pen. Next, the lens is removed, and the sclera is peeled using two 5s forceps. Finally, the optic nerve is severed. This allows the retina to detach from the RPE and to float out of the eyecup. Vitreous humor is removed before cutting each retinal piece into two halves. The retina is then flattened onto the MEA electrodes with either forceps or brushes. Following this, a Teflon insert is placed on the retina to provide good tissue-electrode contact and the MEA with the mounted retina is placed inside the MEA chamber and perfused with ACSF as mentioned above.

Spike Sorting

The recorded extracellular voltage traces are passed through a preamplifier before being fed to an amplifier for a total gain of 1100. The recorded signals are then filtered with a bandwidth of 1 Hz–3 kHz to isolate the spiking potentials. The signals from the electrodes are sampled at a rate of 50 kHz/channel. The recorded voltage traces are filtered offline with a 12-pole Bessel filter with a low cut-off frequency of 51Hz. Due to their temporal kinetics, electrical stimulation artifacts are also isolated during this filtering process. Next, the filtered potentials

are passed through an automated spike sorting stage. Finally, a manual check is done to ensure minimal spike sorting errors (for example, assignment of spikes to wrong cell clusters).

Cell Validation

The putative spiking events are assigned manually scores of 1 (lowest) - 5 (highest), based on their 1) waveform shape 2) ISI histogram lockout 3) Cross-correlograms against other sources, and 4) stability over time. Only clusters with a weighted average score of 2.833 or higher are further analyzed. After the isolation of reliable clusters, the spike times are sent to MATLAB using NeuroExplorer (Plexon Inc., TX, USA). Using MATLAB, linear filters (based on spike-triggered averages) are estimated for the different RGCs. The efficacy of these STA filters is then evaluated using generalized linear models (GLMs).

Below is a brief overview of systems identification, spike-triggered averaging, and GLMs as applied in this thesis.

Systems Identification

The use of statistical methods to construct mathematic models for describing the behaviour of a particular system, based on observed data/measurements, is called systems identification **(Söderström & Stoica, 1989)**. A 'system' can be anything from a pendulum to biological tissue, such as the retina. Such systems models can be broadly classified as white-, grey- or black-box models **(Estrada-Flores et al., 2006; Söderström & Stoica, 1989)**. White-box models are those where the mechanistic operations of the subcomponents of the systems are explicitly modelled. An example of these, would be Newton's laws of motions, or the Hodgkin-Huxley models, used to capture spike generation and spike propagation in neurons. Though the white-box approach allows explicit access to the subsystem components, such models can become very complicated. In contrast, black-box models try to capture the observable input-output relation without involving the subsystem components. The subsystem dynamics are treated essentially like a black box (not observable) **(Figure 1.16)**. Such models, though lacking in the explicit knowledge of the internal workings of a system, are highly tractable. Grey-box models are a hybrid mix of both black- and white-box models **(Estrada-Flores et al., 2006; Söderström & Stoica, 1989)**.

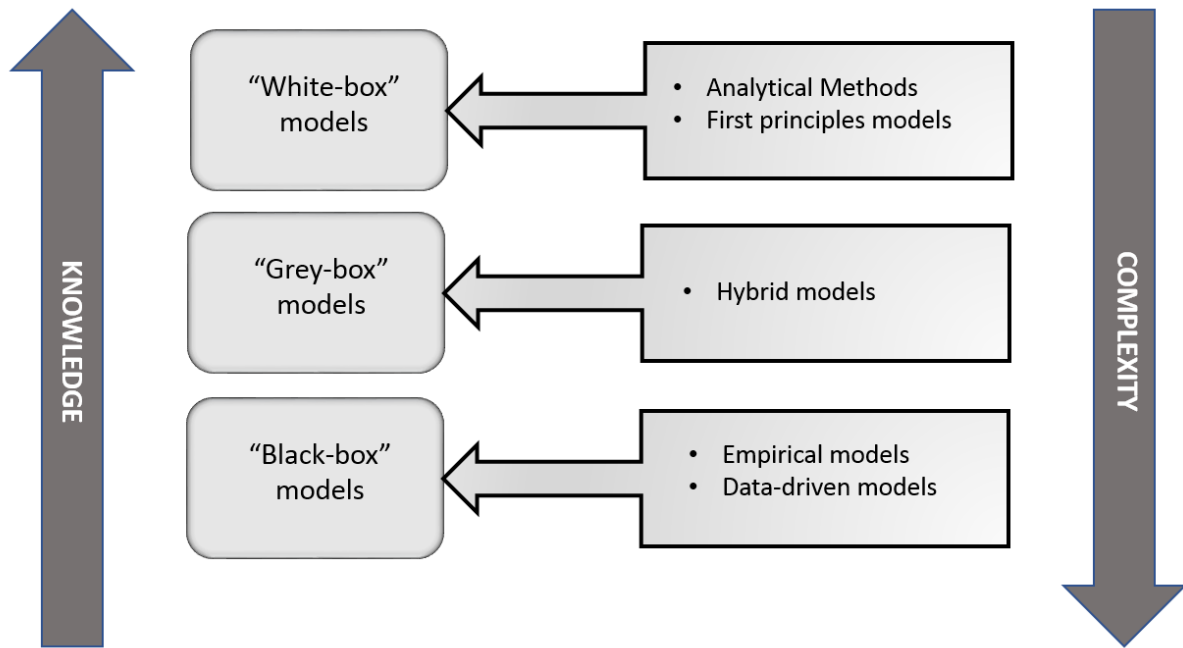


Figure 1.16: The three different classes of models based on complexity of implementation and required knowledge of the system and its subcomponents.

Ultimately, the type of system identification done depends on the question at hand. In neuroscience, both white- (**Hodgkin & Huxley, 1952**) and black-box models (**Chichilnisky, 2001**) have found great use. To date, many models of retinal responses to electrical stimulation have been white-box, with explicit modeling of spike generation based on the Hodgkin-Huxley equations. Black-box models of retinal responses to electrical stimulation have been limited mostly to the identification of voltage-/current- response curves for RGCs. In this thesis, the black-box modeling approach of retinal responses to prosthetic stimulation was extended by using white noise stimulation and reverse correlation.

White Noise Stimulation and Analysis

Traditional visual electrophysiology used flashes, drifting bars, gratings, and spots as their primary visual stimuli (**Enroth-Cugell & Pinto, 1972; Hubel & Wiesel, 1968; Levick & Zacks, 1970; Rodieck, 1965**). Though these stimuli are capable of strongly driving the retina, they suffer from numerous disadvantages, such as confounds brought on by adaptation of responses, and an inefficient sampling of stimulus space. White noise stimulation presents a way around these confounds (**Chichilnisky, 2001; Marmarelis & Naka, 1973a, 1973b, 1973c; Pillow & Simoncelli, 2003; Schwartz et al., 2006**). The term ‘white’ refers to the uniform power distribution of the component frequencies (spatial or temporal) in the stimulus – in

analogy to the relatively flat power spectrum of white light. Therefore, the stimulus is unbiased in its sampling.

In this method, stimuli, which fluctuate randomly around a mean are presented at a certain temporal rate, to the neural tissue. The randomness of the stimuli helps mitigate adaptation, and helps to sample the stimulus space better. By correlating the neural spikes to the stimuli immediately preceding them, the neural network is characterized by a linear input filter and a nonlinear spike-generator (an *LN* model); in other words, a black-box representation (**Chichilnisky, 2001**). The linear input filter is obtained by averaging all the stimuli preceding spikes. This process is called spike-triggered averaging (**Figure 1.17**).

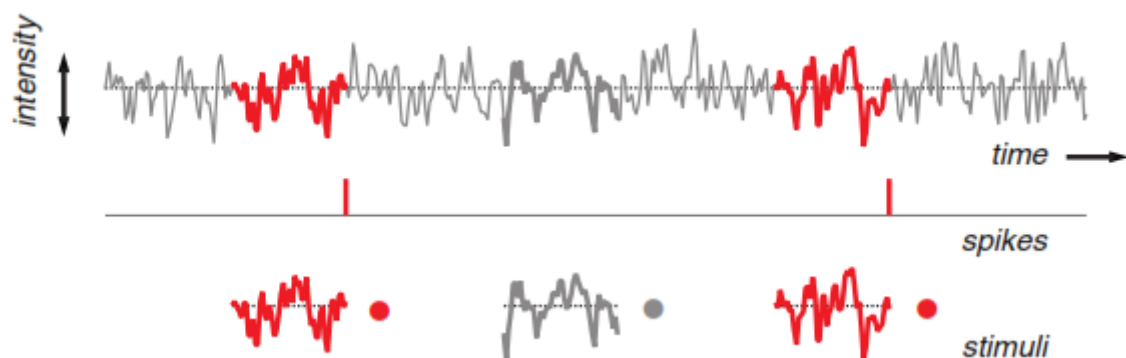


Figure 1.17: White Noise Stimulation and Reverse Correlation: The grey trace represents the random fluctuation of a stimulus around a certain mean. The superimposed red trace represents the stimulus fluctuations that correlated with the occurrence of spikes. By averaging the stimuli preceding these spikes, a spike-triggered average or linear input filter is obtained. Figure adapted from Fairhall et al., 2006

Provided in the next section, is the mathematical proof of why STAs represent the linear input filter of the neuron.

Spike-Triggered Average

Let $R(s)$ be the expected response of a cell to a given stimulus s . It is given by

$$R(s) = \sum_f fP(f|s)$$

..... equation 1.1

Where

$R(s)$ is the expected response

s is the stimulus

f is the average spike count in time-bin immediately following s

P is probability of spike count f in time-bin given a stimulus s

The *STA* can, in turn, be expressed as a sum of stimulus vectors s , where each stimulus vector is weighted by its probability of occurrence $P(s)$ and its expected response $R(s)$. This product is normalized by the average firing rate $\langle f \rangle$. Mathematically, this can be formalized as per the equation 1.2:

$$STA = \frac{\sum_s sP(s)R(s)}{\langle f \rangle}$$

..... equation 1.2

In the *LN* model, the firing rate is assumed to be equal to the output of a static nonlinear function N acting on the dot product of the stimulus vector s and the weight vector w . Hence

$$R(s) = N(w \cdot s)$$

..... equation 1.3

Inserting equation 1.3 into equation 1.2 we obtain

$$STA = \frac{\sum_s sP(s)N(w \cdot s)}{\langle f \rangle}$$

..... equation 1.4

Since the stimuli s are drawn from a circular distribution, for every s there is another stimulus s^* which is radially symmetric around W and for which $P(s) = P(s^*)$. Therefore $s + s^*$ is in the direction of W , implying that $N(w \cdot s) = N(w \cdot s^*)$ (**Figure 1.18**)

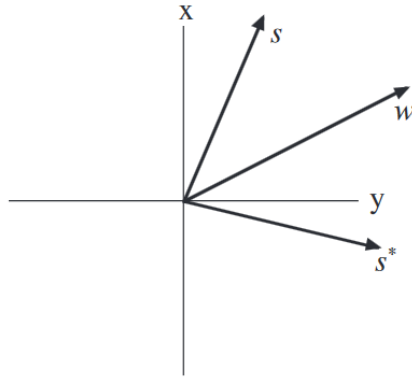


Figure 1.18 The s & s^* vectors represent equi-length stimulus vectors drawn randomly from a circular distribution with equal probability. When we average all the stimuli preceding spikes, we obtain the STA vector which is in the direction of input filter W . Figure adapted from Chichilnisky, 2001 and reused with permission

Now the equation 1.4 can be rewritten as

$$STA = \frac{\sum_s P(s)N(w.s)s}{\langle f \rangle} + \frac{\sum_s P(s^*)N(w.s^*)s^*}{\langle f \rangle}$$

..... equation 1.5

This simplifies to the following:

$$STA = \frac{\sum_s (s + s^*)P(s)N(w.s)}{\langle f \rangle}$$

..... equation 1.6

But as shown above

$$(s + s^*) \propto w.$$

..... equation 1.7

Hence

$$STA \propto w$$

This is why the STA is taken to represent the input filter of the cell. For a more elaborate version of this proof, the reader is referred to **Chichilnisky, 2001**.

Another more intuitive way to think about the STA is, as a vector pointing to the mean of a subset of all the presented stimuli, where the stimulus subset consists only of stimuli that are immediately followed by spikes.

The efficacy of these STAs (linear filters) in capturing the response properties of RGCs was estimated using GLMs (generalized linear models). In the following section, a brief overview of the theoretical framework of GLMs and the linear nonlinear Poisson (LNP model), a special case of GLMs, is presented. The outcome of this GLM analysis is provided in the **summary of results** section and in **Appendix 4**.

Linear Nonlinear Poisson Models

One of the most commonly used statistical models in neuroscience is the LNP model. The LNP model, a special case of the GLM, consists of a linear filter (either spatiotemporal or just temporal) that convolves with the stimulus (**Chichilnisky, 2001**) (**Figure 1.19**). The convolution product is then sent to a nonlinear transform that determines the spiking rate. This spiking rate is converted to spike trains by sampling from a Poisson distribution.

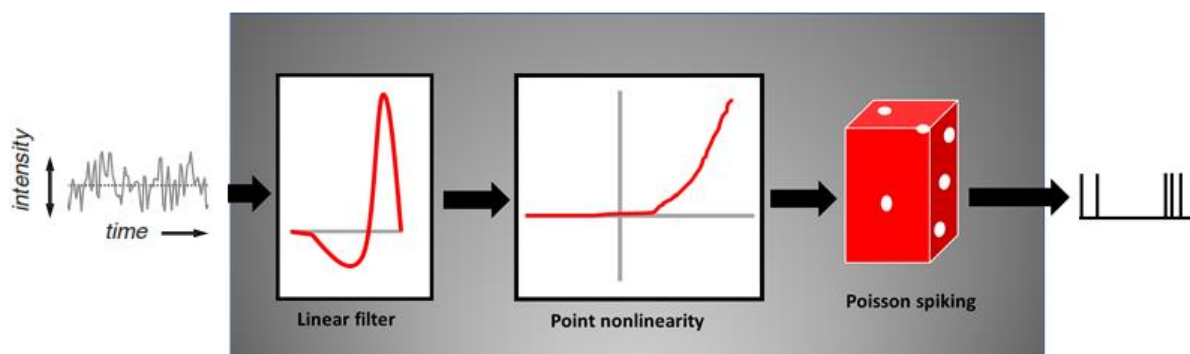


Figure 1.19 LNP model. The linear filter is convolved with the stimulus. This product is sent to a spike rate determining nonlinear function. The instantaneous firing rate is converted to spike times by sampling from a Poisson distribution. Figure adapted from Pillow, 2007 and reused with permission under CC BY-SA 4.0 license

The success of LNP models at describing the response properties of neurons in various sensory systems (including the visual system) and their ease of implementation have made them very popular in neuroscience (**Pillow, 2007; Schwartz et al., 2006; Williamson et al., 2015**). That being said, there are a few notable drawbacks that must be kept in mind when working with

the LNP framework. The first is, that neuronal spikes are not Poissonal (memoryless) in nature. Due to the relative and absolute refractory period, the timing of a spike does depend on the preceding spikes. Therefore, a Poisson spike generator can lead to un-physiological spike times (**Pillow, 2007**). Depending on the question at hand, this could be a major confound. To correct for this, a memory filter can be added. The memory filter convolves with the generated spikes to create a small negative feedback that is combined with the convolution product of the input filter and stimulus (**Figure 1.20**).

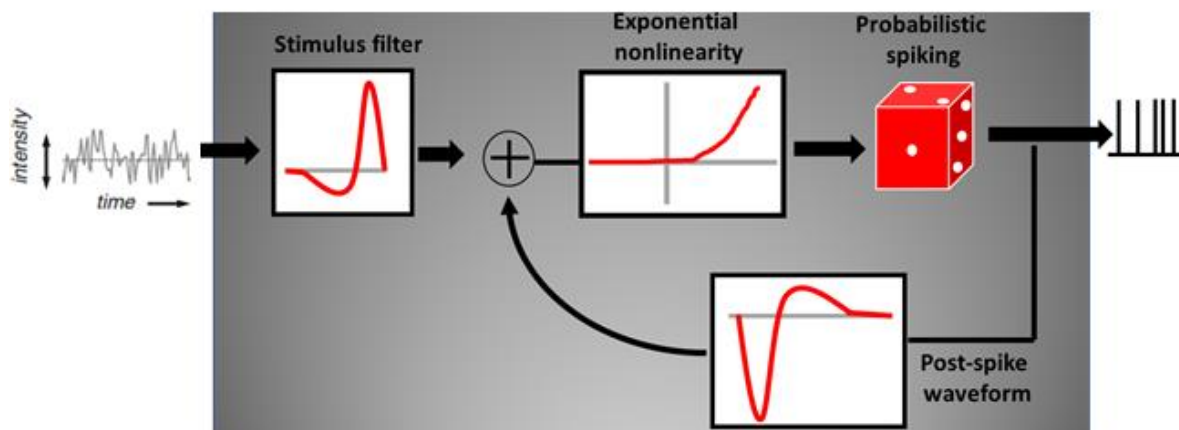


Figure 1.20 LNP model with memory. The spiking of real neurons does not follow a Poisson process (due to the refractory period). Hence a post-spike memory filter is introduced. This corrects for the un-physiological spike times of a pure LNP model. Figure adapted from Pillow, 2007 and reused with permission under CC BY-SA 4.0 license

A second shortcoming of the LNP model is the explicit assumption of a linear convolution between the stimulus and the cell's input filter. Therefore, differences between the predicted spike trains of the model and recorded spike trains will be due to non-stationarity/noise in the responses and essential nonlinearities that have been overlooked. Though an LNP model alone cannot capture these nonlinear response properties, by using a combination of the LNP model, the broader GLM framework, and a suitable experimental/stimulus design, it is possible to quantify how much nonlinearity is being missed by the LNP.

Generalized Linear Models

A mathematical model maps input variables X of a given domain to the observed output Z of either the same or different domain. A GLM is a special class of models which consists of three components namely a random component, linear predictor and a link function (Dobson, 2002; Pillow, 2007).

Random Component

The random component of the model determines the distribution of the observed target/output variable Z . The stochastic distribution can be any of the distributions in the exponential family namely Poisson, Gaussian, exponential, gamma, Bernoulli and is usually determined by the application (Koopman, 1936; Pitman, 1936).

Linear Predictor

The linear predictor (Y) linearly weights the input variables X according to the formula given below.

$$Y = W_0 + \sum_{i=1}^N W_i X_i$$

Where W and $X \in Real Numbers$.

Link Function

The link function is used to connect the deterministic linear predictor WX , to the observed stochastic variable Z . The choice of the link function depends partly on the domains of X and Z , that need to be mapped.

In this thesis, the Poisson distribution is used to model the distribution of the observed spike counts Z .

Therefore

$$P(y \sim \text{spikes}) = (\Delta\lambda)^y \frac{e^{-\Delta\lambda}}{y!}$$

Where

Δ is the size of the time-bin

y is the observed spike count in a bin of size Δ

λ is the theoretical firing rate given linear predictor k and stimulus x

The results of this GLM/LNP analysis are provided in the next section.

Summary of Results

Tickling the retina: integration of subthreshold electrical pulses can activate retinal neurons.

The best-restored vision to date for a patient with RP was with a retinal prosthetic device (**Stingl et al., 2015**). However, this restored acuity is still well below the limit that is theoretically possible with a prosthetic device (**Stett et al., 2000**). One major reason for this could be the indiscriminate activation of different classes of retinal ganglion cells, which leads to a reduction in restored visual acuity. A key reason for indiscriminate activation is the use of large suprathreshold voltage/current pulses, instead of waveforms specific to cell type. Though there have been recent studies, which explore alternate waveforms for preferential activation of different RGC classes (**Twyford & Fried, 2016**), there has been to date no systematic approach to answering this question. Therefore, we decided to investigate the response properties of RGCs using a linear systems approach, based on white noise stimulation and reverse correlation (**Sekhar et al., 2016**). To this end, it was necessary to establish appropriate parameters for the Gaussian white noise stimulus distribution, such as mean voltage, standard deviation, and stimulation frequency. A combination of these parameters to reliably obtain electrical STAs was determined by performing numerous pilot experiments. Though voltage and current pulses of different lengths could have also been explored, we decided to settle on voltage pulses of 1 ms as this is the standard stimulus paradigm used by the Tuebingen retinal implant (**Zrenner et al., 2011**). We performed different experiments where we stimulated the retina with a mean voltage of -1000 mV and an S.D of 35%, at frequencies of 10, 20, 25, and 50 Hz. We were able to obtain STAs at all these frequencies except 10 Hz. As the frequency of stimulation increased, the temporal sampling of the STAs improved. However, since we were interested in network activation, the first 10 ms post stimulation is always ignored to avoid direct spikes (**Boinagrov et al., 2014; Jensen et al., 2005**). Therefore, at higher stimulation frequencies, we ignored a larger percentage of the time-bin after each stimulus pulse. At 50 Hz (the highest stimulus frequency we presented), 50% (10/20 ms) of the time-bin is ignored. Therefore, a stimulation frequency of 25 Hz was finally chosen as a suitable compromise between better sampling of the underlying temporal filter and maximal utilization of the time-bin. Our inability to recover any STAs at 10 Hz strongly implies that an inter-pulse interval of 99 ms was too large for cells to integrate across multiple voltage pulses. Next, numerous pilot experiments were performed to find a mean voltage and

standard deviation for the Gaussian white noise distribution that would offer a suitable compromise between sufficient signal strength for multi-pulse integration and an overall reduction in single-pulse activation. Multiple experiments were done with mean voltages of -700 mV, -800 mV, and -1000 mV at an SD of 35% (**Appendix 1**). While we could generate electrical STAs under all these conditions, STAs of many cells calculated at a mean of -1000mV showed significant single-pulse activation (in contrast to only integrative-based activation). An example STA showing single-pulse activation due to direct RGC activation is shown in **figure 1e** of **Sekhar et al., 2016**. A mean voltage of -800 mV was finally chosen as an ideal compromise between increasing integrative responses and lowering responses to single-pulse stimulation. Additionally, different SDs of 20%, 35% and 45% were also tested using a mean voltage of -800 mV. While we were able to generate STAs at all these SDs, many of the STAs calculated at 45% SD had significant single-pulse activation. Taking all these results into consideration, a mean voltage of -800mV, at an SD = 35%, presented at a frequency = 25Hz was chosen as the standard stimulus paradigm (**Figure 1a,b** of **Sekhar et al., 2016**). Using this stimulus paradigm, 27 cells were collected using 54 unique trials of electrical white noise of a 100 s each. Previous work has shown that direct responses of RGCs to electrical stimulation tend to be solitary spikes with very precise spike timings, while network-driven RGC responses usually occur in the form of bursts with lower spike-time precision (**Fried et al., 2005**). Therefore, the bursting response of RGCs to network stimulation could artificially increase the width of the electrical STAs of the 27 cells. To correct for this, we developed a method called 'first spike-triggered averaging'. First, bursting events were identified using inter-spike intervals (**Rodieck et al., 1962; Zeck & Masland, 2007**). Next, only the first spike of each bursting event is considered for calculating the electrical STA. The stimulus corresponding to that first spike is weighted by the number of spikes in that burst (**Figure 2a** of **Sekhar et al., 2016**). In doing so, we noticed that, while some cells showed a reduction in their STA widths, other cells showed almost no change (**Figure 2 c,e,g** of **Sekhar et al., 2016**). This suggested that there are different coding schemes employed by different cells to electrical stimulation. Finally, we show the STA of a single cell obtained under three different mean voltages (-800 mV, -1000 mV and -1200mV). Only at -1200 mV, we observed significant single-pulse activation in addition to the integrative responses for this cell (**Figure 3a** of **Sekhar et al., 2016**). The threshold of this cell was found to be -1500 mV (**Figure 3b** of **Sekhar et al., 2016**). Moreover, data included from another study showed that the population threshold

(calculated from 59 RGCs) was -1312 mV. Taken together these two results provide strong evidence that the retinal network can integrate multiple subthreshold pulses. To summarize, the manuscript “Tickling the retina: integration of subthreshold electrical pulses can activate retinal neurons.” was a methods paper that demonstrated, that white noise stimulation and reverse correlation can yield electrical STAs for network-driven RGCs indicative of subthreshold multi-pulse integration.

Correspondence between visual and electrical input filters of ON and OFF mouse retinal ganglion cells

The major motivation behind using electrical white noise stimulation was to find if different cell types (ON, OFF, ON-OFF, etc.) have distinct electrical input filters. This is an important precursor to finding electrical waveforms specific to each cell type, that can be used for preferential stimulation. The experimental design consisted of full-field flash stimulation, visual Gaussian white noise, and electrical Gaussian noise followed once again by flash and visual noise (**Figure 1 of Sekhar et al., 2017**). A cell-classification index was calculated based on the methods in **Carciari et al., 2003** (using PSTH fits to the flash responses). We classified cells with an index greater than .5 as ON cells, between -.5 and .5 as ON-OFF cells and lesser than -.5 as OFF cells. The short-latency deflections in the STAs immediately preceding spiking were called D1, while the secondary long-latency deflections (if present) were labeled D2. The timings of the peak of these deflections was called the D1 and D2 latencies. It was found that spiking responses of ON and OFF cells, during electrical stimulation, corresponded to an upward and downward D1 deflection from the baseline in the electrical STAs, respectively (**Figure 3 & 4 of Sekhar et al., 2017**). No correlation was found between electrical and visual STAs with respect to the D1 widths or D1 latencies (**Figure 6 a,c of Sekhar et al., 2017**). However, the latency and widths for the electrical STA D1 deflections of ON cells were found to be significantly shorter than their corresponding visual STA D1 deflections. While the D1 latencies of electrical STAs for OFF cells were significantly shorter than their corresponding D1 latencies in visual STAs, the D1 widths of electrical and visual STAs for OFF cells were found to be comparable (**Figure 6 b,d of Sekhar et al., 2017**). These results suggest that, while the electrical and visual STAs both originate due to activation of the network, there still might be differences in the mechanisms between the electrically- and visually-driven STAs. Next, we analyzed how strongly electrical STAs deviated from sine waves, since sinusoids had been used in previous studies for preferential stimulation of selected RGC types in the wild type retina (**Im & Fried, 2016**) without much success. For a sine wave 1) the ratio of the latency of crest to the trough is .33, 2) the ratio of the widths of the crest to trough is 1:1, and 3) ratio of amplitudes of the crest to trough is 1:1. Comparing these ratios for those cells which had both a D1 and D2 deflection in their electrical STAs, we found that, except for the D1: D2 latency ratio, both D1: D2 width and D1: D2 amplitude ratios deviated from that of a sine wave. This could potentially explain why selective stimulation with sine waves was not possible. This

result is depicted in **figure 5** of **Sekhar et al., 2017** which shows that the scatter plot of D1 vs. D2 widths for the E-STAs deviates from the unity line for the majority of the cells. Finally, in order to understand how these electrical STAs change with photoreceptor loss and retinal rewiring (**Gargini et al., 2007; Marc et al., 2003**), electrical STAs were calculated at P84 *rd10* mice. It was found that there was a statistically significant decrease in both the D1 latency and width for the *rd10* retina in comparison to the wild type retina (**Figure 7 & 8** of **Sekhar et al., 2017**). So, in summary the results of the manuscript “Correspondence between visual and electrical input filters of ON and OFF mouse retinal ganglion cells”, shows for the first time, using the technique of white noise stimulation and reverse correlation, that ON and OFF cells have very distinct electrical STAs, and that these electrical STAs deviate strongly from a classical sine wave approximation. This finding has important implications for preferential activation of different visual pathways, and therefore improving the visual acuity restored with a prosthetic device. The results of this manuscript were corroborated by a later study (**Ho et al., 2017**). In this study, a photovoltaic device, was used to subretinally stimulate the wild type and degenerate rat retina using binary white noise. In doing so, **Ho et al** reported that ON and OFF RGCs had distinct electrical STAs, whose polarities were the opposite of their corresponding visual STAs. Moreover, like us, they also found that the latencies of the electrical STAs were shorter than the visual STAs. Finally, **Ho et al** reported electrical STAs of both polarities, in very late stage degenerate RCS rats, similar to **figure 7** of **Sekhar et al., 2017**.

Characterizing retinal responses to electrical stimulation using generalized linear models

As described in the previous chapter, the spike-triggered average (STA) of a cell represents a first-order approximation of a cell's input filter. The STA assumes that the cell's filter convolves linearly with the stimulus. It is, therefore, necessary to estimate how much of the stimulus-dependent variability is not captured by the STA model, due to this assumption of linearity. To estimate this deviation from linearity, we presented the same retinal cell with multiple interleaved trials of unique (non-repeating) and frozen (repeating) white noise in a 1:1 ratio. This ratio was validated by the following procedure: We fit GLMs to RGC responses that were shown only multiple trials of unique white noise or only multiple trials of frozen white noise. We then checked how the predictive performance of the GLMs on a held-out trial, changed when reducing the number of trials that were used for training. By doing this, we validated that an appropriate number of unique and frozen trials that are required to obtain robust fits for the GLMs was 18 unique and 18 frozen or 1:1 (**Figure 1** of **Appendix 4**). **Figure 2** of **Appendix 4** shows the rasters of an example cell, to 18 trials of unique and frozen noise each, along with the recovered STA. A generalized linear model (GLM) with a log-link function, Poisson spiking distribution, and linear predictor function acting on the stimulus, is trained on all the trials of unique stimuli. Such a model is also called an LNP model (**Figure 4a** in **Appendix 4**). The LNP model's predictive performance is then measured on the frozen trials. The spiking responses not predicted by the LNP model (on the frozen trials) are due to a combination of the simplifying assumption of a linear input filter and the intrinsic stimulus-independent variability of the retinal ganglion cell (RGC) spiking. To tease apart the remaining stimulus-dependent variability not captured by the LNP model from the intrinsic stimulus-independent variability, we analyzed the variability in RGC responses to the multiple trials of frozen white noise. This is done by estimating a second GLM, fitted directly to the PSTH averaged over multiple trials of frozen stimuli (**Figure 4b** in **Appendix 4**). Since there is no assumption of a linear filter acting on the stimulus, any spiking variability not captured by the PSTH model on a held-out trial, represents the intrinsic stimulus-independent variability of the RGC. Therefore, we could estimate an upper limit of the stimulus-dependent spiking variability that can be captured by a statistical model (linear or nonlinear). Moreover, the degree to which the GLM (trained on frozen stimuli), outperforms the LNP model for a given cell, represents the extent of nonlinearity in RGC coding not captured by the simple linear filter. In doing this

analysis for our cells, we found that the LNP model of ON, OFF, and ON-OFF cells captured only a fraction of the total stimulus-dependent variability (**Figure 5 of Appendix 4**). This implies that there is a certain degree of nonlinearity in how RGCs encode for electrical stimulation, and that more sophisticated nonlinear models must be explored to capture the full extent of these responses. It should be noted, that the results of **Appendix 4** are provisional as this work is still in progress. While the finding that there are nonlinearities in RGC responses to electrical stimulation that cannot be captured by a simple LNP model, is not surprising, currently work is being carried out to record from more OFF cells in order to compare the model performances between ON and OFF cells (**Figure 6 of Appendix 4**). Additionally, other model performance measures such as signal to noise ratio and log-likelihood are also being implemented. A comparison between how ON and OFF cells encode for electrical stimulation, with respect to their variability and linearity/nonlinearity, using multiple model performance measures would be a truly novel contribution to the field of prosthetic stimulation.

Discussion

In this thesis, we studied the response properties of RGCs to electrical stimulation using white noise analysis. Even though there had been previous studies, which had attempted this, they had used very different paradigms. For example, in the work of **Freeman et al., 2010**, continuous binary noise stimulation was used to recover temporal electrical STAs in the rabbit retina. Though this was a novel finding, retinal implants use pulsatile stimuli and not continuous current or voltage stimulation, as such a paradigm could potentially damage the retina and electrodes over a period of time. Furthermore, **Lorach et al., 2015**, mapped the spatial electrical receptive fields of ON and OFF RGCs using sparse white noise stimulation. In doing so, they found the electrical receptive fields of ON and OFF cells to be comparable in the wild type rat retina. They also did not find any statistically significant correlations between the size of the visual receptive field and the electrical receptive field in the wild type rat retina. In this thesis, we tried to extend these methods to calculate the temporal receptive fields of ON and OFF RGCs in the mouse retina using voltage pulses whose amplitudes were randomly drawn from a Gaussian distribution. As mentioned earlier, establishing the parameters of the Gaussian distribution required several pilot experiments (**Sekhar et al., 2016**).

The central work of this thesis demonstrated first: the ability to generate electrical STAs across different frequencies and white noise distributions (**Sekhar et al., 2016**); second: that ON and OFF cells have characteristic electrical STAs (**Sekhar et al., 2017**); and third: that these linear filters (electrical STAs) only capture a fraction of the total stimulus-dependent spiking responses (**Appendix 4**). Based on each of these results there are many subsequent questions that can be explored.

1) Studying electrical contrast adaptation using STAs

At present, patients have to manually adjust the gain and sensitivity of their prosthesis when moving through visual scenes with different contrast and luminance conditions. These changes to the electrode gain or sensitivity are global across all electrodes (**Zrenner et al., 2011**), which is very different from how the healthy retina adapts to contrast and luminance. The retina's ability to adapt to luminance and contrast has been studied in the past using visual white noise and visual STAs (**Baccus & Meister, 2002; Chander & Chichilnisky, 2001**). Changes in contrast (SD of the visual Gaussian distribution) have been found to affect the amplitude of

the visual STAs, with higher-contrast stimuli leading to a decrease and lower-contrast stimuli leading to increases in STA amplitude, respectively (**Chander & Chichilnisky, 2001**). This effect is seen when the nonlinear spike generator function of the respective STAs (high and low contrast) are superimposed using a scaling factor. These contrast driven STA-amplitude changes are believed to reflect the adaptations in the sensitivity of the retina (**Chander & Chichilnisky, 2001**). Changes in the latencies of these STA peaks are also observed (**Baccus & Meister, 2002**). It should, therefore, be possible to use electrical STAs to study how the retina adapts to electrical stimulation at different levels of contrasts. Though retinal responses to changes in electrical contrast have been studied already, these studies used sudden changes in a stimulation pulse amplitude (driven by visual luminance) as a surrogate for contrast change (**Goetz et al., 2015**). Moreover, the effects of these contrast changes were studied based on changes in firing rates for the retinal cell responses. However, using the white noise method described in this thesis, it would be possible to understand in-depth how these contrast changes affect the gain and sensitivity of the retinal responses through changes in the amplitude of the electrical STA and spike generating nonlinear function. This study of electrical STAs could be done in both the wild type and degenerate retina in order to understand how photoreceptor loss and retinal rewiring affects the retinal circuitry's ability to adapt to different contrasts. While initial studies showed, that late-stage degenerate retina cannot respond to decreases in electrical contrast (**Goetz et al., 2015**), the use of electrical STAs will help to more deeply investigate why.

A model studying this process could in turn shed light on how to automatically adjust electrode settings locally for different contrast and luminance conditions.

2) Effect of electrical cross talk on STAs and RGC activation thresholds

The data in this thesis was collected using a single stimulating electrode with the immediate surrounding electrodes being used for recording. Our rationale for analyzing only the 7-8 neighboring electrodes is because the percentage of cells that are electrically responsive, to even large suprathreshold voltages pulses, reduces sharply when we extend our analysis beyond the nearest neighboring electrodes. This result can be seen in **figure 3** of **Jalligampala et al., 2017**. Moreover, initially we did analyze cells further away (>400 micrometers) from the stimulating electrode. However, we could not recover any electrical STAs. In addition to this, due to the subthreshold nature of our stimuli, the data yield per tissue tended to be low. While

we could have increased our yield by stimulating with multiple electrodes, such a paradigm can introduce electric cross-talk between the stimulating electrodes and induce changes in the retinal activation thresholds (**Khalili Moghadam et al., 2013; Matteucci et al., 2016**). Initially we did perform experiments, where we used multiple stimulating electrodes on the MEA (separated by a distance of at least 1mm), in order to understand if multi-electrode subthreshold stimulation had an effect on the RGC thresholds and therefore the shape of the electrical STAs. However, the results of our analysis were not conclusive. Therefore, to avoid this potential confound, we limited ourselves to a single stimulating electrode. Quantifying the effect of white noise stimulation with multiple electrodes, however, would be interesting for two reasons: First, if electric cross-talk produced by multiple electrode subthreshold stimulation alters RGC thresholds, it could shed light on how different spatial patterns of electrical stimulation affect population encoding by the retina in a prosthetic setting. This, in turn, could help to optimize the spatial electrode configuration used by present implants (**Khalili Moghadam et al., 2013; Matteucci et al., 2016**). Second, if electric cross-talk has no effect or only a weak effect on RGC activity, it would be possible to increase our data yield by the use of multiple stimulating electrodes (separated by a certain minimal distance).

3) Preferential activation of ON and OFF pathways in wild type and degenerate retina

The ability to preferentially activate different classes of RGCs electrically is a much-researched topic as it has major implications for the effectiveness of retinal prosthetics. There have already been studies, which showed that ON and OFF cells display responses distinct from each other when activated indirectly (through the network) with the same stimulus (**Im & Fried, 2015**). It was also found that strong correlations exist between electrically and visually driven responses patterns for ON cells based on parameters such as inter-spike interval, latency, peak firing rate, and spike count. These correlations though present for OFF cells were much weaker. Furthermore **Twynford & Fried, 2016** showed that ON and OFF cells in the wild type rabbit retina respond to different phases of an ongoing low-frequency sine wave (5 and 10 Hz). Though these results lend evidence to the existence of stimuli that can preferentially activate different cell types, there has been, till date, no systematic exploration of the input stimulus space for ON and OFF cells. The choice of the sine wave as a stimulus was ad hoc and not grounded in any estimate of the RGCs input filter. Such ad hoc choices can lead to sub-optimal stimuli that fail to preferentially activate the retina. Indeed when isolated sine waves

were presented, the preferential activation of different RGC classes was only weak (**Im & Fried, 2016**). When the stimulus space for ON and OFF cells was explored systematically using white noise, we showed that electrical STAs are not always well approximated by sine waves (**Sekhar et al., 2017**). It would be therefore interesting to see, if preferential activation can be achieved using modified sine waves, which have asymmetries in their D1 and D2 amplitudes and widths.

Moreover, it is important to remember that the results mentioned above were in the wild type retina. It is, therefore, not guaranteed that these findings will be preserved in the degenerate retina, the end target of a prosthetic device. In the past, it has been shown that physiological findings in the wild type retina do not necessarily translate to the late-stage degenerate retina, due to the photoreceptor loss and retinal rewiring (**Gargini et al., 2007; Marc et al., 2003**). For example, **Twyford & Fried, 2016**, showed that ON and OFF cells in the wild type rabbit retina respond to different phases of an ongoing sine wave. However, these differential responses disappear with the addition of synaptic blockers suggesting that such phase-specific retinal responses are photoreceptor mediated. Therefore, experiments in search of electrical STAs in the late-stage degenerate retina which are specific to cell type is crucial.

We could show that electrical STAs for p84 *rd10* retina are significantly shorter in their latencies and widths in comparison to the electrical STAs of the wild type retina (**Sekhar et al., 2017**). Therefore, a higher stimulation frequency would be required to better sample *rd10* STAs. This would need further optimization of the stimulation parameters that are currently being used for the wild type retina. Once the stimulation parameters for the *rd10* E-STAs have been optimized, it is necessary to correlate them with their cell type. However, due to the photoreceptor loss, traditional visual stimuli based classification schemes are no longer viable. Therefore, cell-type classification in the degenerate retina would require exploration of techniques such as immunohistochemistry, cellular morphology, intra- and extra-cellular physiology, etc. Though challenging, such experiments are essential in order to find waveforms in the degenerate retina which are specific to cell type, thereby leading to better retinal prosthesis.

4) Differences between visually and electrically driven STAs

The absence of any correlations between the widths and latencies of electrical and visual STAs is interesting as it suggests that the network activation mechanisms of electrical and visual stimulation, though similar are not identical. Using more invasive techniques, such as synaptic blockers or patch clamping, it would be interesting to study the origin of these network mediated differences.

5) Statistical modeling of the wild type retina and degenerate retina

In the third and final paper, we found that there are nonlinearities in how ON, OFF and ON-OFF cells encode for electrical stimulation that cannot be captured by a simple LNP model. Therefore, future work in this direction should try and use more sophisticated nonlinear models to capture the spiking dynamics of RGCs. Being able to predict spike times to novel electrical stimuli with greater accuracy will in turn help find waveforms for preferential stimulation. However, a major difficulty in implementing the models for the third paper was the high stimulus-independent spiking variability in the recorded RGC responses. One reason for this could be due to adaptation/desensitization of RGC responses to prolonged electrical stimulation. This adaptation over recording time will lead to increase in the variability of RGC responses to repeated blocks of electrical stimuli. Another reason for the high variability could be our site of stimulation. In our experiments, the retina was stimulated and recorded from the RGC side. However, since we are targeting the retinal network (bipolar cells and photoreceptors), stimulating from the RGC side increases activation thresholds due to the greater distance between the electrodes and the intended target of stimulation. This increase in threshold could, in turn, decrease our signal strength. Therefore, developing an experimental setup that would allow electrical stimulation from the photoreceptor side and recording from the RGC side would help to decrease the distance between electrodes and the retinal network, thereby reducing activation thresholds, reducing the variability and ultimately making the modeling much easier. Furthermore, exploring alternate stimulus distributions should be considered. In designing our stimuli, we focused on minimizing single-pulse activation. However, this came at the cost of low signal strength, and therefore, higher variability in stimulus-driven responses. Hence, exploring stimulus distributions with higher means, in order to reduce stimulus-driven variability while still maintaining low single-pulse activation, should be undertaken. This would require several new pilot experiments. Finally,

once the models for the wild type retina have been fully developed it would be necessary to see how these models change for the late stage degenerate retina. By comparing the models of wild type RGC responses to *rd10* RGC responses it should be possible to characterize more formally the effects of photoreceptor loss and subsequent rewiring. Such a mathematical formalization is crucial to understanding how the neural code is altered in the degenerate retina (in comparison to the wild type retina). This understanding could, in turn, help develop better visual processing algorithms for retinal implants, to compensate for the altered neural code.

References

- Acland, G. M., Aguirre, G. D., Ray, J., Zhang, Q., Aleman, T. S., Cideciyan, A. V, Pearce-Kelling, S. E., Anand, V., Zeng, Y., Maguire, A. M., Jacobson, S. G., Hauswirth, W. W., Bennett, J. (2001). Gene therapy restores vision in a canine model of childhood blindness. *Nature Genetics*, 28(1), 92–95.
- Alexander, P., Thomson, H. A. J., Luff, A. J., & Lotery, A. J. (2015). Retinal pigment epithelium transplantation: concepts, challenges, and future prospects. *Eye*, 29(8), 992–1002.
- Ayton, L. N., Blamey, P. J., Guymer, R. H., Luu, C. D., Nayagam, D. A., Sinclair, N. C., Shivdasani, M. N., Yeoh, J., McCombe, M. F., Briggs, R. J., Opie, N. L., Villalobos, J., Dimitrov, P. N., Varsamidis, M., Petoe, M. A., McCarthy, C. D., Walker, J. G., Barnes, N., Burkitt, A. N., Williams, C. E., Shepherd, R. K., Allen, P. J.; Bionic Vision Australia Research Consortium. (2014). First-in-Human Trial of a Novel Suprachoroidal Retinal Prosthesis. *PLoS ONE*, 9(12), e115239.
- Baccus, S. A., & Meister, M. (2002). Fast and Slow Contrast Adaptation in Retinal Circuitry. *Neuron*, 36(5), 909–919.
- Baden, T., Berens, P., Franke, K., Román Rosón, M., Bethge, M., & Euler, T. (2016). The functional diversity of retinal ganglion cells in the mouse. *Nature*, 529(7586), 345–350.
- Baker, S. A., & Kerov, V. (2013). Photoreceptor Inner and Outer Segments. *Functional Organization of Vertebrate Plasma Membrane . Current Topics in Membranes*. 72, 231–265.
- Baylor, D. A., Lamb, T. D., & Yau, K. W. (1979). Responses of retinal rods to single photons. *The Journal of Physiology*. 288(1), 613–34.
- Binder, S. (2011). Scaffolds for retinal pigment epithelium (RPE) replacement therapy. *British Journal of Ophthalmology*, 95(4), 441–442.
- Boinagrov, D., Pangratz-Fuehrer, S., Goetz, G., & Palanker, D. (2014). Selectivity of direct and network-mediated stimulation of the retinal ganglion cells with epi-, sub- and intraretinal electrodes. *Journal of Neural Engineering*, 11(2), 26008.

- Boyden, E. S., Zhang, F., Bamberg, E., Nagel, G., & Deisseroth, K. (2005). Millisecond-timescale, genetically targeted optical control of neural activity. *Nature Neuroscience*, *8*(9), 1263–1268.
- Buskamp, V., Duebel, J., Balya, D., Fradot, M., Viney, T. J., Siegert, S., Groner, A.C, Cabuy, E., Forster, V., Seeliger, M., Biel, M., Humphries, P., Paques, M., Mohand-Said, S., Trono, D., Deisseroth, K., Sahel, J.A., Picaud, S., Roska, B. (2010). Genetic Reactivation of Cone Photoreceptors Restores Visual Responses in Retinitis Pigmentosa. *Science*, *329*(5990), 413–417.
- Caprioli, J., & Coleman, A. L. (2010). Blood Pressure, Perfusion Pressure, and Glaucoma. *American Journal of Ophthalmology*, *149*(5), 704–712.
- Carcieri, S.M., Jacobs, A.L., Nirenberg, S. (2003). Classification of Retinal Ganglion Cells: A Statistical Approach. *Journal of Neurophysiology*, *90*(3), 1704–1713.
- Casten, R., & Rovner, B. (2008). Depression in Age-Related Macular Degeneration. *Journal of Visual Impairment & Blindness*, *102*(10), 591–599.
- Chander, D., & Chichilnisky, E. J. (2001). Adaptation to temporal contrast in primate and salamander retina. *The Journal of Neuroscience*, *21*(24), 9904–16.
- Chichilnisky, E. J. (2001). A simple white noise analysis of neuronal light responses. *Network: Computation in Neural Systems*, *12*(2), 199–213.
- da Cruz, L., Dorn, J.D., Humayun, M.S., Dagnelie, G., Handa, J., Barale, P.O., Sahel, J.A., Stanga, P.E., Hafezi, F., Safran, A.B.,, Salzmann, J., Santos, A., Birch, D., Spencer, R., Cideciyan, A.V., de Juan, E., Duncan, J.L., Elliott, D., Fawzi, A., Olmos de Koo, L.C., Ho, A.C., Brown, G., Haller, J., Regillo, C., Del Priore, L.V., Arditi, A., Greenberg, R.J.; Argus II Study Group. (2016). Five-Year Safety and Performance Results from the Argus II Retinal Prosthesis System Clinical Trial. *Ophthalmology*, *123*(10), 2248–2254.
- Daiger, S.P., Bowne, S.J., Sullivan, L.S. (2007). Perspective on Genes and Mutations Causing Retinitis Pigmentosa. *Archives of Ophthalmology*, *125*(2), 151–158.
- Dalkara, D., Kolstad, K. D., Caporale, N., Visel, M., Klimczak, R. R., Schaffer, D. V, & Flannery, J. G. (2009). Inner Limiting Membrane Barriers to AAV-mediated Retinal Transduction From the Vitreous. *Molecular Therapy*, *17*(12), 2096–2102.

- Demb, J. B., & Singer, J. H. (2015). Functional Circuitry of the Retina. *Annual Review of Vision Science*, 1(1), 263–289.
- Dobson, A. J. (2002). *An introduction to generalized linear models*. New York, NY: Chapman & Hall/CRC
- Doroudchi, M. M., Greenberg, K. P., Liu, J., Silka, K. A., Boyden, E. S., Lockridge, J. A., Arman A.C., Janani, R., Boye, S.E., Boye, S.L., Gordon, G.M., Matteo, B.C., Sampath, A.P., Hauswirth, W.W., Horsager, A. (2011). Virally delivered Channelrhodopsin-2 Safely and Effectively Restores Visual Function in Multiple Mouse Models of Blindness. *Molecular Therapy*, 19(7), 1220–1229.
- Eberle, D., Kurth, T., Santos-Ferreira, T., Wilson, J., Corbeil, D., & Ader, M. (2012). Outer Segment Formation of Transplanted Photoreceptor Precursor Cells. *PLoS ONE*, 7(9), e46305.
- European Medicines Agency. (2014). *Annual Report 2014*. Retrieved from http://www.ema.europa.eu/docs/en_GB/document_library/Annual_report/2015/04/WC500186306.pdf
- Enroth-Cugell, C., & Pinto, L. H. (1972). Properties of the surround response mechanism of cat retinal ganglion cells and centre-surround interaction. *The Journal of Physiology*, 220(2), 403–39.
- Estrada-Flores, S., Merts, I., De Ketelaere, B., & Lammertyn, J. (2006). Development and validation of “grey-box” models for refrigeration applications: A review of key concepts. *International Journal of Refrigeration*, 29(6), 931–946.
- Euler, T., Haverkamp, S., Schubert, T., & Baden, T. (2014). Retinal bipolar cells: elementary building blocks of vision. *Nature Reviews Neuroscience*, 15(8), 507–519.
- Fairhall, A. L., Burlingame, C. A., Narasimhan, R., Harris, R. A., Puchalla, J. L., & Berry, M. J. (2006). Selectivity for Multiple Stimulus Features in Retinal Ganglion Cells. *Journal of Neurophysiology*, 96(5), 2724–2738.
- Famiglietti, E. V. (1987). Starburst amacrine cells in cat retina are associated with bistratified, presumed directionally selective, ganglion cells. *Brain Research*, 413(2), 404–408.

- Flammer, J., & Orgül, S. (1998). Optic nerve blood-flow abnormalities in glaucoma. *Progress in Retinal and Eye Research*, 17(2), 267–89.
- Freeman, D.K., Rizzo, J.F. III, & Fried, S.I. (2010) Electric stimulation with sinusoids and white noise for neural prostheses. *Frontiers in Neuroscience*. 4(28).
- Frick, K. D., Gower, E. W., Kempen, J. H., & Wolff, J. L. (2007). Economic impact of visual impairment and blindness in the United States. *Archives of Ophthalmology*, 125(4), 544–50.
- Fried, S.I., Hsueh, H.A., Werblin, F.S. (2005). A Method for Generating Precise Temporal Patterns of Retinal Spiking Using Prosthetic Stimulation. *Journal of Neurophysiology*, 95(2), 970–978.
- Fujikado, T., Kamei, M., Sakaguchi, H., Kanda, H., Morimoto, T., Ikuno, Y., Nishida, K., Kishima, H., Maruo, T., Konoma, K., Ozawa, M., Nishida, K. (2011). Testing of Semichronically Implanted Retinal Prosthesis by Suprachoroidal-Transretinal Stimulation in Patients with Retinitis Pigmentosa. *Investigative Ophthalmology & Visual Science*, 52(7), 4726-33.
- Gargini, C., Terzibasi, E., Mazzoni, F., & Strettoi, E. (2007). Retinal organization in the retinal degeneration 10 (rd10) mutant mouse: A morphological and ERG study. *The Journal of Comparative Neurology*, 500(2), 222–238.
- Ghosh, F., Juliusson, B., Arner, K., & Ehinger, B. (1999). Partial and Full-Thickness Neuroretinal Transplants. *Experimental Eye Research*, 68(1), 67–74.
- Ghosh, F., Wong, F., Johansson, K., Bruun, A., & Petters, R. M. (2004). Transplantation of full-thickness retina in the rhodopsin transgenic pig. *Retina*, 24(1), 98–109.
- Goetz, G., Smith, R., Lei, X., Galambos, L., Kamins, T., Mathieson, K., Sher, A., Palanker, D. (2015). Contrast sensitivity with a subretinal prosthesis and implications for efficient delivery of visual information. *Investigative Ophthalmology and Visual Science*, 56(12), 7186–7194.

- Guo, T., Lovell, N. H., Tsai, D., Twyford, P., Fried, S., Morley, J. W., Suaning, G.J., Dokos, S. (2014). Selective activation of ON and OFF retinal ganglion cells to high-frequency electrical stimulation: A computational modeling study. *36th Annual International Conference of the IEEE Engineering in Medicine and Biology Society*, Milan, Italy (pp. 6108–6111). IEEE. doi: 10.1109/EMBC.2014.6945023
- Hahm, B.J., Shin, Y.W., Shim, E.J., Jeon, H. J., Seo, J.M., Chung, H., & Yu, H. G. (2008). Depression and the vision-related quality of life in patients with retinitis pigmentosa. *British Journal of Ophthalmology*, 92(5), 650–654.
- Hamel, C. (2006). Retinitis pigmentosa. *Orphanet Journal of Rare Diseases*, 1(1), 40.
- Han, X., & Boyden, E. S. (2007). Multiple-Color Optical Activation, Silencing, and Desynchronization of Neural Activity, with Single-Spike Temporal Resolution. *PLoS ONE*, 2(3), e299.
- Hartong, D. T., Berson, E. L., & Dryja, T. P. (2006). Retinitis pigmentosa. *The Lancet*, 368(9549), 1795–1809.
- Hecht, S. Schlaer, S. Pirenne, M.H. (1942). ENERGY, QUANTA, AND VISION. *The Journal of General Physiology*, 25(6), 819–840.
- Hodgkin, A. L., & Huxley, A. F. (1952). A quantitative description of membrane current and its application to conduction and excitation in nerve. *The Journal of Physiology*, 117(4), 500–544.
- Ho, E., Smith, R., Goetz, G.A., Lei, X., Galambos, L., Kamins, T.I., Harris, J., Mathieson, K., Palanker, D., Sher, A. (2017). Spatio-temporal characteristics of retinal response to network-mediated photovoltaic stimulation. *Journal of Neurophysiology*. [Epub ahead of print]
- Hubel, D. H., & Wiesel, T. N. (1968). Receptive fields and functional architecture of monkey striate cortex. *The Journal of Physiology*, 195(1), 215–43.
- Humayun, M. S., Dorn, J. D., da Cruz, L., Dagnelie, G., Sahel, J.A., Stanga, P. E., Cideciyan, A.V., Duncan, J.L., Elliott, D., Filley, E., Ho, A.C., Santos, A., Safran, A.B., Arditi, A., Del Priore, L.V., Greenberg, R. J. Argus II Study Group. (2012). Interim Results from the International Trial of Second Sight’s Visual Prosthesis. *Ophthalmology*, 119(4), 779–788.

- Im, M., & Fried, S. I. (2015). Indirect activation elicits strong correlations between light and electrical responses in ON but not OFF retinal ganglion cells. *The Journal of Physiology*, *593*(16), 3577–3596.
- Im, M., & Fried, S. I. (2016). Temporal properties of network-mediated responses to repetitive stimuli are dependent upon retinal ganglion cell type. *Journal of Neural Engineering*, *13*(2), 25002.
- Jalligampala, A., Sekhar, S., Zrenner, E., & Rathbun, D. L. (2017). Optimal voltage stimulation parameters for network-mediated responses in wild type and rd10 mouse retinal ganglion cells. *Journal of Neural Engineering*, *14*(2), 26004.
- Jensen, R. J., & Rizzo, J. F. III (2007). Responses of ganglion cells to repetitive electrical stimulation of the retina. *Journal of Neural Engineering*, *4*(1), S1–S6.
- Jensen, R. J., Ziv, O. R., & Rizzo, J. F. (2005). Thresholds for Activation of Rabbit Retinal Ganglion Cells with Relatively Large, Extracellular Microelectrodes. *Investigative Ophthalmology & Visual Science*, *46*(4), 1486–96.
- Jones, B. W., Pfeiffer, R. L., Ferrell, W. D., Watt, C. B., Marmor, M., & Marc, R. E. (2016). Retinal remodeling in human retinitis pigmentosa. *Experimental Eye Research*, *150*, 149–165.
- Kamao, H., Mandai, M., Okamoto, S., Sakai, N., Suga, A., Sugita, S., , Kiryu, J., Takahashi, M. (2014). Characterization of Human Induced Pluripotent Stem Cell-Derived Retinal Pigment Epithelium Cell Sheets Aiming for Clinical Application. *Stem Cell Reports*, *2*(2), 205–218.
- Khalili Moghadam, G., Wilke, R., Suaning, G. J., Lovell, N. H., & Dokos, S. (2013). Quasi-Monopolar Stimulation: A Novel Electrode Design Configuration for Performance Optimization of a Retinal Neuroprosthesis. *PLoS ONE*, *8*(8), e73130.
- Kolb, H., & Famiglietti, E. V. (1974). Rod and Cone Pathways in the Inner Plexiform Layer of Cat Retina. *Science*, *186*(4158), 47–49.
- Koopman, B. O. (1936). On Distributions Admitting a Sufficient Statistic. *Transactions of the American Mathematical Society*, *39*, 399–409.

- Lagali, P. S., Balya, D., Awatramani, G. B., Münch, T. A., Kim, D. S., Buskamp, V., Cepko C.L., Roska, B. (2008). Light-activated channels targeted to ON bipolar cells restore visual function in retinal degeneration. *Nature Neuroscience*, *11*(6), 667–675.
- Lakowski, J., Baron, M., Bainbridge, J., Barber, A. C., Pearson, R. A., Ali, R. R., & Sowden, J. C. (2010). Cone and rod photoreceptor transplantation in models of the childhood retinopathy Leber congenital amaurosis using flow-sorted Crx-positive donor cells. *Human Molecular Genetics*, *19*(23), 4545–4559.
- Lamb, T. D. (2016). Why rods and cones? *Eye*, *30*, 179–185.
- Lasker/IRRF Initiative for Innovation in Vision Science (2014). *Restoring Vision to the Blind*. Retrieved from http://www.laskerfoundation.org/media/filer_public/f0/10/f010f4b7-ff5e-492d-ba6c-ced1734cf107/irrf_15.pdf
- Levick, W. R., & Zacks, J. L. (1970). Responses of cat retinal ganglion cells to brief flashes of light. *The Journal of Physiology*, *206*(3), 677–700.
- Litzinger, T. C., & Rio-Tsonis, K. D. (2002). Eye Anatomy. *eLS*.
- Livingston, P. M., Carson, C. A., & Taylor, H. R. (1995). The epidemiology of cataract: a review of the literature. *Ophthalmic Epidemiology*, *2*(3), 151–64.
- Lorach, H., Goetz, G., Smith, R., Lei, X., Mandel, Y., Kamins, T., Mathieson, K., Huie, P., Harris, J., Sher, A., Palanker, D. (2015). Photovoltaic restoration of sight with high visual acuity. *Nature Medicine*, *21*(5), 476–482.
- Lorach, H., Marre, O., Sahel, J. A., Benosman, R., & Picaud, S. (2013). Neural stimulation for visual rehabilitation: Advances and challenges. *Journal of Physiology Paris*, *107*(5), 421–431.
- Lu, B., Zhu, D., Hinton, D., Humayun, M. S., & Tai, Y.C. (2012). Mesh-supported submicron parylene-C membranes for culturing retinal pigment epithelial cells. *Biomedical Microdevices*, *14*(4), 659–667.

- MacLaren, R. E., Groppe, M., Barnard, A. R., Cottrill, C. L., Tolmachova, T., Seymour, L., Clark K.R., During, M.J., Cremers, F.P., Black, G.C., Lotery, A.J., Downes, S.M., Webster, A.R., Seabra, M. C. (2014). Retinal gene therapy in patients with choroideremia: initial findings from a phase 1/2 clinical trial. *The Lancet*, 383(9923), 1129–1137.
- MacLaren, R.E., Pearson, R.A., MacNeil, A., Douglas, R.H., Salt, T.E., Akimoto, M., Swaroop, A., Sowden, J.C., Ali, R.R. (2006). Retinal repair by transplantation of photoreceptor precursors. *Nature*, 444(7116), 203–207.
- MacNeil, M. A., & Masland, R. H. (1998). Extreme diversity among amacrine cells: implications for function. *Neuron*, 20(5), 971–82.
- Mantravadi, A. V., & Vadhar, N. (2015). Glaucoma. *Primary Care: Clinics in Office Practice*, 42(3), 437–449.
- Marc, R. E., Jones, B. W., Watt, C. B., & Strettoi, E. (2003). Neural remodeling in retinal degeneration. *Progress in Retinal and Eye Research*, 22(5), 607–655.
- Marmarelis, P. Z., Naka, K. I. (1973a). Nonlinear analysis and synthesis of receptive-field responses in the catfish retina: I. Horizontal cell ganglion cell chain *Journal of Neurophysiology*. 36, 605–18
- Marmarelis, P. Z., Naka, K. I. (1973b). Nonlinear analysis and synthesis of receptive-field responses in the catfish retina: II. One-input white-noise analysis. *Journal of Neurophysiology*. 36, 619–33
- Marmarelis, P. Z., Naka, K. I. (1973c). Nonlinear analysis and synthesis of receptive-field responses in the catfish retina: III. Two-input white-noise analysis. *Journal of Neurophysiology*. 36, 634–48
- Martin, K. R., Klein, R. L., & Quigley, H. A. (2002). Gene delivery to the eye using adeno-associated viral vectors. *Methods*, 28(2), 267–275.
- Masland, R. H. (2012). The Neuronal Organization of the Retina. *Neuron*, 76(2), 266–280.
- Matteucci, P. B., Barriga-Rivera, A., Eiber, C. D., Lovell, N. H., Morley, J. W., & Suaning, G. J. (2016). The Effect of Electric Cross-Talk in Retinal Neurostimulation. *Investigative Ophthalmology & Visual Science*, 57(3), 1031.

- Meister, M., Pine, J., & Baylor, D. A. (1994). Multi-neuronal signals from the retina: acquisition and analysis. *Journal of Neuroscience Methods*, 51(1), 95–106.
- Menger, N., & Wässle, H. (2000). Morphological and physiological properties of the A17 amacrine cell of the rat retina. *Visual Neuroscience*, 17(5), 769–80.
- Moschos, M., Chatzirallis, A., & Chatziralli, I. (2015). Psychological aspects and depression in patients with retinitis pigmentosa. *European Journal of Ophthalmology*, 25(5), 459–462.
- Nagel, G., Szellas, T., Huhn, W., Kateriya, S., Adeishvili, N., Berthold, P., Ollig, D., Hegemann, P., Bamberg, E. (2003). Channelrhodopsin-2, a directly light-gated cation-selective membrane channel. *Proceedings of the National Academy of Sciences*, 100(24), 13940–13945.
- Nakazawa, T. (2016). Ocular Blood Flow and Influencing Factors for Glaucoma. *Asia-Pacific Journal of Ophthalmology*, 5(1), 38–44.
- Nirenberg, S., & Pandarinath, C. (2012). Retinal prosthetic strategy with the capacity to restore normal vision. *Proceedings of the National Academy of Sciences*, 109(37), 15012–15017.
- Olsen, T. (1986). On the calculation of power from curvature of the cornea. *British Journal of Ophthalmology*, 70(2), 152–154.
- Owen, C. G., Jarrar, Z., Wormald, R., Cook, D. G., Fletcher, A. E., & Rudnicka, A. R. (2012). The estimated prevalence and incidence of late stage age related macular degeneration in the UK. *British Journal of Ophthalmology*, 96(5), 752–756.
- Owsley, C., McGwin, G., Scilley, K., Meek, G. C., Seker, D., & Dyer, A. (2007). Impact of cataract surgery on health-related quality of life in nursing home residents. *British Journal of Ophthalmology*, 91(10), 1359–1363.
- Pascolini, D., & Mariotti, S. P. (2012). Global estimates of visual impairment: 2010. *British Journal of Ophthalmology*, 96(5), 614–618.
- Pearson, R.A., Barber, A.C., Rizzi, M., Hippert, C., Xue, T., West, E.L., Duran, Y., Smith, A.J., Chuang, J.Z., Azam, S.A., Luhmann, U.F., Benucci, A., Sung, C.H., Bainbridge, J.W., Carandini, M., Yau, K.W., Sowden, J.C., Ali, R.R. (2012). Restoration of vision after transplantation of photoreceptors. *Nature*, 485(7396), 99–103.

- Pérez Fornos, A., Sommerhalder, J., da Cruz, L., Sahel, J. A., Mohand-Said, S., Hafezi, F., & Pelizzone, M. (2012). Temporal Properties of Visual Perception on Electrical Stimulation of the Retina. *Investigative Ophthalmology & Visual Science*, 53(6), 2720-31.
- Pillow, J; (2007) Likelihood-based approaches to modeling the neural code. In: Doya, K and Ishii, S and Pouget, A and Rao, RP, (eds.) Bayesian Brain: Probabilistic Approaches to Neural Coding. (pp. 53-70). MIT Press: Cambridge.
- Pillow, J., & Simoncelli, E. P. (2003). Biases in white noise analysis due to non-Poisson spike generation. *Neurocomputing*, 52–54, 109–115.
- Pitman, E. J. G. (1936). Sufficient statistics and intrinsic accuracy. *Mathematical Proceedings of the Cambridge Philosophical Society*, 32(4), 567–579.
- Polosukhina, A., Litt, J., Tochitsky, I., Nemargut, J., Sychev, Y., De Kouchkovsky, I., Huang, T., Borges, K., Trauner, D., Van Gelder, R.N., Kramer, R. H. (2012). Photochemical Restoration of Visual Responses in Blind Mice. *Neuron*, 75(2), 271–282.
- Reichenbach, A., & Bringmann, A. (2013). New functions of Müller cells. *Glia*, 61(5), 651–678.
- Resnikoff, S., Pascolini, D., Etya'ale, D., Kocur, I., Pararajasegaram, R., Pokharel, G. P., & Mariotti, S. P. (2004). Global data on visual impairment in the year 2002. *Bulletin of the World Health Organization*, 82(11), 844–51.
- Rodieck, R. W. (1965). Quantitative analysis of cat retinal ganglion cell response to visual stimuli. *Vision Research*, 5(12), 583–601.
- Rodieck, R. W., Kiang, N. Y.-S., & Gerstein, G. L. (1962). Some Quantitative Methods for the Study of Spontaneous Activity of Single Neurons. *Biophysical Journal*, 2(4), 351–368.
- Rovner, B. W., & Casten, R. J. (2001). Neuroticism Predicts Depression and Disability in Age-Related Macular Degeneration. *Journal of the American Geriatrics Society*, 49(8), 1097–1100.
- Rudnicka, A. R., Kapetanakis, V. V., Jarrar, Z., Wathern, A. K., Wormald, R., Fletcher, A. E., Cook, D.G., Owen, C. G. (2015). Incidence of Late-Stage Age-Related Macular Degeneration in American Whites: Systematic Review and Meta-analysis. *American Journal of Ophthalmology*, 160(1), 85–93.e3.

- Schwartz, O., Pillow, J. W., Rust, N. C., & Simoncelli, E. P. (2006). Spike-triggered neural characterization. *Journal of Vision*, *6*(4), 484–507.
- Schwartz, S. D., Hubschman, J.P., Heilwell, G., Franco-Cardenas, V., Pan, C. K., Ostrick, R. M., Mickunas, E., Gay, R., Klimanskaya, I., Lanza, R. (2012). Embryonic stem cell trials for macular degeneration: a preliminary report. *The Lancet*, *379*(9817), 713–720.
- Sekhar, S., Jalligampala, A., Zrenner, E., & Rathbun, D. L. (2016). Tickling the retina: integration of subthreshold electrical pulses can activate retinal neurons. *Journal of Neural Engineering*, *13*(4), 46004.
- Sekhar, S., Jalligampala, A., Zrenner, E., & Rathbun, D. L. (2017). Correspondence between visual and electrical input filters of ON and OFF mouse retinal ganglion cells. *Journal of Neural Engineering*, *14*(4), 46017.
- Shepherd, R. K., Shivdasani, M. N., Nayagam, D. A. X., Williams, C. E., & Blamey, P. J. (2013). Visual prostheses for the blind. *Trends in Biotechnology*, *31*(10), 562–571.
- Shivdasani, M. N., Sinclair, N. C., Dimitrov, P. N., Varsamidis, M., Ayton, L. N., Luu, C. D., Perera, T., McDermott, H.J., Blamey, P. J. Bionic Vision Australia Consortium. (2014). Factors Affecting Perceptual Thresholds in a Suprachoroidal Retinal Prosthesis. *Investigative Ophthalmology & Visual Science*, *55*(10), 6467-6481.
- Skalicky, S., & Goldberg, I. (2008). Depression and Quality of Life in Patients With Glaucoma: A Cross-sectional Analysis Using the Geriatric Depression Scale-15, Assessment of Function Related to Vision, and the Glaucoma Quality of Life-15. *Journal of Glaucoma*, *17*(7), 546–551.
- Stanzel, B. V., Liu, Z., Somboonthanakij, S., Wongsawad, W., Brinken, R., Eter, N., Corneo, B., Holz, F.G., Temple, S., Stern, J.H., Blenkinsop, T. A. (2014). Human RPE Stem Cells Grown into Polarized RPE Monolayers on a Polyester Matrix Are Maintained after Grafting into Rabbit Subretinal Space. *Stem Cell Reports*, *2*(1), 64–77.
- Stett, A., Barth, W., Weiss, S., Haemmerle, H., & Zrenner, E. (2000). Electrical multisite stimulation of the isolated chicken retina. *Vision Research*, *40*(13), 1785–1795.

- Stingl, K., Bartz-Schmidt, K. U., Besch, D., Chee, C. K., Cottrill, C. L., Gekeler, F., Groppe, M., Jackson, T.L., MacLaren, R.E., Koitschev, A., Kusnyerik, A., Neffendorf, J., Nemeth, J., Naeem, M.A., Peters, T., Ramsden, J.D., Sachs, H., Simpson, A., Singh, M.S., Wilhelm, B., Wong, D., Zrenner, E. (2015). Subretinal Visual Implant Alpha IMS – Clinical trial interim report. *Vision Research*, *111*, 149–160.
- Strauss, O. (2005). The Retinal Pigment Epithelium in Visual Function. *Physiological Reviews*, *85*(3), 845–881.
- Sunness, J. S. (1999). The natural history of geographic atrophy, the advanced atrophic form of age-related macular degeneration. *Molecular Vision*, *5*, 25.
- Szikra, T., & Križaj, D. (2006). The dynamic range and domain-specific signals of intracellular calcium in photoreceptors. *Neuroscience*, *141*(1), 143–155.
- Söderström, T., & Stoica, P. (1989). *System Identification*. Hemel Hempstead, UK, Prentice Hall International
- Twyford, P., & Fried, S. (2016). The Retinal Response to Sinusoidal Electrical Stimulation. *IEEE Transactions on Neural Systems and Rehabilitation Engineering*, *24*(4), 413–423.
- Vaney, D.I (1986). Morphological identification of serotonin-accumulating neurons in the living retina. *Science*, *233*(4762), 444–446.
- Vaney D.I., He S., Taylor W.R., Levick W.R. (2001) Direction-Selective Ganglion Cells in the Retina. In: Zanker J.M., Zeil J. (eds) Motion Vision. Springer, Berlin, Heidelberg
- Vinores, S. A., Küchle, M., Derevjanič, N. L., Henderer, J. D., Mahlow, J., Green, W. R., & Campochiaro, P. A. (1995). Blood-retinal barrier breakdown in retinitis pigmentosa: light and electron microscopic immunolocalization. *Histology and Histopathology*, *10*(4), 913–23.
- Warre-Cornish, K., Barber, A. C., Sowden, J. C., Ali, R. R., & Pearson, R. A. (2014). Migration, Integration and Maturation of Photoreceptor Precursors Following Transplantation in the Mouse Retina. *Stem Cells and Development*, *23*(9), 941–954.
- Weiland, J. D., & Humayun, M. S. (2014). Retinal Prosthesis. *IEEE Transactions on Biomedical Engineering*, *61*(5), 1412–1424.

- Williamson, R. S., Sahani, M., & Pillow, J. W. (2015). The Equivalence of Information-Theoretic and Likelihood-Based Methods for Neural Dimensionality Reduction. *PLOS Computational Biology*, *11*(4), e1004141.
- Wilson M.R., Gallardo M. (2010) Glaucoma Risk Factors: Ethnicity and Glaucoma. In: Schacknow P., Samples J. (eds) *The Glaucoma Book*. Springer, New York, NY
- World Health Organization. (2010). Global Data on Visual Impairments 2010. Retrieved from <http://www.who.int/blindness/GLOBALDATAFINALforweb.pdf?ua=1>
- Yin, L., Greenberg, K., Hunter, J. J., Dalkara, D., Kolstad, K. D., Masella, B. D., Wolfe, R., Visel, M., Stone, D., Libby, R.T., Diloreto, D Jr., Schaffer, D., Flannery, J., Williams, D.R., Merigan, W. H. (2011). Intravitreal Injection of AAV2 Transduces Macaque Inner Retina. *Investigative Ophthalmology & Visual Science*, *52*(5), 2775–2783.
- Young, R. W. (1987). Pathophysiology of age-related macular degeneration. *Survey of Ophthalmology*, *31*(5), 291–306.
- Zeck, G. M., & Masland, R. H. (2007). Spike train signatures of retinal ganglion cell types. *European Journal of Neuroscience*, *26*(2), 367–380.
- Zrenner, E. (2002). Will Retinal Implants Restore Vision? *Science*, *295*(5557), 1022–1025.
- Zrenner, E. (2013). Fighting Blindness with Microelectronics. *Science Translational Medicine*, *5*(210), 210ps16.
- Zrenner, E., Bartz-Schmidt, K. U., Benav, H., Besch, D., Bruckmann, A., Gabel, V.P., Gekeler, F., Greppmaier, U., Harscher, A., Kibbel, S., Koch, J., Kusnyerik, A., Peters, T., Stingl, K., Sachs, H., Stett, A., Szurman, P., Wilhelm, B., Wilke, R. (2011). Subretinal electronic chips allow blind patients to read letters and combine them to words. *Proceedings of the Royal Society B: Biological Sciences*, *278*(1711), 1489–1497.

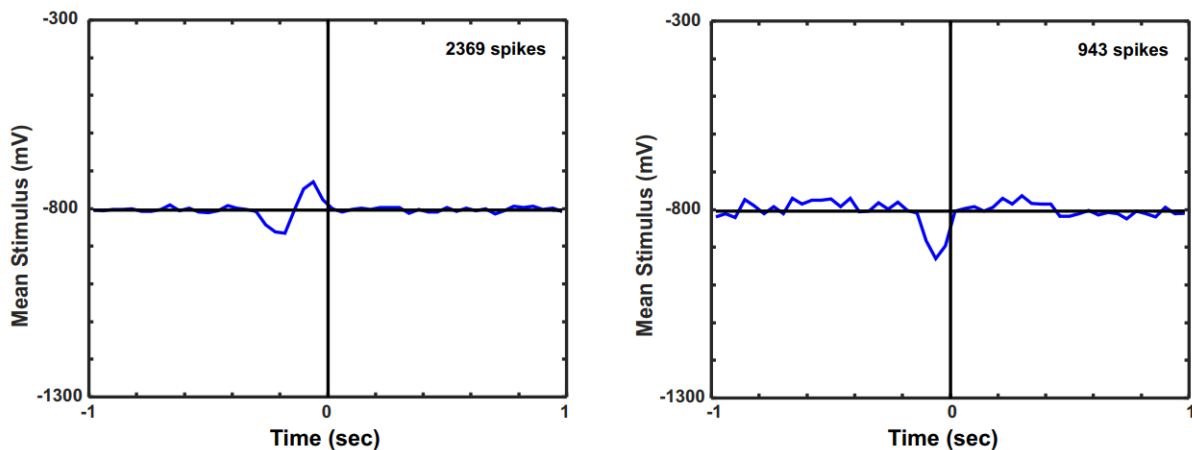
Appendix 1

Electrical STAs at alternate stimulus conditions

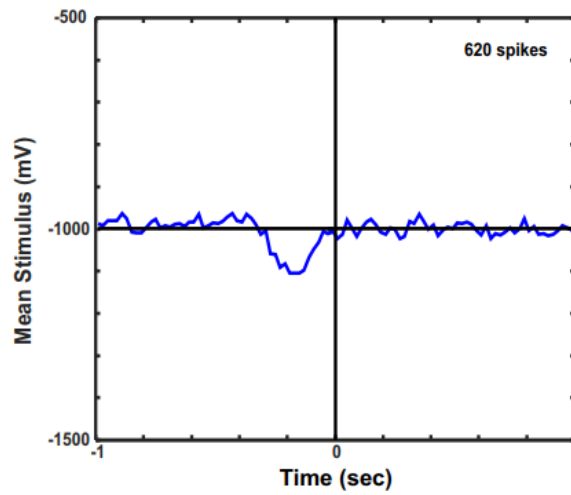
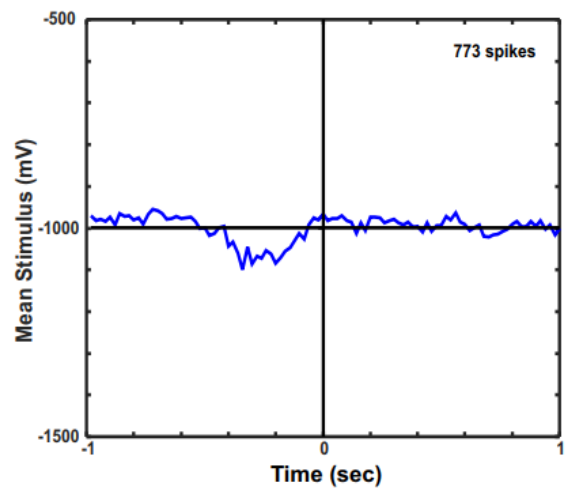
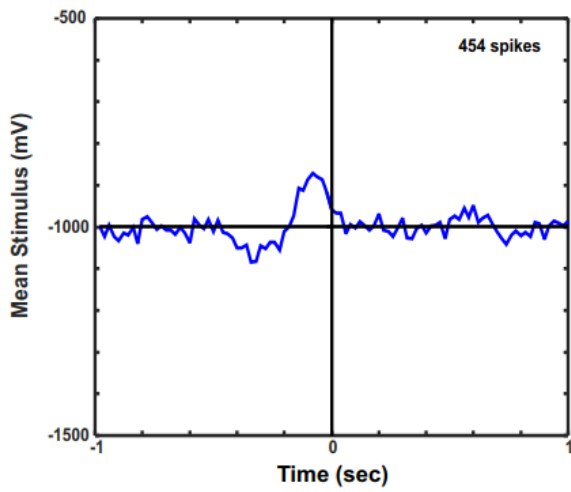
In **Appendix 2**, a detailed presentation of the electrical Gaussian white noise stimulus and evidence that the retina can integrate multiple subthreshold pulses is provided. The majority of the data in **Appendices 2-4** is obtained using electrical white noise sampled at a rate of 25 Hz from a distribution of mean voltage -800mV, 35% SD. Though most of the electrical STAs in this dissertation were obtained with these stimulus conditions, we were able to recover STAs at alternate conditions as well. The ability to obtain E-STAs at multiple contrasts, mean voltages and frequencies speaks to the robustness of the electrical white noise method. Here provided below are some of the E-STAs obtained under alternate stimulus paradigms, plotted at their original spike times (without correcting for bursts).

As mentioned previously we finally settled on a stimulation frequency of 25Hz, as it offered a good compromise between a well-sampled E-STA at 50Hz (but neglecting 50% of the time-bin) and a poorly sampled E-STA at 20Hz (but only neglecting 20% of the time-bin).

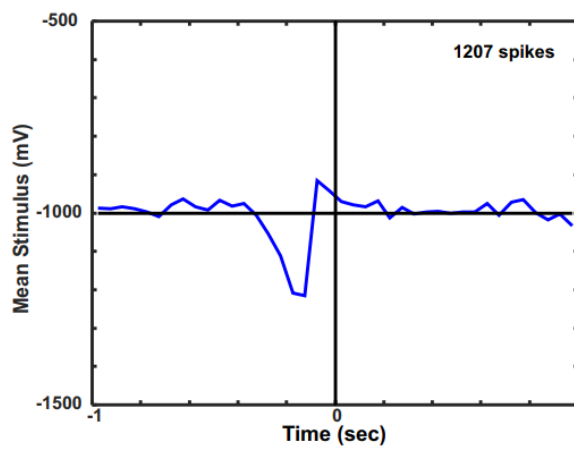
Electrical STAs at -800mV, 25Hz, 20%SD



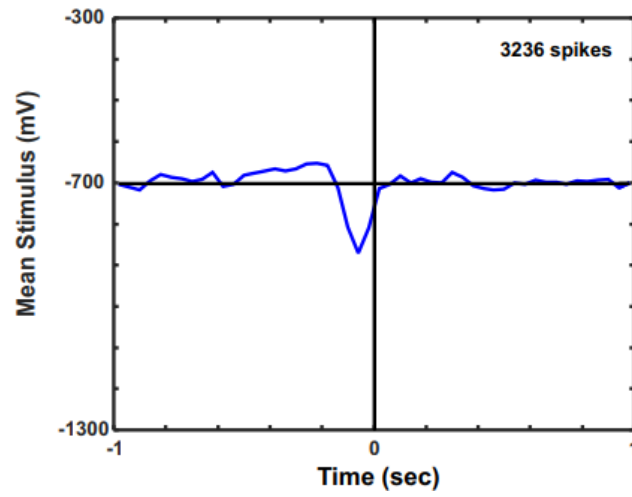
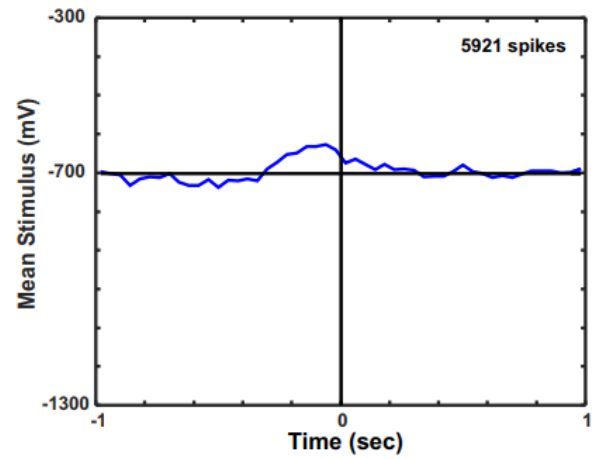
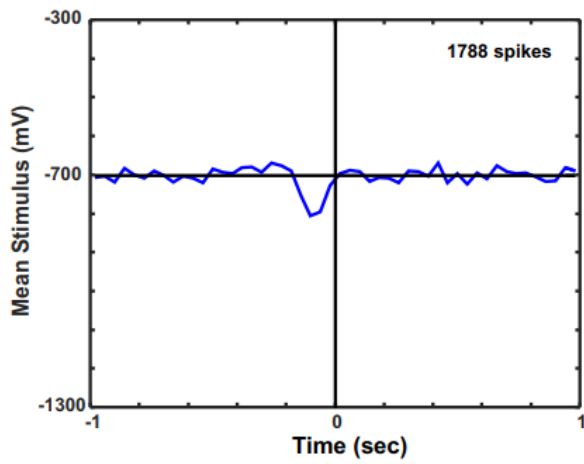
Electrical STAs at -1000mV, 50Hz, 35%SD



Electrical STAs at -1000mV, 20Hz, 35%SD



Electrical STAs at -700mV, 25Hz, 35%SD



Appendix 2

Manuscript 1: Tickling the retina: integration of subthreshold electrical pulses can activate retinal neurons.

Sudarshan Sekhar, Archana Jalligampala, Eberhart Zrenner, Daniel L. Rathbun

Published 17th May 2016 in the Journal of Neural Engineering

Abstract

Retinal Implants have been able to provide, to date, the best-restored visual acuity to patients with retinitis pigmentosa. Present implants use current or voltage pulses of a fixed amplitude presented at a certain frequency, adjusted to each patient. The amplitudes of the individual pulses are designed such that each pulse can activate RGCs, thereby eliciting visual phosphenes in patients. In other words, the individual pulses are suprathreshold. Despite encouraging results in many patients, with such a paradigm, the restored visual acuity falls well below the theoretical limit possible. This is because, there are still many unanswered questions that need to be addressed, such as reducing thresholds for retinal activation, reducing fading of percepts at high stimulation frequencies, inability to preferentially activate different retinal pathways, etc. In an attempt to resolve many of these issues, recent studies have tried alternate stimulus paradigms such as sine waves, sawtooths, diamond-shaped waves, etc. However, the choice of these alternate stimuli has been somewhat ad hoc without a strong justification. Therefore, in this study, we attempted to estimate a linear electrical filter for various retinal ganglion cells using subthreshold white noise electrical stimulation and reverse correlation. The ability to estimate a linear filter would provide a more educated guess at alternate stimulus waveforms that could be used to activate the retina. Our analysis showed that the retina could integrate multiple subthreshold pulses to generate a variety of different electrical input filters. The ability to obtain different electrical STAs raises the possibility that these different filters could correlate with visual cell type. This would have important implications for preferential stimulation of the retina, a major question in the field of retinal prosthetics.

Contributions SS and DLR designed the experiments; SS executed the experiments and analysis; SS, AJ, DLR, and EZ composed the manuscript; AJ contributed additional unpublished data.

Tickling the retina: integration of subthreshold electrical pulses can activate retinal neurons

S Sekhar^{1,2,3,4}, A Jalligampala^{1,2,3}, E Zrenner^{1,2,4} and D L Rathbun^{1,2,4}

¹Institute for Ophthalmic Research, Eberhard Karls University, D-72076 Tübingen, Germany

²Werner Reichardt Centre for Integrative Neuroscience (CIN), D-72076 Tübingen, Germany

³Graduate Training Center of Neuroscience/International Max Planck Research School, D-72074 Tübingen, Germany

⁴Bernstein Center for Computational Neuroscience Tübingen, D-72076 Tübingen, Germany

E-mail: sudsa89@gmail.com and daniel.rathbun@uni-tuebingen.de

Received 12 October 2015, revised 11 April 2016

Accepted for publication 12 April 2016

Published 17 May 2016



CrossMark

Abstract

Objective. The field of retinal prosthetics has made major progress over the last decade, restoring visual percepts to people suffering from retinitis pigmentosa. The stimulation pulses used by present implants are suprathreshold, meaning individual pulses are designed to activate the retina. In this paper we explore subthreshold pulse sequences as an alternate stimulation paradigm. Subthreshold pulses have the potential to address important open problems such as fading of visual percepts when patients are stimulated at moderate pulse repetition rates and the difficulty in preferentially stimulating different retinal pathways. **Approach.** As a first step in addressing these issues we used Gaussian white noise electrical stimulation combined with spike-triggered averaging to interrogate whether a subthreshold sequence of pulses can be used to activate the mouse retina. **Main results.** We demonstrate that the retinal network can integrate multiple subthreshold electrical stimuli under an experimental paradigm immediately relevant to retinal prostheses. Furthermore, these characteristic stimulus sequences varied in their shape and integration window length across the population of retinal ganglion cells. **Significance.** Because the subthreshold sequences activate the retina at stimulation rates that would typically induce strong fading (25 Hz), such retinal ‘tickling’ has the potential to minimize the fading problem. Furthermore, the diversity found across the cell population in characteristic pulse sequences suggests that these sequences could be used to selectively address the different retinal pathways (e.g. ON versus OFF). Both of these outcomes may significantly improve visual perception in retinal implant patients.

Keywords: systems biology, retinal prosthesis, white noise analysis, spike triggered average

(Some figures may appear in colour only in the online journal)

Introduction

Retinitis pigmentosa (RP) and age-related macular degeneration (AMD) are two retinal diseases that cause visual impairment in many people world over. Both RP and AMD are caused by a progressive loss of photoreceptors that remains irreversible and untreatable, eventually leading to complete blindness. Fortunately, the inner retina remains relatively intact. A host of different approaches including

gene therapy, stem cells, optogenetic stimulation and retinal implants are being explored in order to find a treatment for these diseases [1, 2]. To date retinal implants are the only effective treatment approved for clinical use [3–5]. In the subretinal configuration, the implant is embedded in the area where the photoreceptors used to be. The goal of subretinal stimulation is to elicit phosphene perception through activation of the retinal network i.e. indirect retinal ganglion cell (RGC) stimulation. In contrast, epiretinal devices aim to

activate RGCs directly with all image processing performed by the device without help of the retinal network, using direct RGC stimulation. The success of retinal implants—in particular, subretinal—emphasizes that the retinal circuitry of patients who have been blind for many years may still be functional and capable of carrying out important visual processing despite the retinal rewiring that is known to take place during disease progression [6, 7]. To capitalize on such network processing, we have focused our attention on improving our understanding of network stimulation.

Despite the effectiveness of subretinal network stimulation, there remain many unresolved problems. Among them are fading (of visual percepts at high frequencies of constant amplitude pulse stimulation [8]) and the inability to preferentially stimulate different retinal pathways. A solution to the fading problem would give patients better temporal resolution by allowing higher frequency of repetitive stimulation. Complementarily, stimulation specific to select RGC-types could, for example, improve visual contrast by reducing antagonistic signals from competing visual pathways. Though there has been some progress in recent years in addressing these questions [9–11], the exact mechanisms of how the retinal circuitry behaves under electrical stimulation is still poorly understood. To address this limited understanding, we applied linear systems analysis techniques developed in the field of visual cellular neurophysiology as detailed below.

Gaussian-distributed ‘white noise’ stimuli have been used for many years in visual neuroscience to recover temporal filters from the retinal network [12–14]. In this method, a series of luminance values drawn randomly from a Gaussian distribution is presented to the retina [15]. Such a ‘white noise’ stimulus effectively samples the practically infinite space of time-varying luminance patterns. Each of the stimulus sequences immediately preceding a RGC action potential (also called a spike) is combined to produce the spike-triggered average (STA). The Gaussian distribution ensures that the resulting STA is a close estimate of the linear filter of the RGC [12–14]. The advantages of the STA are two-fold. First, it provides a useful model of how the cell and its inputs from the retinal network can integrate multiple subthreshold stimuli over time in order to cross the spike generation threshold. Second, it is an efficient method for sampling from a large, parameter space of potential stimuli.

This white noise method, due to its advantages, is gaining momentum in the field of retinal prosthetics [16, 17]. However, previous studies likely only examined suprathreshold extracellular network stimulation using continuous-current binary noise [16], or did not investigate the temporal integration of multiple pulses over time intervals shorter than 500 ms [17]. Here we present electrical STAs obtained by subthreshold Gaussian white noise stimulation of the retinal network. This paper shows that subthreshold stimulation can be effective, thereby opening up a new domain of electrical waveforms that may selectively activate RGC subtypes and reduce phosphene fading.

Materials and methods

Experimental design

The data contained here represent a first study to describe the degree to which network stimulation of the retina may result from integration of subthreshold pulse sequences. Our data, we contend demonstrates subthreshold integration. Since our aim with this study was to see if we could get RGC responses based on network integration of multiple subthreshold pulses, our principle goal was therefore repeatability across multiple retinal tissues. We therefore conducted enough experiments to collect data from at least 20 RGCs for initial evaluation. Based on the frequency of basic RGC types (ON, OFF, ON/OFF) [18], this should be sufficient to provide a random sampling from the main RGC types. Our data was collected using a 60 channel Microelectrode array (MEA). Only those electrodes immediately surrounding the stimulating electrode were analyzed. Waveforms of spikes from a putative spike train were analyzed based on: (1) the presence of a lockout period in the ISI histogram and autocorrelogram indicating that spike trains from multiple cells were not lumped together (2) absence of a peak in the cross-correlogram with other ‘cells’ that would indicate splitting of a single cell’s spike train into multiple ‘cells’ (3) good isolation in spike clustering space of a biphasic waveform whose shape is typical of extracellularly recorded action potentials and (4) stability of this waveform over the entire recording. Each of these individual characteristics was rated from 1 to 5 (1 being the worst and 5 being the best) and a weighted average was calculated. Only those cells which had an overall rating of 2.8333 or higher were included here. We initially had 44 spike clusters. After applying our selection criteria we had 28 cells. Outliers were not excluded from the population analysis. The present data was collected from 3 retinal tissues from 3 mice.

Our null hypothesis was that integrative electrical STAs were not obtainable under such conditions. Upon initial analysis, we investigated the hypothesis that temporal smear alone was responsible for apparently integrative STAs. This secondary hypothesis was rejected, allowing us to also reject the original null hypothesis. The unit of investigation were well-isolated wild-type mouse (C57Bl/6J) RGCs.

Animals

The mice were kept under a standard white cyclic lighting, mimicking regular daily rhythms. They had free access to food and water. In total, 3 adult wild-type C57Bl/6J (Jackson Laboratory, Bar Harbor, ME, USA) were used. Two of these mice were aged postnatal day 32 (P32) and one was P39. In total, one retinal half was used from each of these 3 mice. All procedures were approved by state authorities (Regierungspräsidentium, Tübingen) and conducted under the supervision of the Tübingen University facility for animal welfare (Einrichtung für Tierschutz, Tierärztlichen Dienst und Labortierkunde) and the NIH Guide for the Care and Use of Laboratory Animals. All possible efforts to minimize the number of animals used and their suffering were made.

Retinal preparation

Prior to retinal dissection, CO₂ inhalation was used to anesthetize the mouse. Next, a pinch of the tissue between toes was used to check for withdrawal reflex. Finally, the mouse was euthanized by cervical dislocation. The eyes were then removed under normal room lighting and placed in carbogenated (95% O₂ and 5% CO₂) artificial cerebrospinal fluid (ACSF) solution containing the following (in mM): 125 NaCl, 2.5 KCl, 2 CaCl₂, 1 MgCl₂, 1.25 NaH₂PO₄, 26 NaHCO₃ and 20 Glucose, pH 7.4. During the dissection process (which was performed under dim light conditions) the cornea, ora serrata, lens and vitreous body were removed. Next the optic nerve was cut at the base of the retina and finally the retina was detached from the pigment epithelium. Next all traces of vitreous material from the inner surface of the retina were removed. This is important as vitreous prevents good contact between the nerve fiber layer and electrodes. Retinas were maintained in carbogenated ACSF until needed. All recordings were performed with a planar MEA. A retinal half was oriented and flattened onto the MEA—ganglion cell side down—with two miniature forceps and was allowed to adapt for >30 min. Care was taken not to damage the retina or MEA during this process. In order to create better contact between the retina and the electrodes, a dialysis membrane (CelluSep, Membrane Filtration Products Inc., Seguin, Texas, USA) mounted on a custom Teflon ring was lowered onto the retina [19]. The MEA was then placed under the preamplifier and continuously superfused with carbogenated ACSF (~6 ml min⁻¹) maintained at 33 °C using both a heating plate and a heated perfusion cannula (HE-Inv-8 & PH01; Multi Channel Systems, Reutlingen, Germany).

MEA and data acquisition system

A planar MEA containing 59 circular TiN electrodes (diameter: 30 μm, interelectrode spacing: 200 μm; Multi Channel Systems, Reutlingen, Germany) arrayed in an 8 × 8 rectangular grid layout, and with electrode tracks insulated by Si₃N₄ on a glass substrate was used for recording from RGCs. There were no electrodes on the four corners of the grid. Moreover one electrode was substituted with a large reference electrode. The electrodes had impedances of approximately 50 kΩ at 1 kHz. The data acquisition system consisted of the MEA60 system (MCS, Reutlingen, Germany), RS-232 interface, a 60 channel preamplifier with integrated filters and a blanking circuit (MEA 1060-Inv-BC). The blanking circuit was used to reduce recording noise by grounding any defective electrodes and to choose the stimulating electrode. These operations were controlled by the MEA Select software. All data collection was done using the MC_Rack program which was installed on a personal computer running Windows XP. The computer was also fitted with MC_Card data acquisition hardware and an analog input card to record stimulus trigger signals. The raw data was sampled at a rate of 50 kHz/channel. Using a filter with a bandwidth of 1 Hz–3 kHz and a gain of 1100.

Electrical stimulation and recording

A stimulus generator (STG 2008, MCS, Reutlingen, Germany) was used to generate the stimulus pulses. The pulses were delivered from the ganglion cell side of the retina (epiretinally) via one of the 59 electrodes—chosen based on proximity to electrodes with clean neural signals. Although subretinal implants deliver electrical stimulation from the photoreceptor side of the retina to activate the retinal network, it is well established that the desired network stimulation can be achieved by stimulating from either side of the retina [20, 21]. Therefore, because of the difficulty in simultaneously stimulating and recording from opposite sides of the whole-mount retina, epiretinal electrodes were used for both. Furthermore, to remove the influence of direct RGC activation on our results, a spike latency exclusion period was applied (see results and figure 1(e))—a step that would also be necessary with subretinal stimulation.

RGC responses on the 8 neighboring electrodes at a distance of either 200 or 283 μm were examined. The noise stimulus was programmed in MATLAB (The Mathworks, Natick, MA) with custom scripts, and imported into *MC-Stim* (MCS, Reutlingen, Germany) for presentation. It consisted of monophasic rectangular voltage pulses, each of 1 ms duration, whose amplitudes were drawn for every 40 ms interval from a Gaussian distribution with a mean of –800 mV and a standard deviation of 280 mV. Such pulse waveforms are typical for retinal implants that target network-mediated (indirect) activation of RGCs [3, 22]; and are comparable to biphasic current pulses [21]. Furthermore, the choice of relatively short 1 ms pulses delivered from the epiretinal side was made, in part, to minimize any potential contribution of photoreceptor stimulation to the STA [23]. For stimuli with a mean other than –800 mV the SD was always 35% of the mean (figure 3). A ‘post-time’ of 1 ms was set in *MC-Stim* (MCS, Reutlingen, Germany) to facilitate active discharge of the stimulating electrode via the stimulator. Additionally, a wait time of 1.3–1.4 ms was set in MEA Select to extend the blanking period before recording resumed—thus minimizing stimulation artifacts. A single trial of the noise stimulus ran for 100 s. Fifty-four non-repeating trials were presented in each recording with about 30 s between each trial.

For figure 3, voltage pulses of 1 ms duration were presented in order of increasing magnitude with each pulse repeated 10 times at 5 s intervals before advancing to the next voltage. This stimulus block was repeated twice before proceeding to noise stimulation. Noise stimulation for this cell consisted of 5 non-repeating trials of noise with a mean of –800 mV followed by 5 non-repeating –1000 mV trials and then 5 non-repeating –1200 mV trials. The full set of 15 trials was repeated twice. The population data of figure 3(b) was collected during a separate study that did not include the 28 cells presented here, using the same 1 ms duration, 5 s intervals, and increasing voltage amplitude; but in the context of a broader exploration of stimulus space in which 8 other durations and matching positive voltages were also presented.

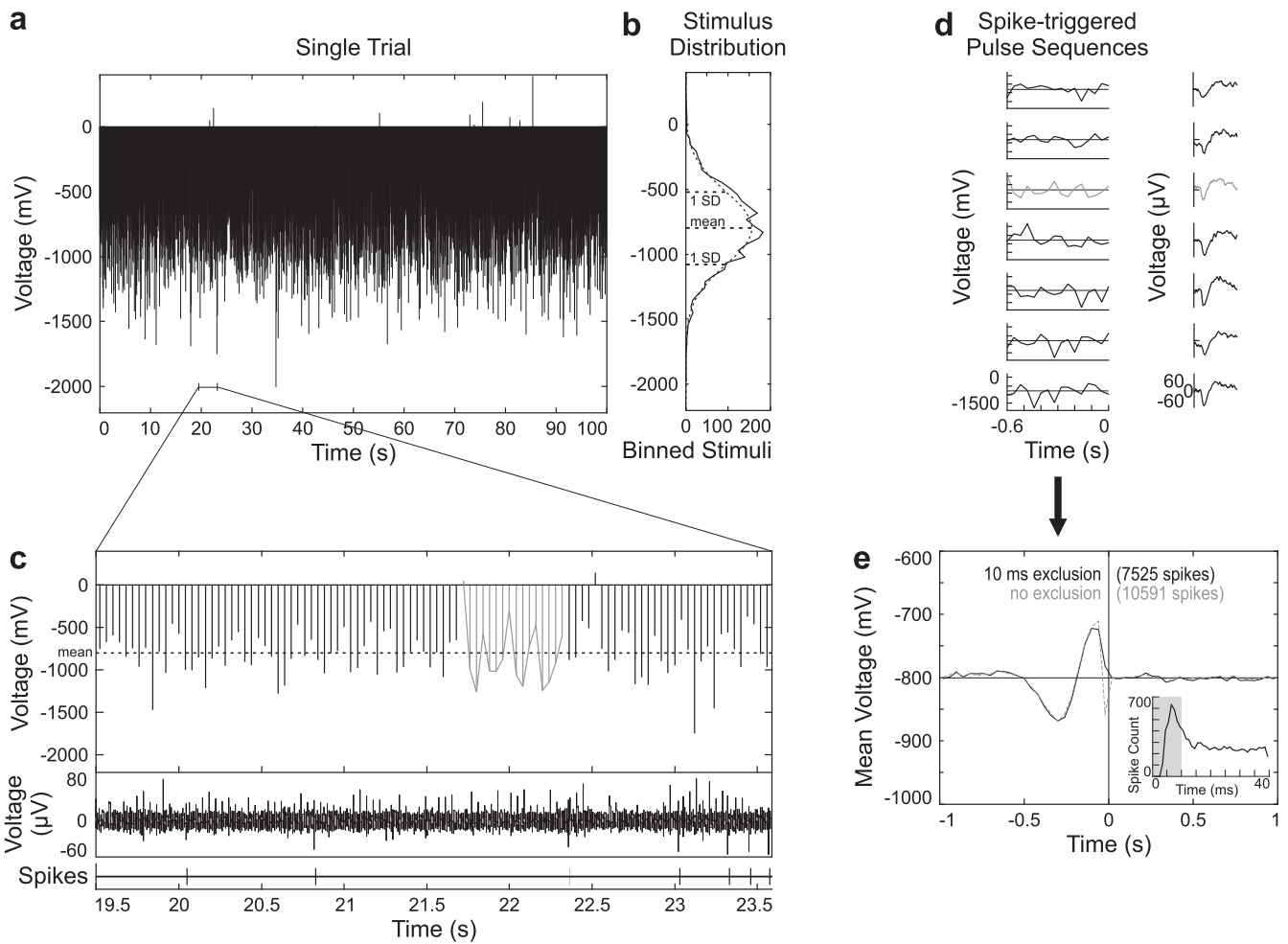


Figure 1. Spike-triggered average method reveals temporal electrical integration. Retinas were stimulated through a microelectrode array in an epiretinal configuration with both the stimulating and recording electrodes against the RGC side of the retina. (a) Single stimulus block containing random pulse amplitude sequence of 1 ms pulses at 25 Hz. (b) Amplitude distribution of pulses in (a) (black) drawn from a Gaussian function (gray, dotted). Dotted lines mark mean and SD voltages, which define the Gaussian function. (c) Expansion from a with accompanying high-pass filtered voltage recording and spike train; (gray) highlights an example pulse sequence preceding the associated spike, below. (d) Sample pulse amplitude sequences of the 7 spikes from (c). Three ms spike waveform excerpts are shown at right. (e) STA for all spikes (gray, dotted). Average post-spike stimuli shown right of 0 s to reflect spike count dependent noise level for each STA. To ignore direct electrical activation of RGCs, spikes following a pulse by ≤ 10 ms were excluded in subsequent analysis (black). Inset shows histogram of spike times after each pulse. Gray area denotes excluded spikes.

Response threshold was determined as the lowest voltage in which the response exceeded mean + 2 · Variance of the ‘spontaneous’ firing rate assessed during the many 1 s epochs preceding each voltage pulse.

Data analysis

The stored raw data were processed using commercial spike sorting software (Offline Sorter, Plexon Inc, TX, USA). To process the data, voltage traces were first high pass filtered with a 12-pole Bessel filter with a cut off frequency of 51 Hz. Following this, putative action potential events (spikes) whose filtered amplitude was greater than four standard deviations from the mean were detected. These events were sorted into clusters with an automated routine (T-distribution expectation maximization) to assign noise events as well as spikes from up to 5 cells recorded on each electrode to their

own separate ‘units’. Finally, as a quality control step, the multiple automated sorting solutions were manually inspected and slightly modified as necessary in order to minimize Type I and Type II errors in attribution of events to different sources. Only units with a distinct waveform, interspike interval lock-out period, and which demonstrated a refractory period in their autocorrelogram were considered to contain the spike train from a single RGC and included in the analysis presented here. Cells which responded to visual but not electrical stimulation were observed, however the number of spikes produced were too few to support reliable spike train isolation. Time stamps assigned to the detection threshold crossing of these sorted spikes were collected with NeuroExplorer (PlexonInc, TX, USA) and exported to MATLAB for further analysis.

Custom scripts written in MATLAB were used for: ‘all’ and ‘first’ spike-triggered averaging, analysis of the statistical

significance of the STAs, pre-ISI versus post-ISI analysis to identify bursts, and calculation of latency and integration period of the negative deflection (see results). Because cathodic pulses are known to be more effective in stimulating the retina in the epiretinal configuration, we focused our analysis on negative deflections in the STA. For STAs, each spike was binned according to the 40 ms stimulus frame in which it occurred.

Statistical analysis

To identify STA deflections, the STA was first smoothed with MATLAB's *spline* function sampled at 1 ms intervals. The time delay of the minimum value in this smoothed STA determined the latency of negative STA deflections. Statistical significance of a STA deflection was calculated using MATLAB's *ztest* function to test whether the deflection was significantly outside the distribution of baseline values for each STA. The mean of the baseline distribution for each cell was taken to be the mean of the fluctuation on the right of time = 0 in the STA for each cell. The sigma was the standard deviation of these fluctuations. The alpha value used by *ztest* (1-tailed) was corrected for multiple comparisons to result in a 5% chance of falsely misidentifying a data point as significant. The integration widths for negative deflections were calculated based on the first values on either side of the deflection peak that were no longer statistically significant from the baseline. The limits for integration boundaries were set to 0 and 1 s.

Results

Determining if retinal circuit can integrate multiple electrical pulses

To determine if the retinal circuit can integrate across multiple electrical pulses, we presented random voltage-controlled pulse sequences while recording RGC spike trains from the mouse retina using a planar MEA (figures 1(a)–(d); experimental methods). We then estimated the electrical filter of each RGC by averaging the stimulus segments preceding each spike—yielding the STA. We found STAs with an integration time spanning multiple pulses were common (figure 1(e)), demonstrating that, in addition to responding to individual suprathreshold pulses, the retinal network can integrate multiple subthreshold pulses. Preliminary experiments with pulse frequencies of 10, 20, 25, 40, and 50 Hz demonstrated a tradeoff between STA sampling density and response rate—with 25 Hz representing a reasonable compromise between the two concerns (data not shown). No integrative STAs were acquired at 10 Hz suggesting that the maximal interval sufficient for integration lies somewhere between 50 and 100 ms.

All 28 well-isolated RGC spike trains yielded negative STA deflections that were statistically significant. We focused our analysis on negative deflections because cathodic pulses are known to be most effective in the epiretinal stimulation

configuration. STA shape varied across the population with 11 cells demonstrating a short latency positive deflection preceded by a longer latency negative deflection (as in figure 1(e)). Another 9 cells displayed the inversion (as in figure 3(a)) with negative deflection preceded by longer latency positive deflection. The remaining 8 cells were monophasic or difficult to classify. Further work is required to develop classification methods that are robust to the variability in STA shape and signal-to-noise ratio.

As our objective, was to investigate only the RGC spikes resulting from retinal network activation and not via direct RGC activation, all spikes within a latency of 10 ms following each stimulus pulse were excluded from our analysis (figure 1(e) *inset*). This exclusion period was based both on previous reports and on our observation that a short-latency negative deflection/peak was eliminated in the STA for less than 20% of cells [20, 24].

Bursting responses sometimes broaden STA deflections

Because network-driven responses of some RGCs tend to occur in bursts, single suprathreshold electrical pulses could evoke multiple spikes of variable latency. This in turn, would smear out the representation of such pulses in the STA across multiple time points thereby implying integration where none exists (figure 2) [25]. To test this, we used interspike intervals (ISIs; figures 2(b), (d) and (f)) to identify response bursts [26, 27] and created STAs using only the timing of the first spike in each burst (figures 2(c), (e) and (g)). The STAs of most cells changed only modestly due to this first spike-triggered average (fSTA) method, and still demonstrated the broad negative deflections expected for multi-pulse integration. Examples of the two extremes of this continuum are shown in figures 2(c) and (g). The fSTAs of a few cells (5/26) had negative deflections with latencies shorter than the interpulse interval of 40 ms—indicating that the STA was dominated by responses to single pulses (figure 2(g)). For the cells with significant negative fSTA deflections (26/28), we found that deflection latency mean \pm SD was 171.5 ± 118.9 ms and temporal integration width was 139.2 ± 70.5 ms. These electrical STA values were comparable to typical mouse RGC visual STA latencies and integration widths, suggesting that the retinal circuit is activated in a similar way by both visual and electrical stimulation [18]. Figure 2(h) shows how width and latency vary across the population. Figures 2(i) and (j) shows how these parameters change when correcting for burst responses with the fSTA method.

Determining how the mean of the voltage distribution affects the STA

In order to stimulate and record from multiple RGCs simultaneously—each of whom might have a different stimulation threshold—we could not optimize the mean voltage level of stimulation for each cell. Instead, we sought to find a mean that would be sufficiently below threshold for a majority of cells. In preliminary experiments, we observed that a mean of

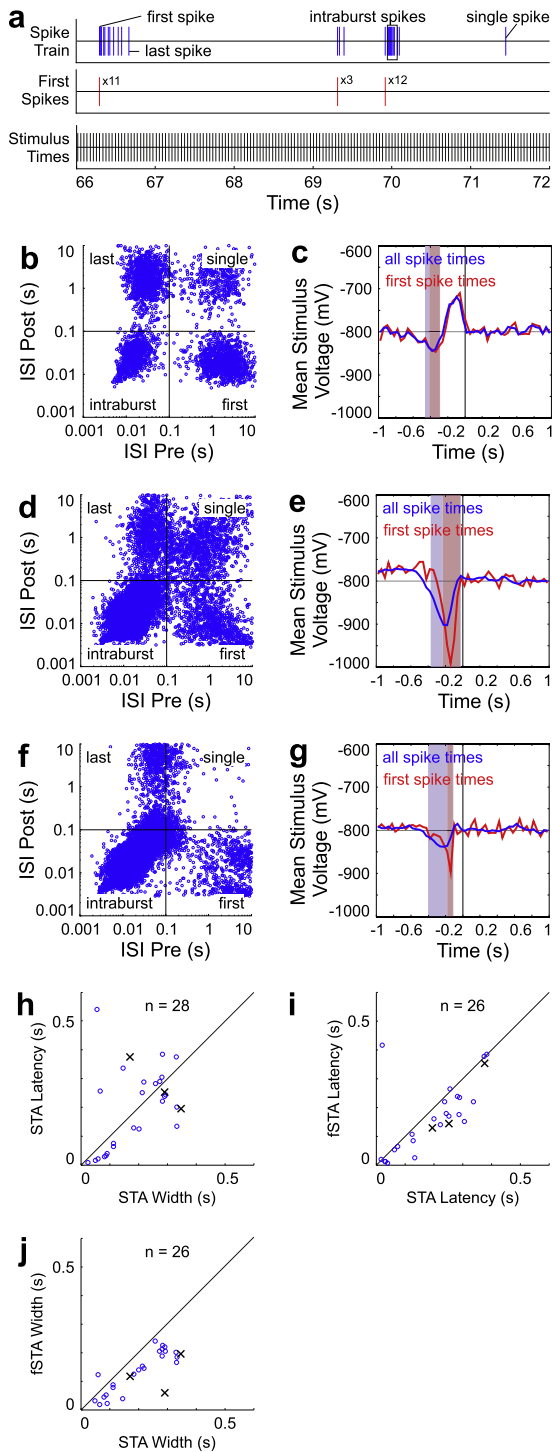


Figure 2. Bursting responses sometimes broaden STA deflections. (a) Sample bursting spike train (top), first spike occurrences (middle) and stimulus pulse times (bottom). (b), (d), (f) Distribution of interspike intervals (ISIs) before (pre) and after (post) each spike for three different RGCs. Quadrants divide spikes into four labeled classes using a criteria of <100 ms for inclusion of spikes into a ‘burst’. (c), (e), (g) Burst correction of STAs. For ‘first’ spike STA (fSTA) calculation, each ‘first’ spike time is weighted according to the total number of spikes in the burst. ‘All’ indicates the standard STA method presented in figure 1. Shaded regions mark negative deflections for each STA. (h) Scatterplot of negative deflection parameters for all RGCs for ‘all’ spike STAs. (i) Negative deflection latency for fSTAs versus ‘all’ spike STAs. (j) Same for widths. The three example cells from (b) to (g) are marked in (h)–(j).

–800 mV maximized the number of cells which responded with an integrative fSTA while simultaneously minimizing the number of cells which yielded fSTAs with sharp peaks driven by single suprathreshold voltage pulses (as discussed below).

Accordingly, we found that the statistics of the voltage pulse distribution (figure 1(b)) influenced the degree to which cells responded to single suprathreshold pulses versus the integration of subthreshold pulse sequences (figure 3). As the mean amplitude increased, more individual pulses passed the cell’s response threshold (–1500 mV according to our definition, see methods), thereby contributing to a short-latency peak in the STA (figure 3(a), bottom). It should be noted that the actual threshold for this cell is most likely somewhere between –1000 mV and –1500 mV. The voltage response curve for the cell shown in figure 3(b) demonstrates that many of the voltages presented to generate the lower STA of figure 3(a) strongly activate this cell. In contrast to the Gaussian noise stimuli used to generate STAs, the stimuli used to measure the voltage response curve of figure 3(b) were presented one at a time separated by 5 s. For a broader context, the mean population voltage response curve from 59 cells (from 12 retinal halves) recorded in another study from our group is overlaid in black. In this other study currently being prepared for publication [28], the same 1 ms pulses and 5 s intervals were used. The mean \pm SD threshold calculated from this population data was found to be -1312 ± 530 mV—supporting our assertion that most pulses in the –800 mV noise stimulus were indeed subthreshold for the majority of cells. Examples of fSTAs with sharp, single-pulse-activated peaks which were produced from a Gaussian of mean –1000 mV (35% contrast, 12 trials) during our preliminary investigations are also shown, demonstrating responses from cells for whom the network was activated too strongly to elicit multi-pulse integration (figures 3(c) and (d)).

Discussion

Electrical STAs from the retina have been shown in previous work using continuous binary noise stimulation [16]. In contrast, the stimuli delivered by implants presently approved for human patients are pulsatile in nature and not continuous—in order to prevent damage to electrodes and retinal tissue. In a related work, the average firing rate following electrical pulses using a ‘sparse noise’ stimulus were reported [17]. Although useful for mapping the spatial extent of electrical sensitivity, such results do not address how multiple pulses may be integrated on the scale of tens to hundreds of ms. Therefore, the electrical filters we have presented in this paper, are the first proof of principle that electrical STAs can be recovered from the retina under conditions immediately relevant to prosthetics. Because the STA provides an approximation of the cell’s preferred stimulus, it might prove useful to move away from the suprathreshold pulsatile stimuli presently used in prostheses, towards exclusively subthreshold stimulus patterns, like those we have shown in this paper.

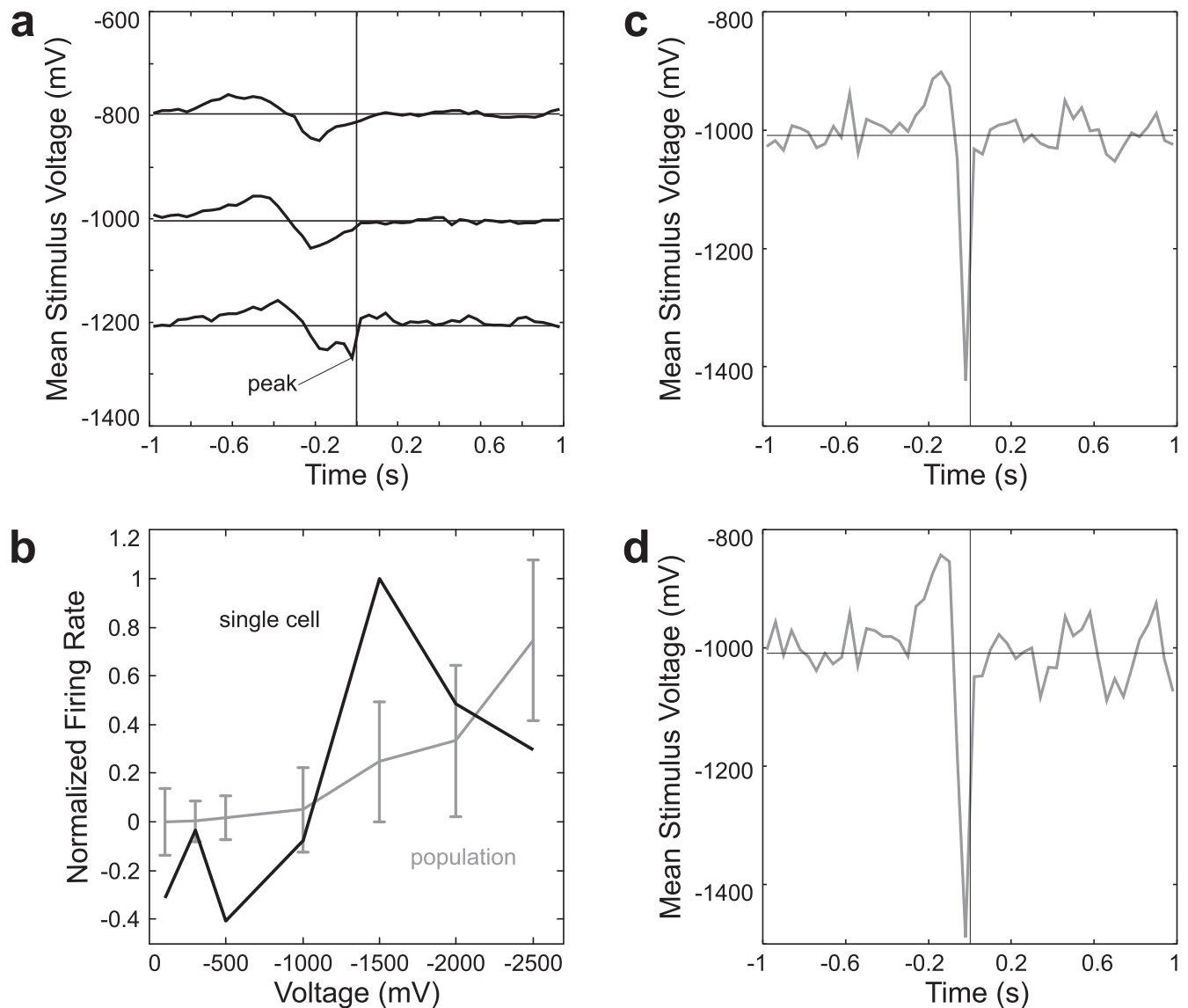


Figure 3. Mean stimulus voltage alters STA. (a) STA calculated at three mean voltages for a single cell. Labeled peak reflects single-pulse responses. (b) Voltage tuning curve of same cell for 1 ms pulses presented at 5 s intervals (*black*, 20 repetitions each, response integration window: 10–100 ms). Population tuning curve for 59 RGCs from another study using the same methods shown for reference (*gray*). For each cell, firing rate was baseline (spontaneous) subtracted and normalized to its maximal response. (c), (d) Sample cell STAs from a pilot study which displayed primarily single-pulse responses (Gaussian noise stimulus: mean = -1000 mV, 35% contrast, 25 Hz pulse rate).

It has previously been shown that different RGCs (e.g. ON versus OFF) have different visual STAs [18]. If electrical STAs also vary for different RGCs, it would in theory be possible to preferentially stimulate different retinal pathways by employing different pulse patterns, thus providing more naturalistic visual percepts. This would have substantial implications for retinal prosthetics. Preliminary studies have shown correlations between certain visual RGC subtypes and their responses to pulsatile electrical stimulation [9]. Using Gaussian white noise electrical stimulation would complement such correlation analyses. In accordance with the hypothesis that preferred electrical stimuli vary with RGC type, we have observed in a few cells, an apparent correlation between visual and electrical STAs. Specifically, whether the short-latency peak of an STA deviates above or below the mean voltage appears to correlate with the ON/OFF visual

response category of that cell. However, further experiments and analysis are needed to fully develop these observations.

The reality of obtaining these STAs may seem surprising, given that RGC spiking has been shown to decrease markedly when stimulated at such frequencies—a potential retinal correlate of phosphene fading [8, 10, 11]. Nevertheless, it has been demonstrated that responses to such high frequencies can persist if the stimulus amplitude is varied [29]. In this case, the response reflects a change in stimulus rather than the presence of the stimulus. Given that threshold measurements are typically made with single isolated pulses, the electrical STAs reported here measured in the context of ongoing stimulation may prove to be a better measure of the best stimulus waveform. Simultaneously, these STAs could provide a solution to the problem of phosphene fading observed during traditional suprathreshold stimulation to the degree

that fading may be limited to suprathreshold pulses. The presentation of subthreshold pulse patterns to patients will be necessary to test this theory.

Limitations of the present study and future work

It has previously been shown that a cell can have multiple linear filters contributing to the spike generation mechanism [30]. The STA would in such a case be an amalgamation of these multiple underlying filters and therefore not the ideal estimate of the cell's preferred stimulus. Moreover, because an STA is a linear approximation of the cell's filter, nonlinearities underlying a cell's response are not captured by the STA. Nevertheless, the ability to get STAs from a tissue is an important and arguably essential precursor to exploring the extent of nonlinearities and possibility of multiple filters.

In order to achieve significant STAs with minimal noise, the stimuli presented here lasted well over an hour. Over that time, nonstationarity in firing rate was noted. One well-known source of nonstationarity is the various timescales of adaptation that have been frequently observed in retinal responses. Accordingly, we are further investigating adaptation and other candidate nonstationarities to better model the electrical responses of RGCs.

As a pilot study, the main goal of these experiments was to ascertain whether RGC STAs could be obtained from subthreshold pulsatile electrical stimulation of the retinal network. We have demonstrated that the fundamental method is sound and that there is evidence to support both cell type-specific stimulation and a role for such stimuli in reducing perceptual fading. It is, however, necessary to expand on this work by testing each of these hypotheses experimentally as well as examining how these STAs change over the course of degeneration. If these hypotheses prove to be correct, these novel stimulation paradigms could, with relative ease, be translated to human trials. This could in turn significantly improve visual percepts restored by implants.

Acknowledgments

Funding

Core funding for this study was provided by the German Federal Ministry of Education and Research (BMBF; 031 A 308). This study is part of the research program of the Bernstein Center for Computational Neuroscience, Tuebingen, funded by the BMBF (FKZ: 01GQ1002). Additional support was received from the Deutsche Ophthalmologische Gesellschaft, the PRO RETINA foundation for prevention of blindness, the Tistou and Charlotte Kerstan Foundation, and the Werner Reichardt Centre for Integrative Neuroscience (CIN) at the Eberhard Karls University of Tübingen. The CIN is an Excellence Cluster funded by the Deutsche Forschungsgemeinschaft (DFG) within the framework of the Excellence Initiative (EXC 307).

Author contributions

SS and DR designed the experiments; SS executed the experiments and analysis; SS, AJ, DR and EZ composed the manuscript; AJ contributed additional unpublished data.

Competing financial interests

DR has received surplus equipment on loan and minor support for supplies from Retina Implant AG. EZ is Advisor to Retina Implant AG, stock holder and co-inventor of patents held by this company. Retina Implant AG had no influence on the planning and execution of the project presented here.

We therefore declare no competing financial interests.

References

- [1] Zrenner E 2013 Fighting blindness with microelectronics *Sci. Transl. Med.* **5** 210–6
- [2] Sahel J A and Roska B 2013 Gene therapy for blindness *Annu. Rev. Neurosci.* **36** 467–88
- [3] Zrenner E et al 2011 Subretinal electronic chips allow blind patients to read letters and combine them to words *Proc. Biol. Sci.* **278** 1489–97
- [4] Stingl K et al 2015 Subretinal visual implant alpha IMS—clinical trial interim report *Vision Res.* **111** 149–60
- [5] Weiland J D and Humayun M S 2014 Retinal prosthesis *IEEE Trans Biomed Eng.* **61** 1412–24
- [6] Biswas S, Haselier C, Mataruga A, Thumann G, Walter P and Müller F 2014 Pharmacological analysis of intrinsic neuronal oscillations in rd10 retina *PLoS One.* **9** e99075
- [7] Jones B W, Pfeiffer R L, Ferrell W D, Watt C B, Marmor M and Marc R E 2016 Retinal remodeling in human retinitis pigmentosa *Exp Eye Res.* **16** 30048–3
- [8] Pérez Fornos A, Sommerhalder J, da Cruz L, Sahel J A, Mohand-Said S, Hafezi F and Pelizzone M 2012 Temporal properties of visual perception on electrical stimulation of the retina *Invest. Ophthalmol. Vis. Sci.* **53** 2720–31
- [9] Im M and Fried S I 2015 Indirect activation elicits strong correlations between light and electrical responses in ON but not OFF retinal ganglion cells *J. Physiol.* **593** 3577–96
- [10] Freeman D K and Fried S I 2011 Multiple components of ganglion cell desensitization in response to prosthetic stimulation *J. Neural Eng.* **8** 016008
- [11] Jensen R J and Rizzo J F 3rd Responses of ganglion cells to repetitive electrical stimulation of the retina *J. Neural Eng.* 2007 **4** S1–6
- [12] Marmarelis P Z and Naka K I 1973 Nonlinear analysis and synthesis of receptive-field responses in the catfish retina: I. Horizontal cell ganglion cell chain *J. Neurophysiol.* **36** 605–18
- [13] Marmarelis P Z and Naka K I 1973 Nonlinear analysis and synthesis of receptive-field responses in the catfish retina: II. One-input white-noise analysis *J. Neurophysiol.* **36** 619–33
- [14] Marmarelis P Z and Naka K I 1973 Nonlinear analysis and synthesis of receptive-field responses in the catfish retina: III. Two-input white-noise analysis *J. Neurophysiol.* **36** 634–48
- [15] Chichilnisky E J 2001 A simple white noise analysis of neuronal light responses *Network* **12** 199–213
- [16] Freeman D K, Rizzo J F and Fried S I 2010 Electric stimulation with sinusoids and white noise for neural prostheses *Front Neurosci.* **4** 1–3
- [17] Lorach H et al 2015 Photovoltaic restoration of sight with high visual acuity *Nat. Med.* **21** 476–82
- [18] Baden T, Berens P, Franke K, Román Rosón M, Bethge M, and Euler T 2016 The functional diversity of retinal ganglion cells in the mouse *Nature* **529** 345–50
- [19] Meister M, Pine J and Baylor D A 1994 Multi-neuronal signals from the retina: acquisition and analysis. *J. Neurosci. Methods* **51** 95–106

- [20] Boinagrov D, Pangratz-Fuehrer S, Goetz G and Palanker D J 2014 Selectivity of direct and network-mediated stimulation of the retinal ganglion cells with epi-, sub- and intraretinal electrodes *J. Neural Eng.* **11** 026008
- [21] Stett A, Barth W, Weiss S, Haemmerle H and Zrenner E 2000 Electrical multisite stimulation of the isolated chicken retina *Vis. Res.* **40** 1785–95
- [22] Loudin J D, Simanovskii D M, Vijayraghavan K, Sramek C K, Butterwick A F, Huie P, McLean G Y and Palanker D V 2007 Optoelectronic retinal prosthesis: system design and performance *J. Neural Eng.* **4** S72–84
- [23] Eickenscheidt M, Jenkner M, Thewes R, Fromherz P and Zeck G 2012 Electrical stimulation of retinal neurons in epiretinal and subretinal configuration using a multicapacitor array *J. Neurophysiol.* **107** 2742–55
- [24] Jensen R J, Ziv O R and Rizzo J F 2005 Responses of rabbit retinal ganglion cells to electrical stimulation with an epiretinal electrode *J. Neural Eng.* **2** S16–21
- [25] Fried S I, Hsueh H A and Werblin F S 2006 A method for generating precise temporal patterns of retinal spiking using prosthetic stimulation *J. Neurophysiol.* **95** 970–8
- [26] Zeck G M and Masland R H 2007 Spike train signatures of retinal ganglion cell types *Eur. J. Neurosci.* **26** 367–80
- [27] Rodieck R W, Kiang N Y and Gerstein G L 1962 Some quantitative methods for the study of spontaneous activity of single neurons *J. Biophys.* **2** 351–68
- [28] Jalligampala A, Rathbun D L and Zrenner E 2014 Electrical responsiveness of retinal ganglion cells (RGCs) in rd10 mouse line *The Eye and the Chip (Detroit, Michigan, USA)*
- [29] Goetz G, Smith R, Lei X, Galambos L, Kamins T, Mathieson K, Sher A and Palanker D 2015 Contrast sensitivity with a subretinal prosthesis and implications for efficient delivery of visual information *IOVS* **56** 7186–94
- [30] Schwartz O, Pillow J W, Rust N C and Simoncelli E P 2006 Spike-triggered neural characterization *J. Vis.* **6** 484–507

Appendix 3

Manuscript 2: Correspondence between visual and electrical input filters of ON and OFF mouse retinal ganglion cells

Sudarshan Sekhar, Archana Jalligampala, Eberhart Zrenner, Daniel L. Rathbun

Published 12th June 2017 in the Journal of Neural Engineering

Abstract

Our goal was to investigate, if different visual cell types had characteristic electrical STAs. To this end, we performed experiments in which we provided full-field visual flash, visual and electrical white noise to the retina. The visual stimuli were used for cell classification, and the electrical noise was used to calculate electrical STAs. It was found that ON and OFF cells (classified based on the flash stimuli) had very distinct electrical STAs. While electrical STAs of ON cells correlated with a decrease in magnitude of the voltage stimulus immediately prior to spiking, electrical STAs of OFF cells correlated with an increase in the magnitude of voltage stimulus prior to spiking. Moreover, these electrical STAs were found to deviate from a classical sine wave, with regards to the amplitude and widths of their two phases. This result could explain why selective activation was not seen when sine wave shaped electrical stimuli were presented to the retina in isolation. Finally, we quantify the functional effects of photoreceptor loss and retinal rewiring by comparing the latency and widths of late-stage *rd10* electrical STAs to those of the wild type electrical STAs. We show that the latency and width of *rd10* STAs are significantly shorter. In general, while our central finding that ON and OFF cells have different electrical STAs is not definitive proof for preferential stimulation, it provides strong evidence that the use of systems engineering tools such as white noise analysis could hold the answer to some of the field's most challenging questions.

Contributions SS and DLR designed the experiments; SS executed the experiments and analysis; SS, AJ, DLR, and EZ composed the manuscript;

Correspondence between visual and electrical input filters of ON and OFF mouse retinal ganglion cells

S Sekhar^{1,2,3,4}, A Jalligampala^{1,2,3}, E Zrenner^{1,2,4} and D L Rathbun^{1,2,4}

¹ Institute for Ophthalmic Research, Eberhard Karls University, 72076 Tübingen, Germany

² Werner Reichardt Centre for Integrative Neuroscience (CIN), 72076 Tübingen, Germany

³ Graduate Training Centre of Neuroscience/International Max Planck Research School, 72074 Tübingen, Germany

⁴ Bernstein Centre for Computational Neuroscience Tübingen, 72076 Tübingen, Germany

E-mail: sudsa89@gmail.com (Sudarshan Sekhar) and daniel.rathbun@uni-tuebingen.de (Daniel Llewellyn Rathbun)

Received 28 April 2017

Accepted for publication 10 May 2017


Published 12 June 2017



Abstract

Objective. Over the past two decades retinal prostheses have made major strides in restoring functional vision to patients blinded by diseases such as retinitis pigmentosa. Presently, implants use single pulses to activate the retina. Though this stimulation paradigm has proved beneficial to patients, an unresolved problem is the inability to selectively stimulate the ON and OFF visual pathways. To this end our goal was to test, using white noise, voltage-controlled, cathodic, monophasic pulse stimulation, whether different retinal ganglion cell (RGC) types in the wild type retina have different electrical input filters. This is an important precursor to addressing pathway-selective stimulation. **Approach.** Using full-field visual flash and electrical and visual Gaussian noise stimulation, combined with the technique of spike-triggered averaging (STA), we calculate the electrical and visual input filters for different types of RGCs (classified as ON, OFF or ON–OFF based on their response to the flash stimuli). **Main results.** Examining the STAs, we found that the spiking activity of ON cells during electrical stimulation correlates with a decrease in the voltage magnitude preceding a spike, while the spiking activity of OFF cells correlates with an increase in the voltage preceding a spike. No electrical preference was found for ON–OFF cells. Comparing STAs of wild type and *rd10* mice revealed narrower electrical STA deflections with shorter latencies in *rd10*. **Significance.** This study is the first comparison of visual cell types and their corresponding temporal electrical input filters in the retina. The altered input filters in degenerated *rd10* retinas are consistent with photoreceptor stimulation underlying visual type-specific electrical STA shapes in wild type retina. It is therefore conceivable that existing implants could target partially degenerated photoreceptors that have only lost their outer segments, but not somas, to selectively activate the ON and OFF visual pathways.

Keywords: prosthesis, white noise analysis, preferential stimulation, linear systems analysis, retinal physiology

 Supplementary material for this article is available [online](#)

(Some figures may appear in colour only in the online journal)

Introduction

Retinitis pigmentosa (RP) and age-related macular degeneration are some of the leading causes of incurable blindness the world over. There has been much effort in recent years to find treatments for these diseases, with research being conducted in fields as diverse as stem cells, gene therapy, optogenetics and prosthetics [1–3]. Many of these approaches have shown great promise as viable treatment options. Retinal prostheses in particular have enjoyed the most success in the restoration of functional vision to RP patients. In fact, three prosthetic companies namely Second Sight, Retina Implant and Pixium Vision have received regulatory approval for their devices in 2011 (Argus-II), 2013 (Alpha-IMS), and 2016 (IRIS 2), respectively [2, 3].

The two main types of retinal prosthesis, categorized by site of implantation, are the subretinal (employed by Retina Implant) and epiretinal (employed by Second Sight and Pixium Vision). Typically, subretinal implants aim to engage the residual retinal network through bipolar cell stimulation while epiretinal implants target the retinal ganglion cells (RGCs) directly without activation of the network. This ability to preferentially stimulate the network versus RGCs directly is possible due to the difference in the ion channel types present in bipolar cells versus RGCs. RGCs prefer fast changing stimuli due to their high concentration of voltage-gated sodium channels which mediate action potentials, whereas bipolar cells and photoreceptors prefer slower changing stimuli due to their high concentration of calcium channels which regulate neurotransmitter release [4]. Although stimulation kinetics support such preferential stimulation from both epiretinal and subretinal locations, stimulation thresholds tend to be lowest for the most proximal neurons (RGCs for epiretinal electrodes, and bipolar cells for subretinal electrodes) [5]. Despite their different strategies, sub- and epiretinal implants both primarily use rectangular pulses of a fixed amplitude for activation of the retina, probably due to their effectiveness in other medical devices such as cochlear implants and pacemakers etc [6, 7].

In recent years there has been a growing body of work exploring alternate waveforms like sine waves [8] and pulse amplitude modulation patterns such as diamond, triangular, sawtooth and random [9] in order to stimulate the retina. The primary motivation for this work is the belief that the present pulsatile stimulation paradigm could be sub-optimal (e.g. due to its inability to selectively stimulate selected visual pathways) and that alternate stimulation waveforms could help resolve this problem. For example, Twyford and Fried showed in wild type rabbit retina that ON and OFF sustained and BT cells respond to the different phases of an ongoing sine wave [8]. Additionally, we recently showed that RGCs can be activated by a stream of subthreshold pulses [10]. In particular this ability to activate the retina through subthreshold electrical stimulation opens up a whole new way of probing the question, ‘What is an RGC’s preferred electrical stimulus pattern?’ through the use of white noise stimulation, both electrical and visual [11].

Prior to Twyford and Fried, Freeman *et al*, also showed that ON and OFF cells respond to different phases of a low frequency

sine wave [4, 8]. Likewise, Twyford *et al* also showed that strategic amplitude modulation could differentially activate RGCs through direct stimulation [12]. However, to our knowledge there has been no systematic examination of how different patterns of indirect (network) activation of RGCs correspond to specific RGC types. In this study we present the first systematic comparison of the retinal network’s electrical and visual temporal input filters based on white noise stimulation. To best characterize the cell type, we quantified the full-field flash response with an ON/OFF selectivity index [13]. Examination of both flash and Gaussian noise responses indicates a clear correspondence between RGC cell type and its electrical input filter.

Methods

The main aim of this study was to test whether electrical input filters (also called spike-triggered averages or STAs) differ between ON and OFF RGCs. Each experiment (figure 1) began with a block of full-field flash stimulation followed by a block of full-field temporal visual Gaussian white noise, and then a ~100s block of spontaneous activity before starting electrical white noise stimulation in 100s stimulus blocks. Following electrical stimulation we recorded one more set of flash, visual Gaussian white noise and spontaneous activity blocks.

To test the hypothesis that ON and OFF cells differ in their electrical STAs, we pooled data from three related studies. The main data set of 27 cells came from a previous study using 54 non-repeating (unique) electrical noise stimulus blocks (90 min total), 80 s flash stimulus blocks and 50 s visual white noise blocks [10]. Another data set, consisted of 13 cells which had been shown 18 blocks of repeating (frozen) and 18 blocks of non-repeating electrical noise (60 min total) in an interleaved fashion. Flash stimulus blocks were 160 s long before electrical stimulation and 80 s long after electrical stimulation. This data set was used to validate the pooling together of E-STAs calculated under repeating versus non-repeating stimulus paradigms and was the only wild type data set where we did not present visual noise stimulation. The final set of 6 cells received 36 blocks of repeating noise (60 min total), 80 s flash stimulus blocks and 50 s visual white noise blocks. We supplemented these wild type data with 31 RGCs from *rd10* retina, which, barring the visual noise stimuli, had an identical experimental design to the main set of 27 cells.

Animals

Except where noted, the methods used in this study matched those we have reported in our previous study [10]. Here we examine the data from 46 RGCs collected from 12 retinal pieces using 11 wild type C57BL/6J mice aged 2 × P32, 2 × P39, 1 × P46, 1 × P51, 1 × P56, 1 × P58, 2 × P59, 1 × P64 and 31 RGCs from three retinal pieces of two *rd10* mice aged P84 (The Jackson Laboratory, Bar Harbor, ME, USA). Based on the frequency of occurrence of the main RGC types (ON, OFF and ON-OFF), this should provide sufficient sampling of these three categories [14]. All

experimental procedures have approval of the state authorities (Regierungspraesidium, Tuebingen) and were conducted under the supervision of the Tuebingen University facility for animal welfare (Einrichtung fuer Tierschutz, Tieraerztlichen Dienst und Labortierkunde) and the NIH Guide for the Care and Use of Laboratory Animals.

Data collection

All mice were anesthetized with CO₂ inhalation and killed by cervical dislocation. The eyes were then removed and dissected quickly to ensure that retinas were perfused with carbogenated ACSF (artificial cerebrospinal fluid) maintained at 33 °C (using a heating plate and heated perfusion cannula) and 7.4 pH within 10 min of death. All data was collected from isolated retina mounted on a standard 60-channel microelectrode array (MEA, 60MEA200/30iR-ITO, Multi Channel Systems, Reutlingen, Germany), constantly perfused with ACSF. Due to the difficulties of stimulating and recording from opposite sides of the retina, and the ability to stimulate the network both epi- and subretinally [5, 15], the retina was placed ganglion cell side down on the MEA. Thus, both stimulation and recording were epiretinal. A single electrode on the MEA was used to deliver electrical stimulation. Only the 7–8 electrodes immediately surrounding the stimulating electrode were analysed (interelectrode distance = 200 or 283 μm). Voltage traces were sampled with MultiChannel Systems hardware (MCS, Reutlingen, Germany) at a rate of 50 kHz/channel, using a filter bandwidth of 1 Hz–3 kHz and a gain of 1100.

Data processing and inclusion criteria

Offline Sorter (Plexon Inc., TX, USA) was used to process the raw data. Raw data were high-pass filtered before putative action potential events (spikes) were extracted. Automated and manual spike sorting were applied to minimize Type I and Type II errors in attribution of waveforms to different sources [10]. Spike trains included in this study exhibited (1) the presence of a clear lock-out period in the ISI histogram and autocorrelogram (2) the absence of a peak in the cross-correlogram between different cells which would indicate that a single cell had been wrongly split into 2 or more units (3) good separation in principal component space of a biphasic waveform whose shape is typical of extracellularly recorded action potentials and (4) stability of the waveform shape and firing rate over the entire experiment. These were the cell inclusion criteria. Time stamps of these sorted spikes were collected with NeuroExplorer (Plexon Inc., TX, USA) and exported to MATLAB. All analyses and statistical tests were performed in MATLAB (The Mathworks, Natick, MA).

Visual stimulation

Flash stimulus blocks consisted of cycling 2 s ON (40 klx) and 2 s OFF (20 lx) full-field luminance (mean illuminance = 20 klx, 99.9% Michelson contrast). For the 50 s visual white noise blocks, the brightness of each stimulus frame was

drawn randomly from a Gaussian distribution with 35% contrast (i.e. standard deviation, SD, of the Gaussian distribution was 35% of the mean, which was also 20 klx) at the rate of 10 Hz. Visual stimuli were presented with a linearized, commercially available DLP-based projector (K10; Acer Inc., San Jose, California, USA). Other than during visual stimulation, a shutter was placed in front of the projector and the experimental setup was surrounded by dark curtains with room lights turned off to minimize stray light.

Electrical stimulation

Our aim was to test our hypothesis, that there is a correspondence between electrical spike-triggered averages (STAs) and visual response type. Therefore, we presented 1 ms long voltage pulses whose amplitudes were drawn randomly at a rate of 25 Hz from Gaussian distributions with mean -800 mV and SD 35%. The choice of 1 ms long voltage pulses is well established amongst subretinal implants [16, 17] and are comparable to biphasic current pulses [18–20]. The stimulus pulses were programmed in MATLAB using custom scripts and imported into MC-Stim (MCS, Reutlingen, Germany) for presentation. A stimulus generator (STG 2008, MCS, Reutlingen, Germany) was used to generate pulses.

Analysis

Electrical and visual STAs (E-STAs and V-STAs, respectively) were calculated by averaging the ± 1 s of stimulus surrounding each spike. Significance testing of STA deflections has been described previously [10]. Briefly, the maximal upward- and downward-going deflections from the mean, preceding time zero, were first detected. These deflections were judged to be significant if they were statistically distinguishable from the 1 s of noise following time zero. Once an STA passed this initial criterion, it was cubic spline interpolated at intervals of 1 ms. The deflection with the shorter latency was assigned to be D_1 . The width of D_1 was defined as the full span of time around the D_1 maximum over which the STA did not cross the stimulus mean. The latency of D_1 was defined as the time of the maximal point of the deflection. Once the STA crossed the stimulus mean to the left of D_1 , the maximal point of the STA from that crossing to the next crossing was tested for significance. If it was significant, this longer-latency deflection was assigned to be D_2 , otherwise, the cell was not assigned a D_2 . The procedure for width and latency calculation of D_2 were identical to D_1 . We were only interested in examining integrative electrical responses, so the contribution of single-pulse activations to the E-STA was removed by setting the first time point of each E-STA to the stimulus mean (see supplement 1 (stacks.iop.org/JNE/14/046017/mmedia)). Example voltage response curves demonstrating the voltage-dependency of single-pulse activation can be seen in supplement 2.

For comparisons of visual and electrical responses (figures 4 and 6), the short latency deflection of the STA (D_1) was used. Deflections demonstrating a decrease in voltage magnitude or brightness relative to the stimulus mean were negatively

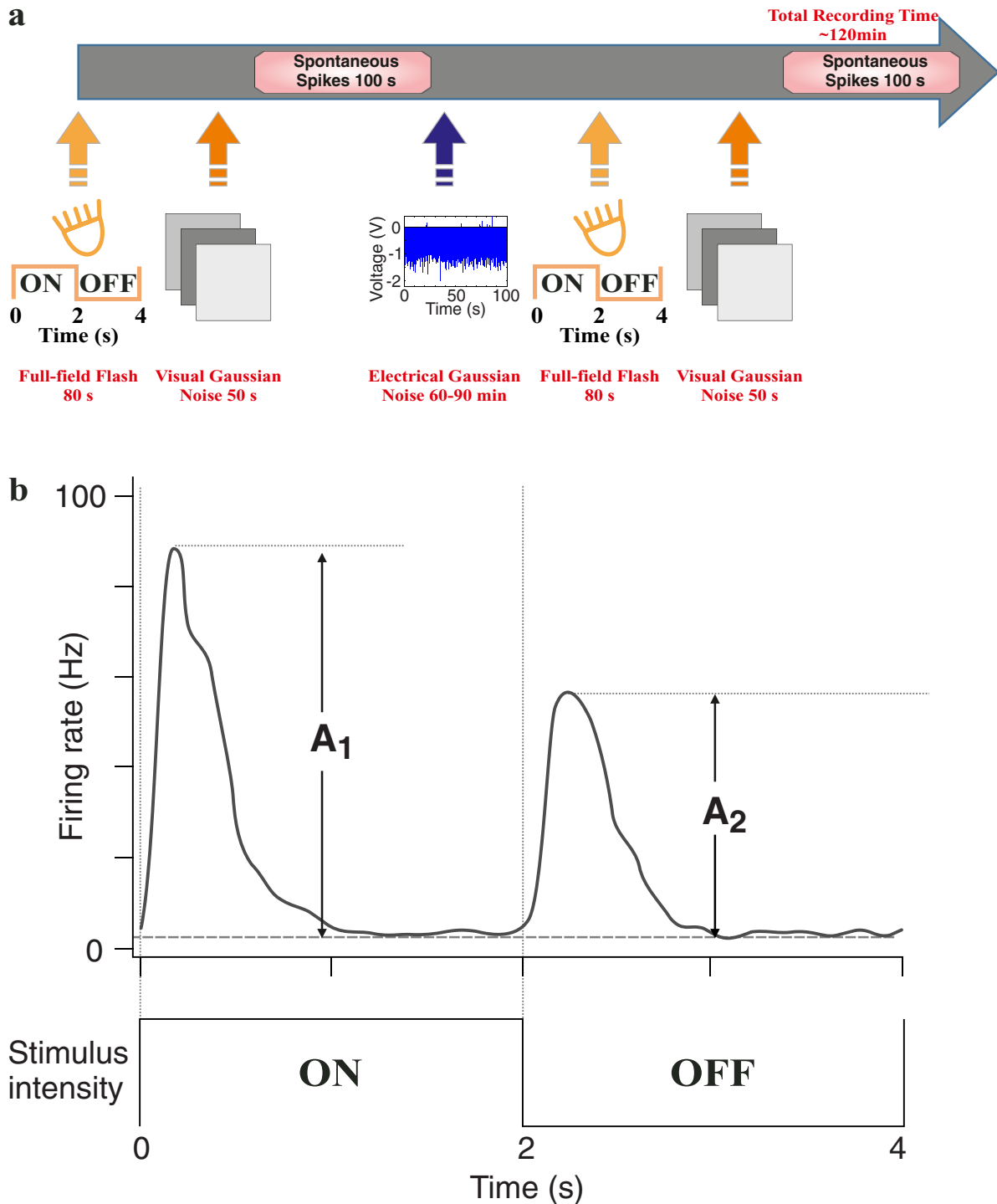


Figure 1. Methods. (a) Experimental design: full-field flash (20 repetitions of 2 s ON and 2 s OFF) and visual full-field Gaussian noise (50 s at 10 Hz) were presented at the start and end of each experiment to classify RGCs. The primary stimulus was at least one hour of electrical noise presented in 100 s blocks. (b) Cell classification. Spike time histograms of the flash responses were quantified according to Carciari *et al* [13] (see *Methods*).

signed while the converse were positively signed. When comparing the first and second deflections of the E-STA (figure 5), the term ‘upward’ was used for negatively signed deflections while ‘downward’ was used for positive deflections to reflect their orientation as displayed. Electrical STAs were burst corrected as described in [10], and include singleton spikes that were not part of a burst. The inclusion of singleton spikes did not significantly alter the E-STA. Spiking events with an

onset latency within 10 ms following a voltage stimulus pulse were disregarded to exclude direct RGC stimulation from our analysis.

The responses to flash stimulation were quantified according to the methods of Carciari *et al* [13] (figure 1(b)). Briefly, a mean peristimulus time histogram (PSTH) was generated using 10 ms bins. The PSTH was smoothed with a Gaussian filter ($\sigma = 50$ ms). The maximal firing rate of each phase was

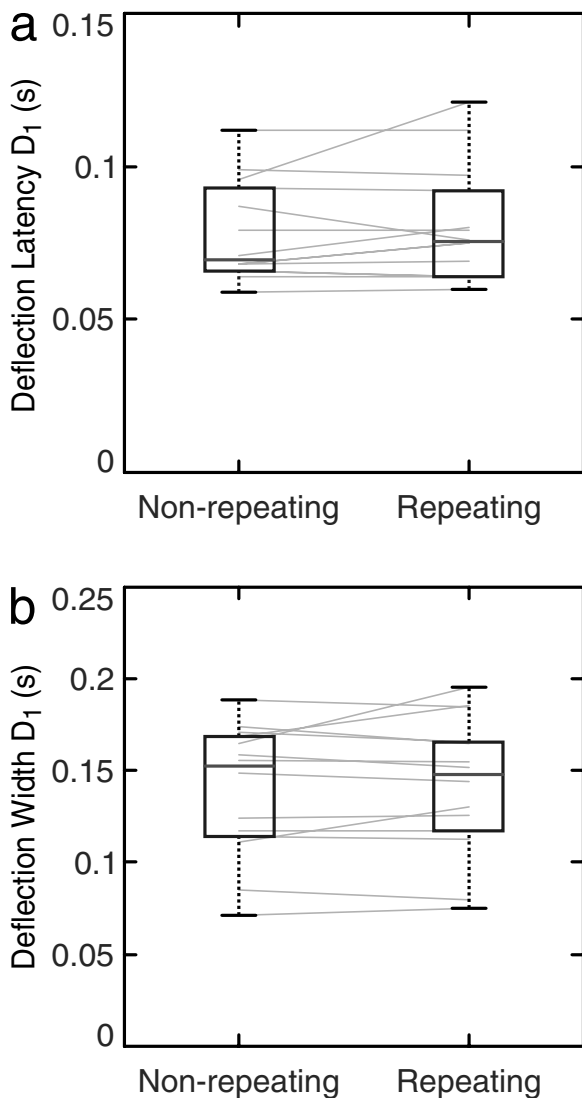


Figure 2. Comparison of responses to repeating and non-repeating electrical noise stimuli. (a) Latency of the short-latency E-STA deflections calculated using 18 trials of non-repeating white noise versus 18 trials of repeated white noise, interleaved. (b) Width of the short-latency E-STA deflections calculated using 18 trials of non-repeating white noise versus 18 trials of repeated white noise.

identified to determine its latency and amplitude. An ON/OFF index was calculated from the amplitudes of ON (A_1) and OFF (A_2) responses according to the equation, $(A_1 - A_2)/(A_1 + A_2)$, such that ON cells have a large positive index bounded by 1, OFF cells have a large negative index bounded by -1 , and ON-OFF cells have indices around 0. In scatterplots, cell colour was based on the ON/OFF index with OFF cells < -0.5 coloured blue, ON cells > 0.5 coloured red and ON-OFF cells between these two cut-off values coloured black.

Results

We recorded spike trains from 57 wild type mouse RGCs. Because electrical white noise was presented during the bulk of the recording time, cells which responded to visual stimulation, but not to electrical, were very difficult to isolate. Therefore, the majority of effectively isolated spike trains

were from RGCs that responded during electrical stimulation ($n = 46$). Of these, 33 cells also had visual STAs. We also recorded from 36 *rd10* mouse RGCs, 31 of which had significant E-STAs.

Following up on our previous work [10], we first addressed the concern that calculating electrical STAs (E-STAs) from repeated presentation of the same noise stimulus could influence the STA shape due to overfitting. This comparison was done based on 13 RGCs which were shown 18 blocks of 100s repeating (frozen) and 18 blocks of 100s non-repeating electrical Gaussian white noise interleaved (-800 mV, 25 Hz, 35%). The distribution of the D_1 latency and widths of the E-STAs obtained under these two different conditions were found to be comparable with no statistically significant difference (figure 2; $p > 0.05$, paired two-tailed t -test). This therefore justified the pooling of the above mentioned sets of 27 and 6 cells described in *Methods*. Except for figure 2, all subsequent figures in this paper, containing analysis of these 13 cells was done with all 36 trials of electrical noise.

Finally, in order to understand how the electrical input filters change with photoreceptor loss and retinal rewiring (as seen in patients with RP) we also collected data from 31 RGCs obtained from late stage degenerate *rd10* mice. The *rd10* cells were subject to the identical 54 non-repeating electrical noise stimuli as the core set of 27 cells mentioned above.

Example cells (figure 3) demonstrate our main result that ON and OFF RGCs had electrical STAs (E-STAs) that were well-matched to their visual response type; and that ON-OFF cells often did not follow this pattern. Specifically, ON cells had an upward deflection in both their visual STA (V-STA) and E-STA shortly preceding time zero; whereas, OFF cells had a downward short-latency deflection (D_1) in each STA.

Visual response classification

The visual stimuli (a flash followed by visual Gaussian noise) were only presented at the beginning and end to ensure uninterrupted electrical stimulation during the main experiment. For our 33 cells that were shown both flash and visual noise, flash trials #1–20 were recorded at the beginning of the experiment, whereas trials #21–40 were recorded at the end after at least an hour of electrical stimulation (figure 3, bottom row). All flash response repetitions were used to categorize cells. As indicated by their ON/OFF indices (see *Methods*), the three example cells were classified as ON, OFF and ON-OFF, respectively (figure 3, bottom row). Visual STAs were also calculated from all presentations of the visual noise stimulus. The sign of the short latency V-STA deflection always matched flash response based classification of ON and OFF cells. For the set of 13 cells which were not shown visual noise, we presented 40 flash trials prior to electrical stimulation and 20 flash trials following electrical stimulation. All 60 trials were used to calculate the ON/OFF indices.

E-STAs correspond to cell type

Comparison of the flash stimulus-derived ON/OFF selectivity index with the direction of the short-latency E-STA deflection

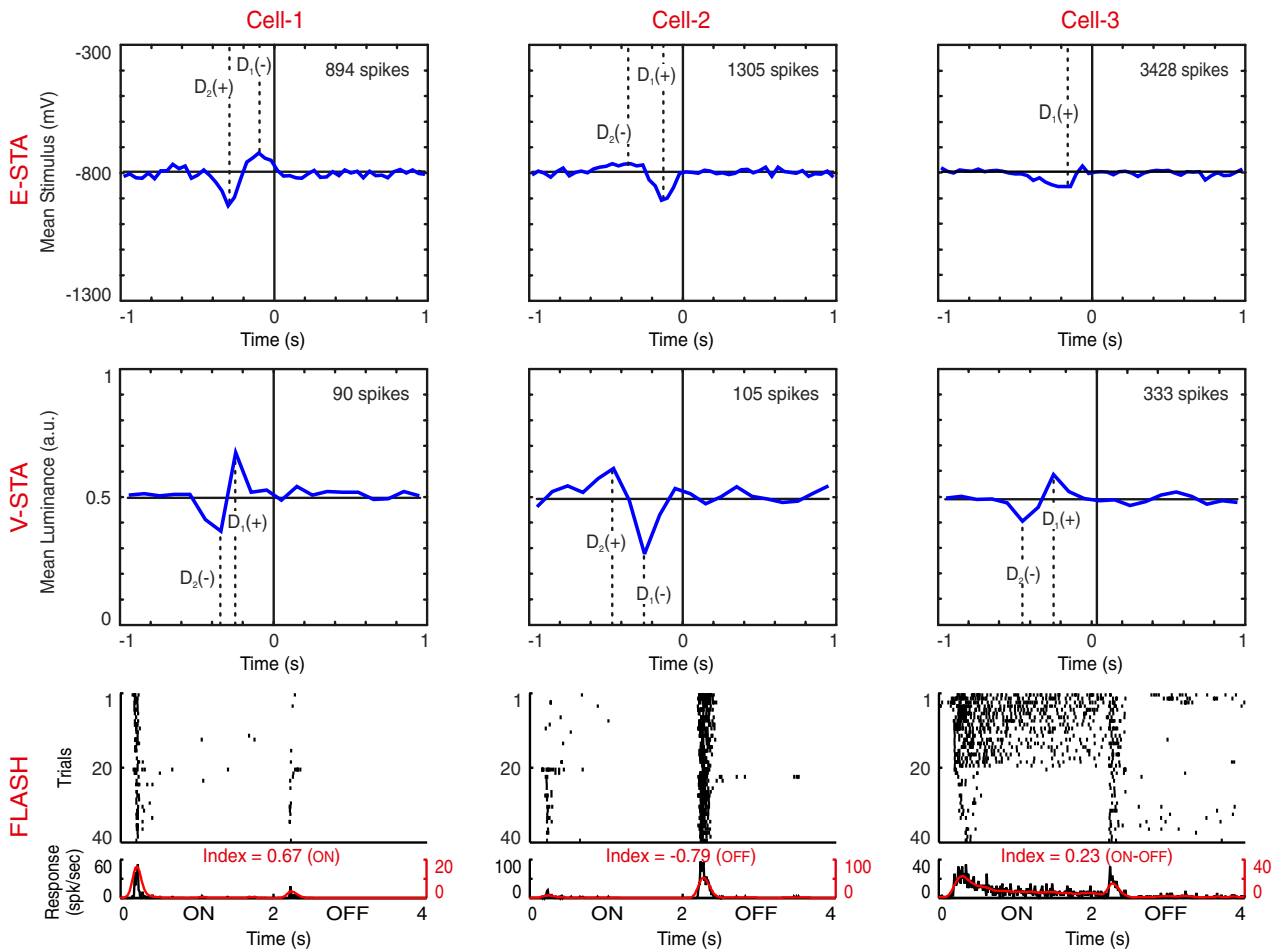


Figure 3. Example cell responses. (Top row) Electrical spike-triggered average (E-STA), (middle row) visual STA (V-STA), (bottom row), flash response spike rastergram and peristimulus time histogram (PSTH) from beginning and end of experiment. The smoothed PSTH (overlaid line corresponding to right vertical axis) was used to classify cell type. Note that an upward V-STA deflection indicates an increase in light immediately prior to response whereas an upward E-STA deflection indicates a decrease in cathodic (negative) voltage magnitude prior to response. Short latency STA deflections are labelled D_1 and the sign of the deflection is indicated. Longer latency deflections, when present, are labelled D_2 .

(negative for upward, positive for downward) demonstrates the robustness of our main result across the population of 46 wild type RGCs (figure 4). While all 20 ON cells had negative deflections and 10/11 OFF cells had positive deflections, ON-OFF cells showed both signs (11 negative, 4 positive) with no apparent correlation between the ON/OFF index and E-STA deflection sign. One reason for this could be our simplistic full-field visual stimuli. Perhaps with more sophisticated stimulation to better discriminate RGC types (e.g. see [14]) or analysis tools such as spike-triggered covariance [21], we might find correlations between electrical and visual responses for ON-OFF cells. Further examination of the deflection latency (figure 4(a)) and width (figure 4(b)) also reveals no clear correlation between latency or width magnitude and the ON/OFF index.

E-STA variability

We next examined the relationship between upward and downward deflections in the E-STA (figure 5). The majority of cells (36/46) had biphasic E-STAs (both upward and downward

deflections were significant). The remaining ten cells had monophasic E-STAs (only significant upward or downward deflection). As already noted, upward deflections had shorter latencies than downward deflections (if present) for all ON cells, whereas downward deflections had shorter latency than upward deflections (if present) for most OFF cells (figure 5(a)). Similar to latencies, we found that upward deflection widths were greater for most OFF cells while downward deflection widths were greater for most ON cells (figure 5(b)). Note that unsigned deflection widths and latencies are used for these figures.

To test whether whole-wave sinusoids might reasonably approximate the biphasic E-STA shapes, we examined the ratios of latencies, widths and amplitudes for D_1 and D_2 . The geometric mean ratio of latencies ($D_1:D_2$) was 0.32, well matched to the 1:3 ratio that would be expected for a sinusoid. In contrast, the geometric mean ratio of widths was 0.48, which is well below the 1:1 ratio that would be expected for sinusoids, indicating that D_2 widths tend to be about twice as broad as D_1 widths. Likewise, the geometric mean ratio of amplitudes, which should be close to 1:1 for sinusoids, was actually 1.52, reflecting that D_2 was almost always weaker

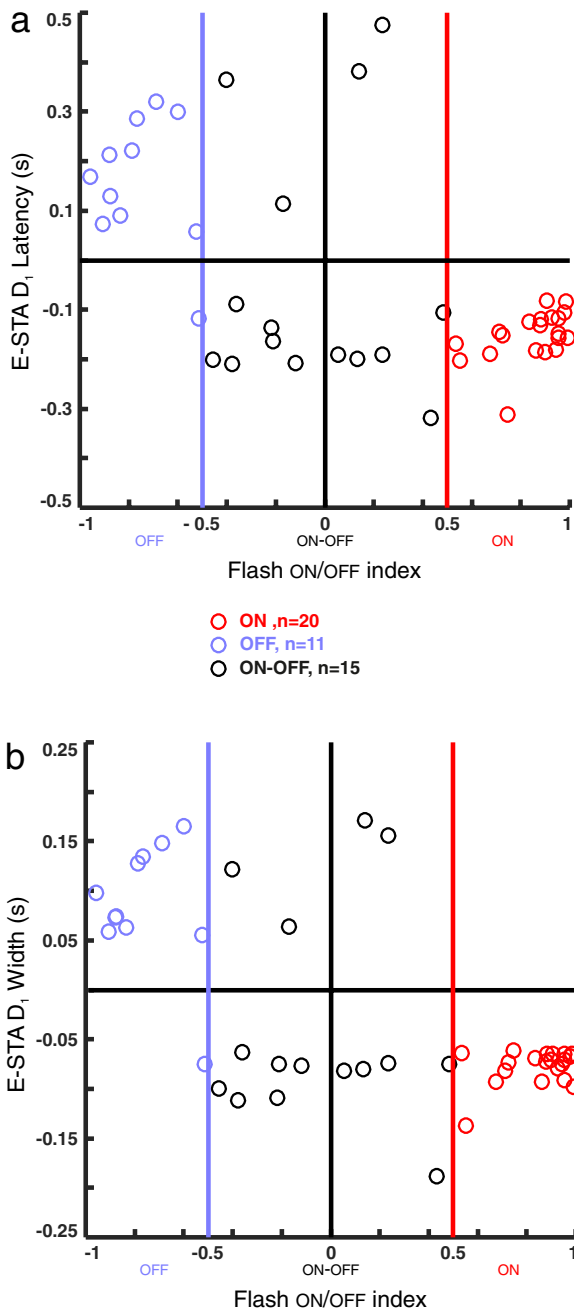


Figure 4. E-STA corresponds to ON/OFF classification index. (a) Latency of the short latency deflection (D_1) plotted against each cell's ON/OFF index. (b) Width of D_1 plotted against each cell's ON/OFF index. By convention, width and latency of D_1 in the E-STA which correspond to a decrease in voltage magnitude (upward deflections) are negatively signed. Red markers represent ON cells (ON/OFF index > 0.5), and blue markers are OFF cells (ON/OFF index < -0.5). Black markers represent ON-OFF cells. Vertical red and blue lines separate ON-OFF cells from ON and OFF cells, respectively.

than D_1 . Examined together, these results indicate that, while a sinusoidal electrical waveform may be a good first approximation to these STAs, significantly more effective electrical stimulation may be achievable with waveforms that better match the E-STA shape.

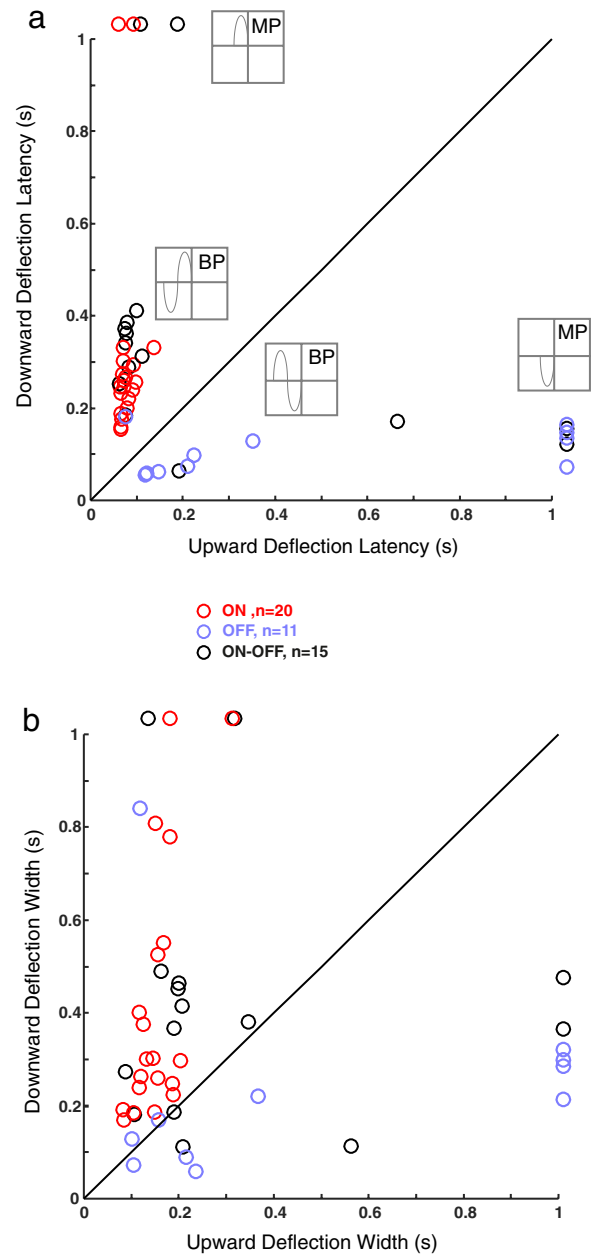


Figure 5. Variability in E-STA shape. (a) For biphasic cells, E-STA downward deflection latency plotted against upward deflection latency. Monophasic cells with no long latency deflection are placed outside the plot area for the missing value. Icons show the basic E-STA shape for each cluster of cells (BP biphasic, MP monophasic). (b) E-STA downward deflection width plotted against upward deflection width. As in (a), missing values are placed outside the plot area. Note, deflection widths and latencies are unsigned in this figure.

Comparison of E-STAs and V-STAs

Although V-STA responses are good at predicting flash responses [22] it is not a certainty that the two will always match. This is because the complex interaction of early and late response phases of receptive field centre and surround inputs can have a profound effect on the STA. Such an effect is most notable in ON-OFF cells for which the sign of the

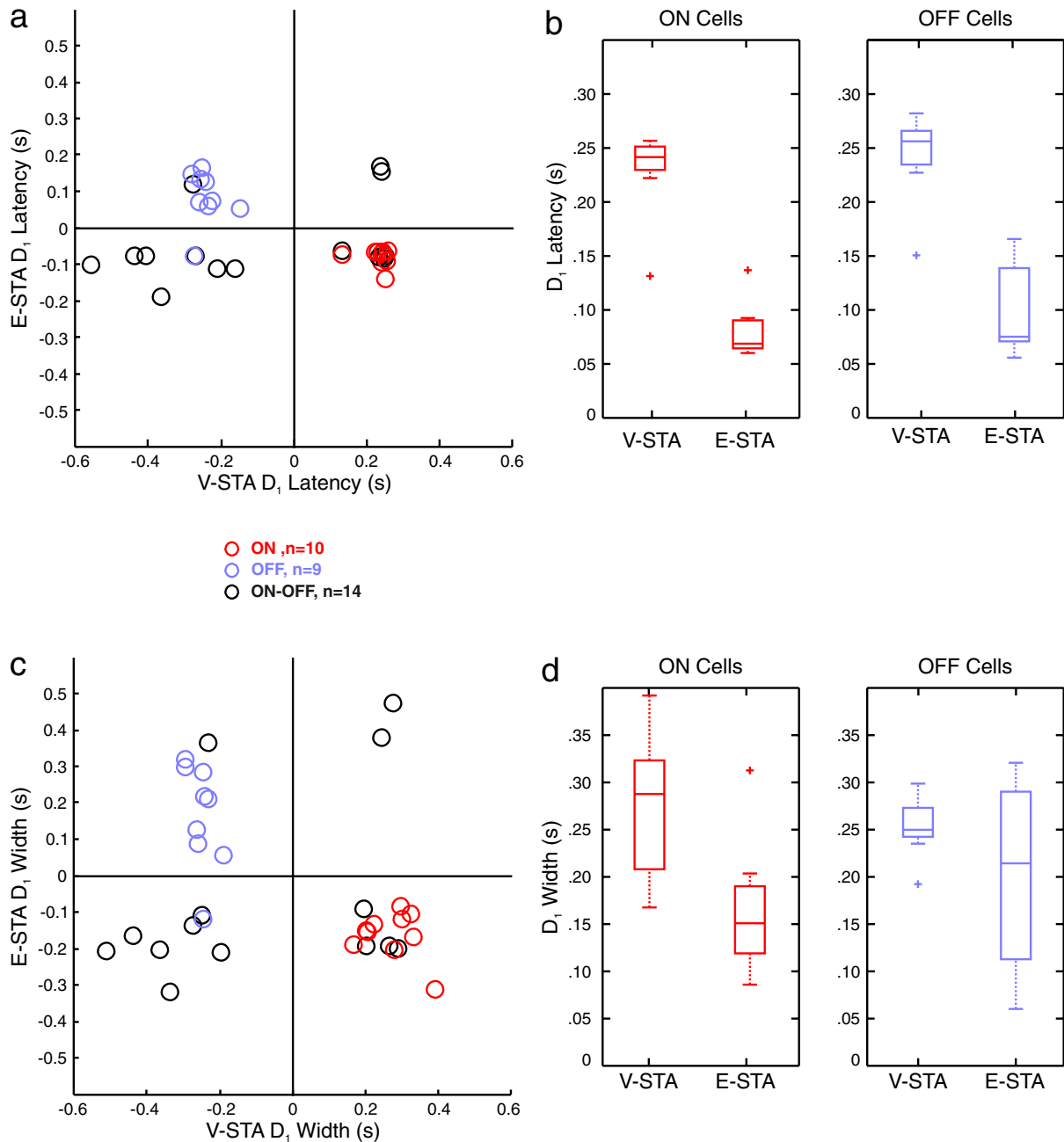


Figure 6. Comparison of E-STA to V-STA. (a) Scatterplot of D_1 latencies. (b) Comparison of D_1 latency distributions. (c) Scatterplot of D_1 widths. (d) Comparison of D_1 width distributions. Values in (a) and (c) are signed as in figure 3; values in (b) and (d) are unsigned.

short latency V-STA deflection could be either an upward ON response (+sign) or a downward OFF response (−sign) depending on the relative timing and weighting of ON and OFF inputs. Therefore, we also examined the relationship of D_1 latencies and widths for E-STAs and V-STAs (figure 6) for the 33/46 cells which had been presented visual noise in addition to flash and electrical noise. We found the same correlations for ON and OFF cell types as shown in figure 4. Specifically, negative deflections of the E-STA were associated with positive V-STA deflections—as would be expected for ON cells. Likewise, positive E-STA deflections (associated with OFF cells) corresponded with negative V-STA deflections; and the ON–OFF cells could be found in all four quadrants of the

scatter plots (figures 6(a) and (c)). Comparing ON cells to OFF cells, both widths and latencies of E-STAs were found to be well matched ($p > 0.05$, two-tailed Student’s t -test), indicating that an ON E-STA can be considered equivalent to an OFF E-STA that has been inverted around the mean (figures 6(b) and (d)). Although not included in this figure, the additional set of 13 cells without V-STAs does not change this last result. Comparing E-STAs to V-STAs, both latencies and widths were smaller for E-STAs in ON cells, while only latencies were smaller for E-STAs in OFF cells ($p < 0.05$). These faster E-STAs suggest that, though the visually and electrically activated mechanisms may be similar, they are unlikely to be identical.

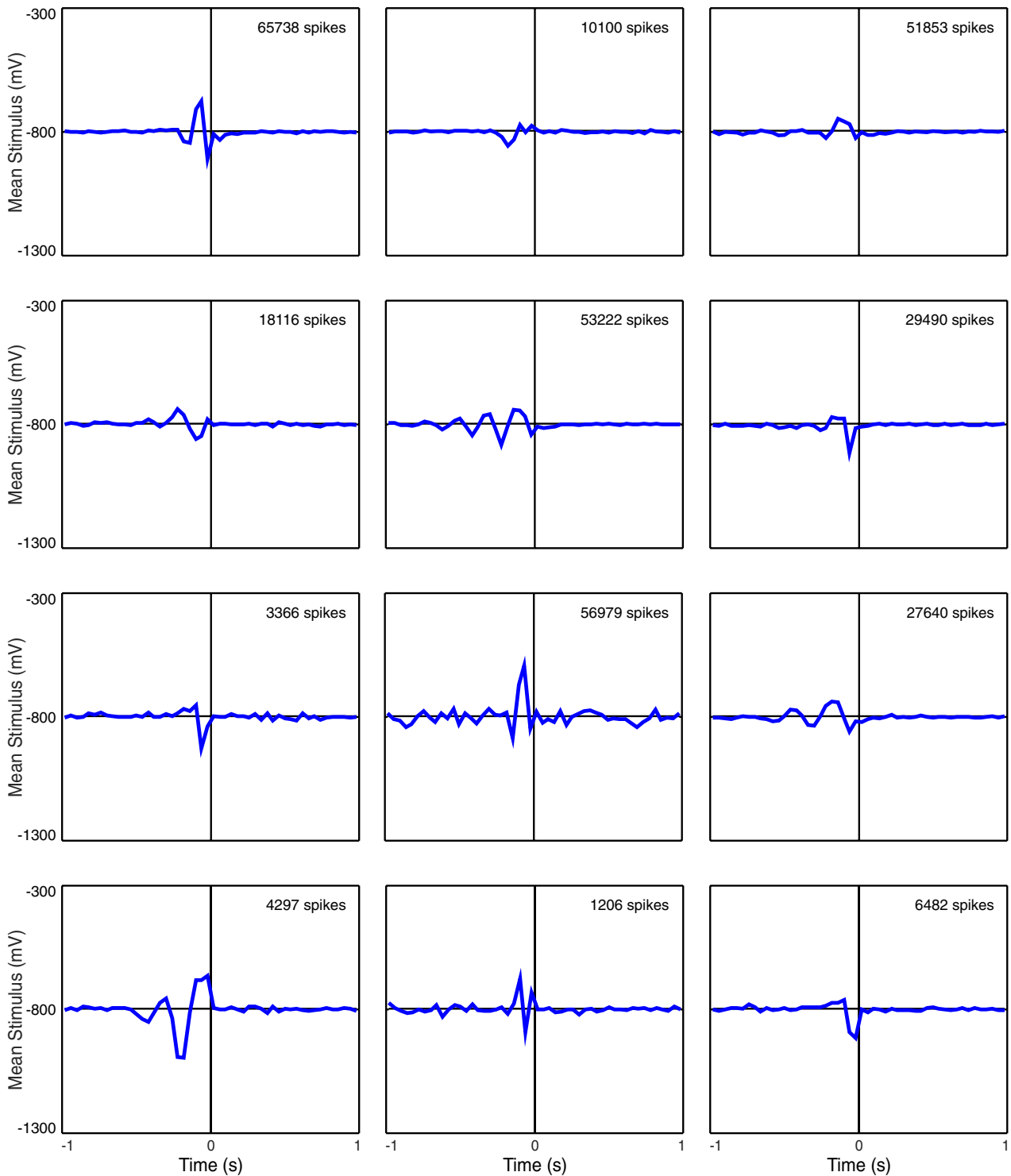


Figure 7. Example E-STAs from P84 *rd10* RGCs.

Comparison of wild type and *rd10* E-STAs

Since the majority of present implants are used in patients who have been blind for many years, we wanted to determine whether E-STAs in the wild type retina differ from those in late stage degenerate retina. Figure 7 shows 12 example *rd10* E-STAs representing the diversity of shapes observed across 31 *rd10* RGCs.

Comparing the first significant deflections immediately preceding zero of *rd10* E-STAs to those of the 46 wild type E-STAs, we found that both latencies and widths in *rd10* are significantly shorter in comparison to the wild type retina (figure 8; two-tailed *t*-test, $p < 0.05$). These differences demonstrate that the loss of photoreceptors and subsequent rewiring in diseased retina significantly alters the E-STA. Such changes are consistent with photoreceptor stimulation

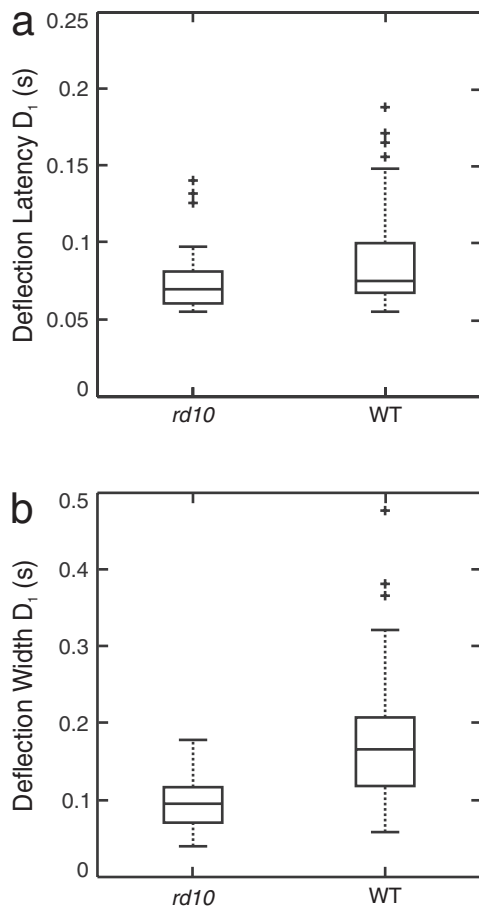


Figure 8. Comparison of E-STAs between wild type (WT) and *rd10* RGCs. (a) D_1 latencies. (b) D_1 widths. Values are unsigned.

underlying the slower, broader E-STA shapes found in the healthy retina.

Discussion

The main aim of this study was to verify if the major visual pathways (ON, OFF and ON-OFF) in the wild type mouse have different electrical input filters. Though there have been studies that show that different RGC types vary in their responses to electrical stimulation [12, 23, 24] and that ON and OFF cells respond to different phases of an ongoing sine wave [8], there has to date been no comparison of the electrical input filters of these different RGC types. Our study is, to our knowledge, the first comparison of an RGC's temporal electrical and visual input filters based on cell type. Our demonstration that there is a correspondence between the visual and network-mediated electrical input filters of different RGC types adds strong support to the growing body of literature on selective stimulation. Moreover, we have demonstrated the effectiveness of using white noise analysis in the field of retinal prosthetics as a tool to address important unanswered questions.

In this study we have shown that the E-STAs of ON cells have a short latency upward deflection (corresponding to decreasing voltage magnitude) while the E-STAs of OFF cells have a short latency downward deflection (corresponding to

increasing magnitude). This implies, that in theory selective stimulation of these RGC types should be possible. Previous studies foreshadowed this result by demonstrating that ON and OFF cells respond during opposite phases of an ongoing sine wave electrical stimulus [4, 8]. Extrapolating from these present and previous results, we hypothesize that a pulse train modulated by the diminishing phase of an electrical sinusoid in the range of 1–10 Hz presented epiretinally, would preferentially activate ON cells while the rising phase would preferentially activate OFF cells.

Because degenerate *rd10* E-STAs are faster and narrower than wild type E-STAs, it appears that photoreceptor stimulation makes a significant contribution to the E-STA in the wild type retina. It is quite likely, therefore, that the mirror-inverted E-STAs found for ON versus OFF cells reflect the sign inverting and sign preserving synapses of photoreceptors onto the ON and OFF bipolar cell pathways, respectively. If photoreceptor stimulation underlies these visual type-specific E-STAs, it becomes unclear how they could be used in patients blinded by photoreceptor degeneration. Fortunately, photoreceptors persist in the degenerating retina long after their outer segments have been lost [25]. Therefore, presuming that such residual photoreceptors maintain their synaptic connections, it may still be possible to selectively stimulate ON and OFF pathways in the early stages of degeneration.

Regarding the shape of our E-STAs, though a half- or full-period sinusoid might be the simplest approximation of our E-STAs, it might not necessarily be the best. Looking at the distribution of biphasic E-STA latencies, widths, and amplitudes, we see that there is considerable variability between D_1 and D_2 . Specifically, while the mean latency ratio $D_1:D_2$ matches a sinusoid approximation of the STAs, neither amplitude or width ratios matched this approximation. Whereas amplitudes tended to be greater for D_1 , widths tended to be greater for D_2 . These observations suggest that, though sinusoids should be able to preferentially stimulate different pathways in the wild type retina, they might be too simplistic an approximation. This concern is reinforced by an absence of cell type-specific stimulation even when such stimuli were presented [26]. Possibly sinusoids which have an asymmetry in the size and widths of their upward and downward deflections should be investigated.

Limitations and future work

Though the results of this study are novel and interesting, it must be remembered that the data central to this paper were collected from the wild type retina so that cells could be visually classified. Consequently the RGC type-specific E-STAs presented here appear to have a strong photoreceptor contribution. However for cell-type specific stimulation based on E-STAs to be most useful in retinal prosthetics, it must work in the degenerated retina in which most photoreceptors are gone. Therefore, in order to verify if we could obtain E-STAs in late-stage, degenerated retinas where the majority of photoreceptors are lost and the network has undergone significant rewiring [27], we repeated these white noise experiments in

P84 *rd10* mice. We found that it is possible to obtain diverse E-STA filters even in the *rd10* retina. Such short, multipulse STAs were also shown in degenerated RCS rats in a recent conference presentation [28]. Unfortunately because it is not possible to correlate these E-STAs to visual cell type in late stages of degeneration, it will be necessary to develop non-visual techniques for cell type classification in order to determine if specific degenerate E-STAs correspond to specific RGC types.

In the present work, cell-type specific filters appear to be mediated by either inhibition or excitation of photoreceptors which consequently activates ON and OFF bipolar cells, respectively—a multiplexing of the photoreceptor signal. Such cell-type specific filters may still be found in the degenerated retina due to the relatively intact synaptic connections of the inner plexiform layer (IPL). For example, in the wild type retina rod ON bipolar cells, through A-II amacrine cells, multiplex their signal into ON and OFF signals in cone bipolar cells [29]. Although the outer plexiform layer (OPL) circuitry is compromised, there is no current evidence that this IPL circuit is non-functional in the degenerated retina. As the most numerous bipolar cell type [29], with well-preserved inner retinal connections [25], rod bipolar cells may be a particularly attractive target for prosthetic stimulation. Though these are interesting possibilities to explore in future research, they are however beyond the scope of the present manuscript. Moreover, the significance of our main result does not rely on the possibility of achieving cell-type selective stimulation without photoreceptors. Rather the significance is the correspondence between electrical input filter and cell type which has never before been published.

Conclusions

To conclude, we used the tools of temporal white noise stimulation and linear systems analysis to show that ON and OFF cells have distinct electrical input filters. This in turn reflects the successful application of STA analysis to the field of prosthetic vision, which has, till date, been largely absent. Our demonstration that the sign of the short latency deflection correlates between visual and electrical STAs (given that the cell is either ON or OFF), not only provides insight into selective stimulation of retinal pathways, but also, in the broader sense, represents a significant shift from the present method used in prosthetic research of examining parameters one at a time (e.g. frequency, duration, amplitude, etc) to a linear systems method in which the parameter space is more efficiently sampled [11]. It also demonstrates that electrical STAs are sensitive enough to reveal such variability. Although not definitive proof that such variable STAs are applicable to prosthetic stimulation, this result opens the door to such a possibility and necessitates that more research be conducted to fully explore the implications of this new method. Additionally these STAs suggest that half- or full-period sinusoids, which have been previously used for retinal stimulation, might be too simplistic, ignoring

the diversity of electrical filters found across RGCs. Based on these initial results, we feel that the systems approach of using white noise stimulation could hold the key to understanding how to selectively stimulate the varied visual pathways remaining in the degenerated retina.

Acknowledgments

Funding

Core funding for this study was provided by the German Federal Ministry of Education and Research (BMBF; 031 A 308). This study is part of the research program of the Bernstein Centre for Computational Neuroscience, Tuebingen, funded by the BMBF (01GQ1002). Additional support was received from the German Ophthalmology Society (DOG), the PRO RETINA foundation for prevention of blindness, the Tistou and Charlotte Kerstan Foundation, and the Werner Reichardt Centre for Integrative Neuroscience (CIN) at the Eberhard-Karls University of Tübingen. The CIN is an Excellence Cluster funded by the German Research Foundation (DFG) within the framework of the Excellence Initiative (EXC 307, including the senior professorship of Eberhart Zrenner).

Author contributions

SS and DR designed the experiments; SS executed the experiments and analysis; SS, AJ, DR and EZ composed the manuscript. We thank Klaudija Masarini and Norman Rieger for their excellent technical assistance.

Competing financial interests

DR has received surplus equipment on loan and minor support for supplies from Retina Implant AG. EZ is Advisor to Retina Implant AG, stock holder and co-inventor of patents held by this company. However, Retina Implant AG had no influence on the planning and execution of the project presented here.

We therefore declare no competing financial interests.

References

- [1] Sahel J A and Roska B 2013 Gene therapy for blindness *Annu. Rev. Neurosci.* **36** 467–88
- [2] Zrenner E 2013 Fighting blindness with microelectronics *Sci. Trans. Med.* **5** 16
- [3] Weiland J D and Humayun M S 2014 Retinal prosthesis *IEEE Trans. Biomed. Eng.* **61** 1412–24
- [4] Freeman D K, Eddington D K, Rizzo J F 3rd and Fried S I 2010 Selective activation of neuronal targets with sinusoidal electric stimulation *J. Neurophysiol.* **104** 2778–91
- [5] Boinagrov D, Pangratz-Fuehrer S, Goetz G and Palanker D J 2014 Selectivity of direct and network-mediated stimulation of the retinal ganglion cells with epi-, sub- and intraretinal electrodes *J. Neural Eng.* **11** 026008
- [6] Wilson B S and Dorman M F 2008 Cochlear implants: current designs and future possibilities *J. Rehabil. Res. Dev.* **45** 695–730

- [7] Beck H, Boden W E, Patibandla S, Kireyev D, Gutpa V, Campagna F, Cain M E and Marine J E 2010 50th anniversary of the first successful permanent pacemaker implantation in the United States: historical review and future directions *Am. J. Cardiol.* **106** 810–8
- [8] Twyford P and Fried S 2016 The retinal response to sinusoidal electrical stimulation *IEEE Trans. Neural Syst. Rehabil. Eng.* **24** 413–23
- [9] Ryu S B, Ye J H, Lee J S, Goo Y S and Kim K H 2009 Characterization of retinal ganglion cell activities evoked by temporally patterned electrical stimulation for the development of stimulus encoding strategies for retinal implants *Brain Res.* **1275** 33–42
- [10] Sekhar S, Jalligampala A, Zrenner E and Rathbun D L 2016 Tickling the retina: integration of subthreshold electrical pulses can activate retinal neurons *J. Neural Eng.* **13** 046004
- [11] Chichilnisky E J 2001 A simple white noise analysis of neuronal light responses *Network* **12** 199–213
- [12] Twyford P, Cai C and Fried S 2014 Differential responses to high-frequency electrical stimulation in ON and OFF retinal ganglion cells *J. Neural Eng.* **11** 025001
- [13] Carcieri S M and Jacobs A L and Nirenberg S 2003 Classification of retinal ganglion cells: a statistical approach *J. Neurophysiol.* **90** 1704–13
- [14] Baden T, Berens P, Franke K, Román Rosón M, Bethge M and Euler T 2016 The functional diversity of retinal ganglion cells in the mouse *Nature* **529** 345–50
- [15] Eickenscheidt M, Jenkner M, Thewes R, Fromherz P and Zeck G 2012 Electrical stimulation of retinal neurons in epiretinal and subretinal configuration using a multicapacitor array *J. Neurophysiol.* **107** 2742–55
- [16] Oh S, Ahn J H, Lee S, Ko H, Seo J M, Goo Y S and Cho D I 2015 Light-controlled biphasic current stimulator IC using CMOS image sensors for high-resolution retinal prosthesis and *in vitro* experimental results with rd1 mouse *IEEE Trans. Biomed. Eng.* **62** 70–9
- [17] Lorach H et al 2015 Photovoltaic restoration of sight with high visual acuity *Nat. Med.* **21** 476–82
- [18] Loudin J D, Simanovskii D M, Vijayraghavan K, Sramek C K, Butterwick A F, Huie P, McLean G Y and Palanker D V 2007 Optoelectronic retinal prosthesis: system design and performance *J. Neural Eng.* **4** S72–84
- [19] Stett A, Barth W, Weiss S, Haemmerle H and Zrenner E 2000 Electrical multisite stimulation of the isolated chicken retina *Vision Res.* **40** 1785–95
- [20] Zrenner E et al 2011 Subretinal electronic chips allow blind patients to read letters and combine them to words *Proc. Biol. Sci.* **278** 1489–97
- [21] Schwartz O, Pillow J W, Rust N C and Simoncelli E P 2006 Spike-triggered neural characterization *J. Vis.* **6** 484–507
- [22] Sakai H M 1992 White-noise analysis in neurophysiology *Physiol. Rev.* **72** 491–505 <http://physrev.physiology.org/content/72/2/491.long>
- [23] Guo T, Lovell N H, Tsai D, Twyford P, Fried S, Morley J W, Suaning G J and Dokos S 2015 Selective activation of ON and OFF retinal ganglion cells to high frequency electrical stimulation *Conf. Proc. IEEE Eng. Med. Biol. Soc. (Milan, Italy)* **2014** 6108–11
- [24] Goetz G, Smith R, Lei X, Galambos L, Kamins T, Mathieson K, Sher A and Palanker D 2015 Contrast sensitivity with a subretinal prosthesis and implications for efficient delivery of visual information *Investigative Ophthalmol. Vis. Sci.* **56** 7186–94
- [25] Gargini C, Terzibasi E, Mazzoni F and Strettoi E 2007 Retinal organization in the retinal degeneration 10 (*rd10*) mutant mouse: a morphological and ERG study *J. Comp. Neurol.* **500** 222–38
- [26] Im M and Fried S I 2016 Temporal properties of network-mediated responses to repetitive stimuli are dependent upon retinal ganglion cell type *J. Neural Eng.* **13** 025002
- [27] Jones B W, Kondo M, Terasaki H, Lin Y, McCall M and Marc R E 2012 Retinal remodelling *Japan. J. Ophthalmol.* **56** 289–306
- [28] Smith R, Ho E, Goetz G A, Lei X, Kamins T, Harris J, Mathieson K, Palanker D V and Sher A 2016 Spatio-temporal characteristics of retinal responses to subretinal photovoltaic stimulation *Association for Research in Vision and Ophthalmology Conf. (Seattle, USA)* <http://iovs.arvojournals.org/article.aspx?articleid=2561908>
- [29] Euler T, Haverkamp S, Schubert T and Baden T 2014 Retinal bipolar cells: elementary building blocks of vision *Nat. Rev. Neurosci.* **15** 507–19

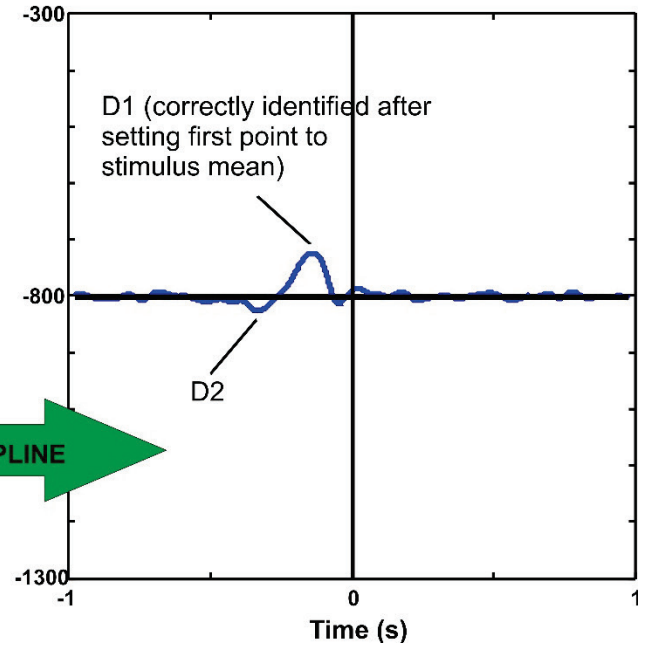
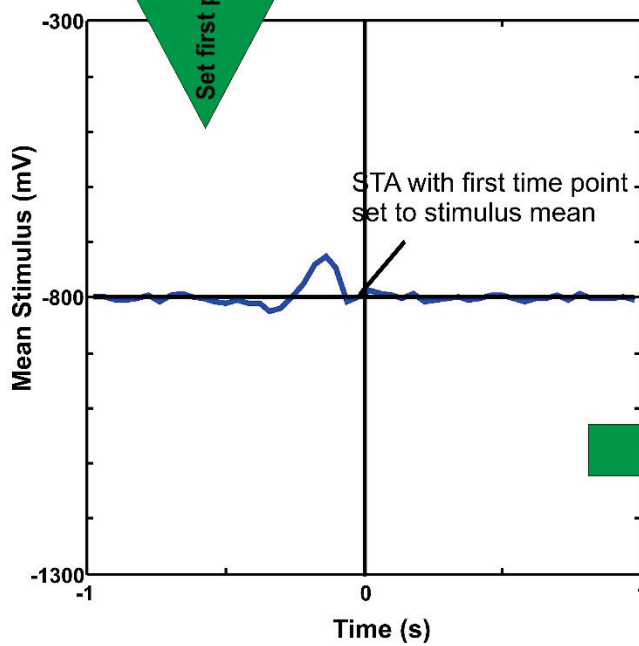
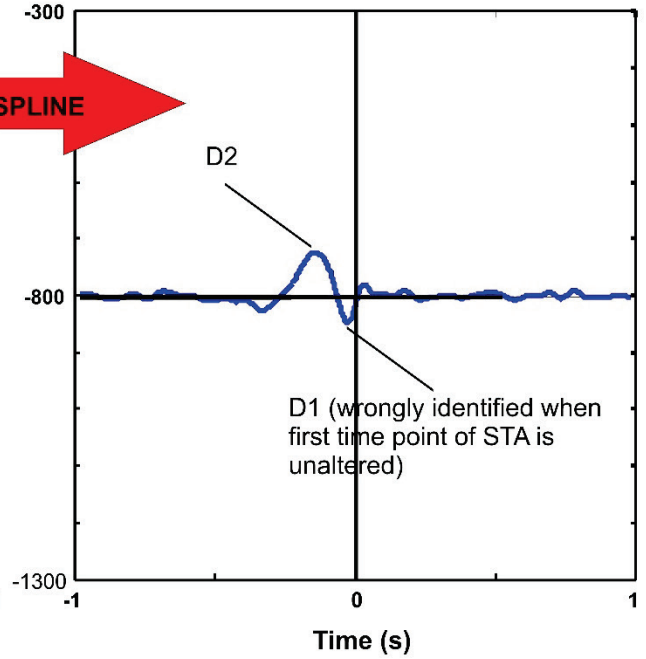
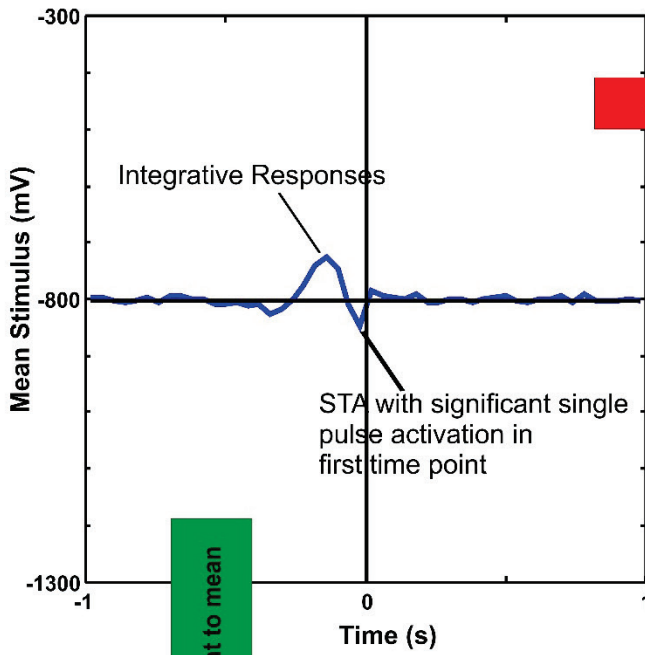
Supplementary Materials

S1. Removing the influence of single pulse activation to better understand integrative activation.

As described in our previous manuscript (Sekhar et al. 2016), when stimulating and recording from multiple RGCs simultaneously, it is not possible to optimize the distribution of stimuli for each of our cells. We therefore chose the stimulus distributions presented in this manuscript to maximize the number of cells responding due to integration of subthreshold pulses. However, as thresholds can vary considerably across cells in an experiment, it is not guaranteed that all pulses will be below threshold for a given cell. This is why the STAs of some cells showed single pulse activation, in addition to integrative responses. Because our goal was only to study the integrative component of the STA, these deflections due to single pulse activation could potentially confound the classification of our electrical STAs. In order to avoid identifying single pulse activations as D_1 , as well as to remove the influence of these activations on the D_1 width and latency, the first time point of every electrical STA was set to the mean of the stimulus prior to detection of D_1 and D_2 . Thus, our objective custom algorithm ignored the first time point of the STA in assigning D_1 and D_2 as well as their parameters. This was even done in STAs where single pulse activation was difficult to clearly identify, in order to standardise the calculation of D_1 latencies and widths across all cells. We provide below an example ON cell which has significant single pulse activation in addition to integrative responses. Using this cell we demonstrate why setting the first time point of each E-STA to the mean of the stimulus is essential for appropriate classification.

RAW STA

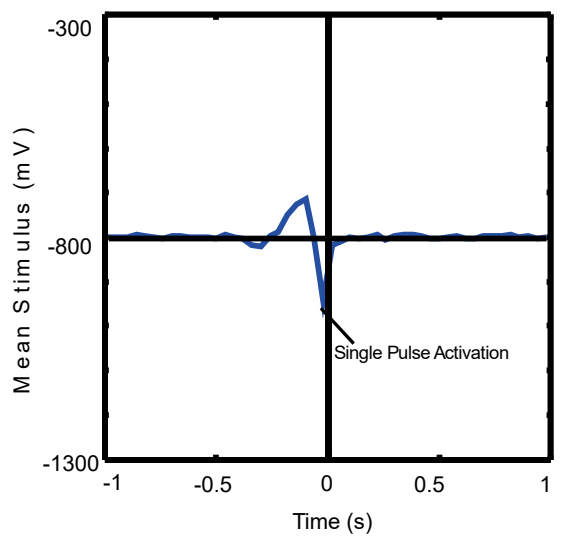
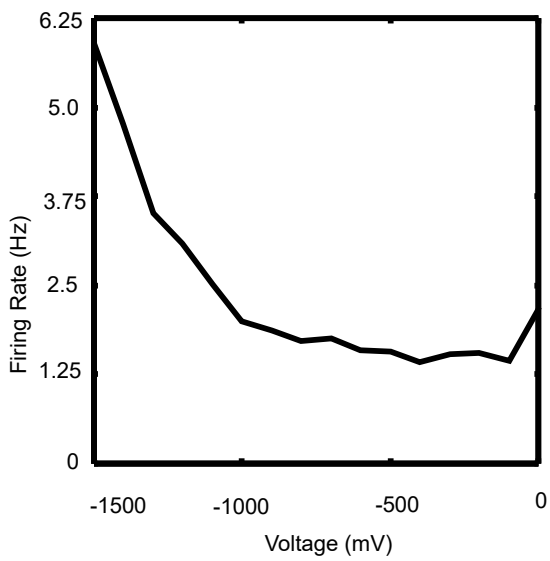
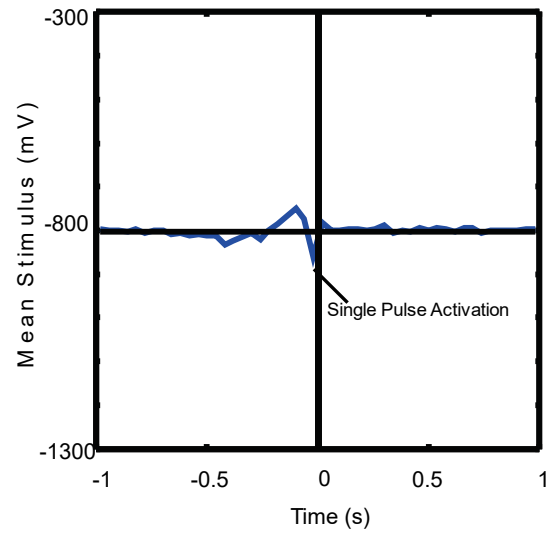
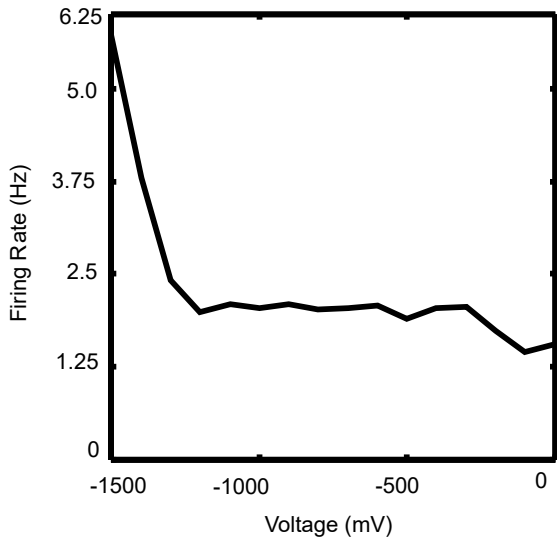
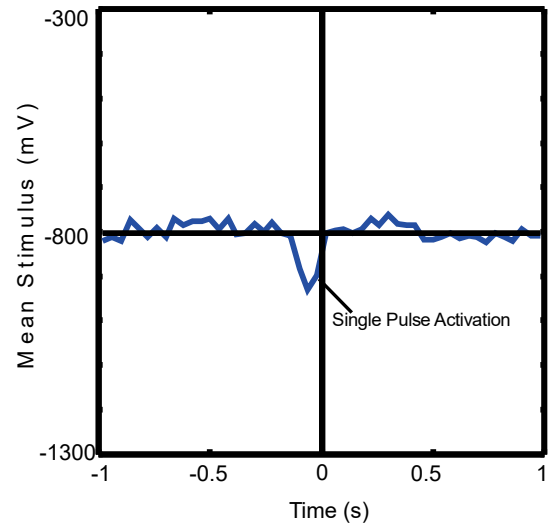
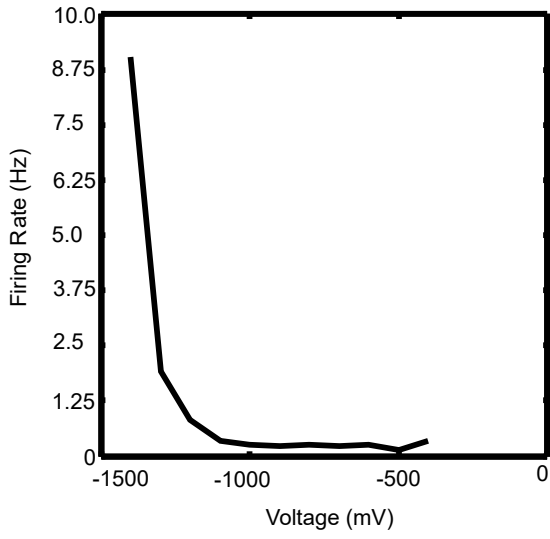
CUBIC SPLINED STA



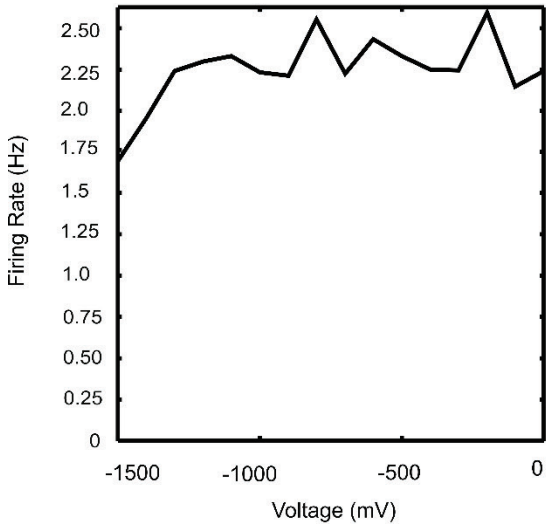
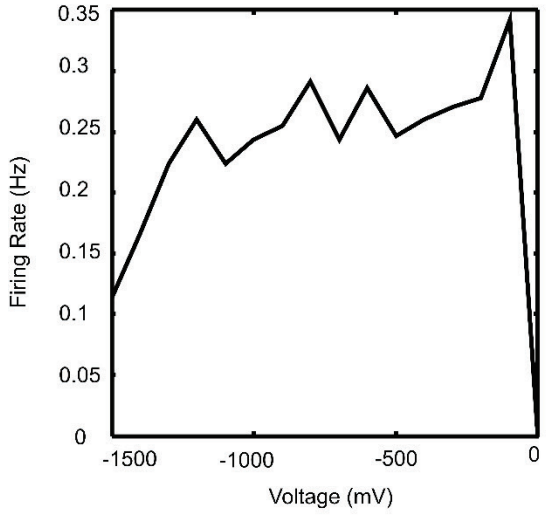
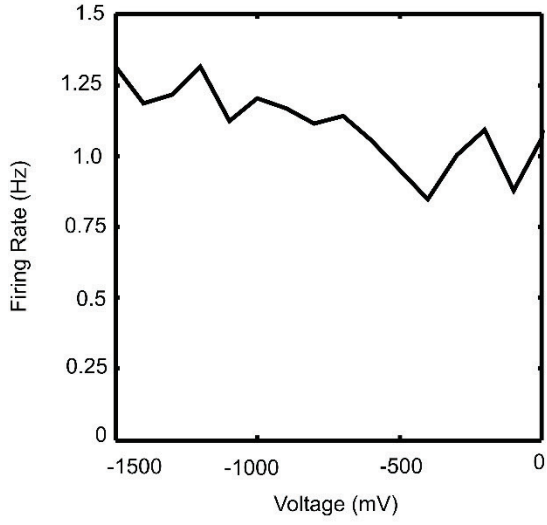
S2. For each of the cells presented in this manuscript, we derived the voltage-response curve in order to better understand the contribution of single pulse activation to the STA. The voltage response curve is calculated in the following way

- i) The stimuli presented are first binned in 100 mV steps ranging from -2500 mV to 500 mV.
- ii) To produce the average response rate, the total number of spikes elicited during the experiment (within 40 ms of stimulus pulse presentation), by stimulus pulses from each bin, was divided by the number of pulses in that bin. The plot of average spikes elicited per binned stimulus against the voltage of each bin was used to determine the voltage-response curve from our ongoing white noise stimulus.

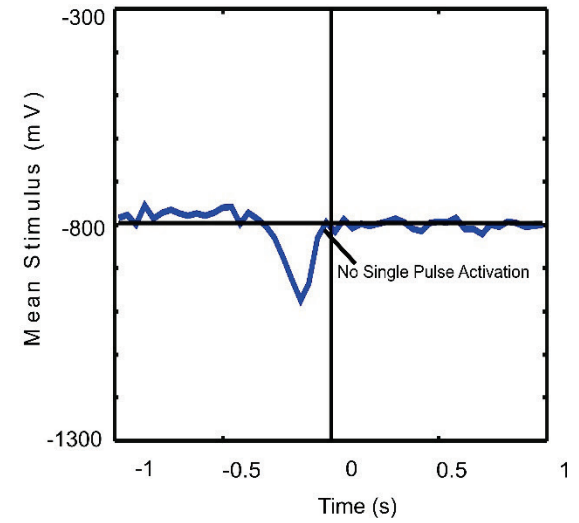
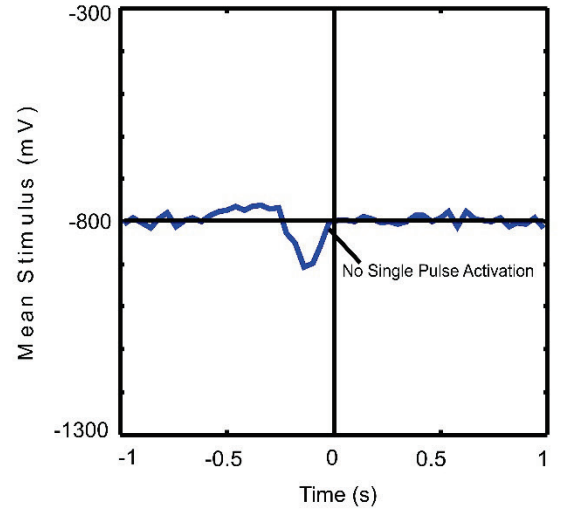
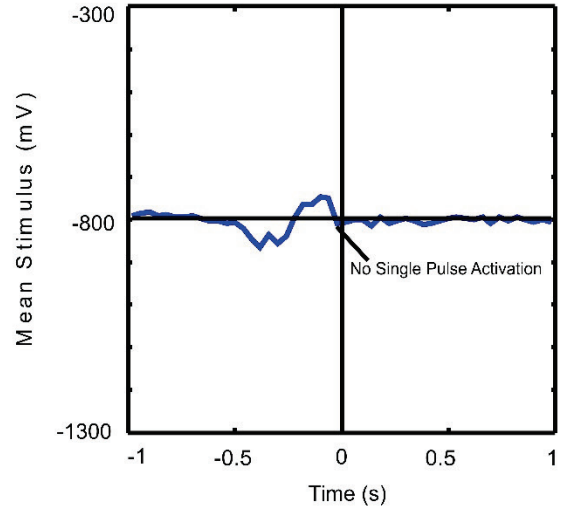
We plot the voltage-response curves and corresponding electrical STAs for 6 example cells below. Those cells with sharp increases in response at relatively low voltage magnitudes (~-1000 to ~-1300mV) also have higher peak firing rates and noticeable single pulse activation (first time point of STA), in addition to the deflections arising from integrative responses (rows 1-3). It is due to these cells with large responses at relatively low voltage magnitudes that we set the first time point of all E-STAs to the mean of the stimulus. In contrast, for those cells whose responses were low and did not vary considerably with voltage, there is no significant single pulse activation, but only the deflections arising from integrative responses (rows 4-6).



Voltage-Response Curve



STA with no single pulse activation



Appendix 4

Manuscript 3: Characterizing retinal responses to electrical stimulation using generalized linear models

Sudarshan Sekhar*, Poornima Ramesh*, Giacomo Bassetto*, Eberhart Zrenner, Daniel L. Rathbun, Jakob Macke. * Equal Contribution

Status: In preparation for submission to the Journal of Neural Engineering

Abstract

In previous works, it was shown that when we combine white noise voltage stimulation with reverse correlation, electrical STAs can be calculated for retinal ganglion cells. Moreover, these electrical STAs were found to correlate with visual cell type. Though in theory STA shaped waveforms could be used for selective activation of different retinal pathways, it is not guaranteed to succeed. This is because the STA is a linear approximation of how the cell interacts with the input stimulus. Though this assumption is very useful, it is ultimately false. Therefore, it is important to quantify to what degree a linear approximation of a RGCs input filter can capture stimulus-dependent spiking variability, and to what extent is spiking variability stimulus independent. In doing so, we obtain an estimate of the nonlinearity and non-stationarity in RGC responses that a simple STA based model overlooks. To this end, we first stimulate the retina with multiple interleaved trials of unique and frozen white noise. Two separate GLM models are then used to fit the RGC spiking responses obtained during the unique and frozen trials. By comparing the performance of these two models for each cell on a held-out trial, an estimate of the linearity, nonlinearity and intrinsic variability in RGC spiking is obtained. Our initial results suggest that there is a large degree of nonlinearities in RGC responses to electrical stimulation that a simple LNP model, cannot capture. This, in turn, implies that more sophisticated nonlinear models would have to be explored for capturing RGC responses to electrical stimulation. These results, also have the potential to shed light on cell types that can be easily targeted with standard prosthetic stimuli, and cell types that would require more elaborate stimulus design.

Contributions SS & DLR designed the experiments with input from PR, GB & JHM; SS executed the experiments; PR & GB performed the analysis with input from JHM and SS; SS, PR, GB, EZ, DLR and JHM wrote the manuscript.

Characterizing retinal responses to electrical stimulation using generalized linear models

Abstract

Objective: The ability to preferentially stimulate different retinal pathways is an area of active research in visual prosthetics. Many recent studies have shown that electrical stimulation can elicit differential responses in varied classes of retinal ganglion cells (RGC). The aim of this study was to characterize these differences in RGC responses using a statistical modeling approach and in turn, to quantify how ON and OFF cells differ in their encoding of prosthetic stimulation.

Approach: We stimulate the murine retina with multiple trials of non-repeating (unique) and repeating (frozen) electrical noise. The RGC spiking responses recorded during the unique noise trials, are subsequently fit with a Linear Nonlinear Poisson (LNP) model. These models then predict RGC responses to the held-out trials of frozen noise. Differences between the model prediction and experimentally recorded spike patterns for the held-out trials are due to a combination of the linear encoding assumption of the LNP model and intrinsic stimulus-independent variability in RGC spiking. Next, we estimate the intrinsic RGC spiking variability by analyzing the RGC response reliability to the multiple trials of frozen stimuli. Finally, by combining the results of these two analyses, we estimate the degree of linearity, nonlinearity and reliability of RGC encoding of prosthetic stimulation.

Results: On comparing model performances for our cells to unique and frozen noise, we found that there is a substantial degree of nonlinearity in both ON and OFF cell responses which a simple linear model cannot account for.

Significance: Our paper is the first to use LNP models to quantify systematically, how ON and OFF cells encode for electrical stimulation. We show that both ON and OFF cell responses deviate from a linear regime and will, therefore, require more elaborate nonlinear models to capture the full extent of their response dynamics to electrical stimulation. Furthermore, in a broader sense, our work represents a systematic way of identifying cell types that can be easily targeted by standard electrical stimuli, and cell types, which would require the development of more sophisticated stimulus paradigms.

Introduction

Age-related macular degeneration (AMD) and retinitis pigmentosa (RP) are the two most common retinal degenerative diseases causing total blindness (**Lorach et al., 2013**). Both these diseases lead to progressive vision loss due to photoreceptor death. Despite this, studies have shown that the retinal circuitry in the inner plexiform layer (IPL) remains relatively intact.

Though there is not yet a cure for these diseases, multiple treatment options are currently being investigated. One such approach involves the use of electrode arrays or photodiode arrays implanted in the eye (also known as retinal implants). These arrays electrically stimulate the diseased retina. Retinal implants have been able to restore some degree of visual perception back to patients (**Humayun et al., 2012; Stingl et al., 2015; Zrenner et al., 2011**). These prosthetic devices can either directly target the retinal ganglion cells (RGCs) or stimulate

the retinal network in order to use the remnant visual processing present in the IPL. Both these strategies have their respective advantages and drawbacks (**Zrenner, 2002, 2013**). At present, retinal implants (regardless of the intended site of stimulation), use a train of constant-amplitude current or voltage pulses, with individual pulses designed to elicit retinal activity. Such pulses are suprathreshold (above the threshold for a cell). Though such a suprathreshold stimulus protocol is well established in the literature and has been effectively used in clinical trials, it leads to indiscriminate activation of various classes of RGCs such as ON, OFF, etc., thereby reducing the restored visual acuity to below the theoretical limit. In acknowledgment of this shortcoming, there has been a lot of work in recent years studying preferentiality of RGC responses to different electrical waveforms such as sine waves, sawtooth, random, triangular, diamond, etc. (**Guo et al., 2014; Twyford et al., 2014; Twyford & Fried, 2016**). In addition to this, recently RGCs were shown to be able to integrate a stream of smaller subthreshold pulses via the retinal network, in order to generate spiking responses (**Sekhar et al., 2016**). Moreover, by combining spike-triggered averaging with this subthreshold stimulus paradigm ON and OFF cells were found to have very distinct electrical input filters (**Sekhar et al., 2017**). Though in theory, it would be possible to use these STA-like waveforms for selective stimulation of various RGC classes, it does not guarantee selective activation. This is because the underlying assumption of an STA model is that the input filter of the cell convolves linearly with its stimulus. Though this a very useful assumption to make, the linear filter approximation overlooks nonlinear response properties of the cell. It is hence necessary to quantify the degree to which a cell's behavior deviates from the simplifying STA (linear) model.

In this study, we analyzed the effectiveness of LNP models in capturing a cell's response to electrical stimulation.

We do so by comparing the prediction performance of two generalized linear models (GLM), one fit only to trials of unique stimuli, and one only to trials of frozen stimuli. The GLM fit to the unique stimulus trials has a filter that convolves linearly with the stimulus. In the second GLM, there is no linear filter. Instead, we directly fit to each binned spike count obtained during the frozen stimulus trials, and thereby approximate a Peri-Stimulus Time Histogram (PSTH) model for the cell. The comparison of these two model performances quantifies how linearly RGCs encode for prosthetic stimulation. The model performance measure (MPM) used is linear correlation coefficient. These analyses methods provide a systematic manner of identifying RGC classes that can be well controlled with simple STA-like stimuli, and RGC classes that would require more elaborate stimulus design. This, in turn, has important implications for the design of future retinal prosthesis.

Methods

We obtained the data central to this study using three different stimulus protocols. In the first stimulus protocol, the cells were shown multiple trials of only unique white noise. In the second stimulus protocol, the cells were shown multiple trials of only frozen white noise. In the final protocol, the cells were shown interleaved trials of both frozen and unique noise with a 1:1 ratio. We verified that 1:1 was an appropriate ratio using the first two stimulus protocols and only used the cells collected under the third protocol for the LNP/GLM modeling. All 3 protocols used 100 s trials whose mean/SD was -800 mV/280 mV with a presentation

frequency of 25 Hz. We also presented visual stimuli before and after electrical stimulation for cell-classification (ON, OFF, ON-OFF) purposes.

Animals

The experimental methods used in this paper are identical to a previous study (**Sekhar et al., 2017**), and are restated here: The data in this paper consists of 53 RGCs obtained from 16 retinal pieces using 15 C57BL/6J mice. The age of the mice are 2 × P32, 2 × P39, 2 × P46, 1 × P49, 1 × P51, 1 × P53, 1 × P56, 2 × P58, 2 × P59, 1 × P64. All experimental procedures have the approval of the state authorities (Regierungspraesidium, Tuebingen) and were conducted under the supervision of the Tuebingen University facility for animal welfare (Einrichtung fuer Tierschutz, Tieraerztlichen Dienst und Labortierkunde) and the NIH Guide for the Care and Use of Laboratory Animals.

Data Collection

The mice were anesthetized using CO₂ inhalation. Following this, the mice were killed by cervical dislocation. After eye removal and dissection, the retinas were perfused with carbogenated ACSF (artificial cerebrospinal fluid) which was regulated at 33°C (using a heating plate and heated perfusion cannula) and at a pH of 7.4. Retinal pieces were mounted ganglion cell side down on a standard 60-channel microelectrode array (MEA, 60MEA200/30iR-ITO, Multi Channel Systems, Reutlingen, Germany), and were constantly perfused with ACSF. A single electrode was used for electrical stimulation and analysis was restricted to the 7-8 electrodes immediately surrounding the stimulating electrode (inter-electrode distance = 200 or 283 μm). Voltage traces were sampled with MultiChannel Systems hardware (MCS, Reutlingen, Germany) at a rate of 50 kHz/channel, using a filter bandwidth of 1 Hz– 3 kHz and a gain of 1100.

Data Processing and Inclusion Criteria

Raw data was first high pass filtered in order to extract putative action potential events (spikes). Following this these putative spikes underwent automated and manual spike sorting in order to reduce Type I and Type II errors in assigning waveforms to different sources. To be included in this study spike trains had to have 1) the presence of a clear lock-out period in the ISI histogram and autocorrelogram 2) the absence of a peak in the cross-correlogram between different cells, which would indicate that a single cell had been wrongly split into 2 or more units 3) good separation in principal component space of a biphasic waveform whose shape is typical of extracellularly recorded action potentials and 4) stability of the waveform shape and firing rate over the entire experiment. Offline Sorter (Plexon Inc, TX, USA) was used to filter and spike sort the data. Time stamps of these sorted spikes were collected with NeuroExplorer (Plexon Inc, TX, USA) and exported to MATLAB. All analyses and statistical tests were performed in MATLAB (The Mathworks, Natick, MA).

Visual Stimulation

Flash stimulus blocks consisted of cycling 2 s ON (40 klx) and 2 s OFF (20 lx) full-field luminance (mean illuminance = 20 klx, 99.9% Michelson contrast). Visual stimuli were presented with a linearized, commercially available DLP-based projector (K10; Acer Inc., San Jose, California, USA). Other than during visual stimulation, a shutter was placed in front of the projector, and

the experimental setup was surrounded by dark curtains with room lights turned off to minimize stray light.

Electrical Stimulation

Electrical stimuli were presented at a rate of 25Hz in 100s trials. The amplitudes of the 1 ms voltage pulses were drawn randomly from a Gaussian distribution with mean of -800 mV and SD 35%. Voltage pulses of length 1ms are commonly used in subretinal implants and are equivalent to biphasic current pulses. The stimulus pulses were programmed in MATLAB using custom scripts and imported into MCStim (MCS, Reutlingen, Germany) for presentation. A stimulus generator (STG 2008, MCS, Reutlingen, Germany) was used to generate pulses. To characterize the degree of linearity and variability in RGC responses, the retina was presented with 18 interleaved trials of unique and frozen electrical noise each. Therefore, in total 36 trials were presented.

LNP Model Implementation

We use LNP models to quantify how well a simple linear model can capture neural responses to electrical stimulation. The LNP model is an encoding model which is a special case of the generalized linear models (GLMs) (Nelder & Wedderburn, 1972). These models have been extensively used in the past to describe the dependence of firing rate of retinal ganglion cells on visual stimuli (Paninski, 2004; Paninski et al., 2007; Pillow, 2006; Pillow et al., 2008). An LNP maps an input variable \mathbf{x} (typically a stimulus) to a measured spike count \mathbf{y} via three components: a linear predictor (often referred to as the receptive field), a nonlinear link-function and model of neural variability. The linear predictor convolves the stimulus with a filter \mathbf{k} which, in stimulus space, corresponds to the direction that elicits the maximum spiking activity from the neuron. The convolution operation projects the stimulus onto the direction of maximal spiking activity.

$$z = k \cdot x$$

The function f (also called inverse-link function) maps z to a variable λ , such that $\lambda = f(z)$.

λ can be thought of as the instantaneous firing rate of the neuron

In this paper

$$\lambda = \log(1 + e^{k \cdot x + b})$$

where

b is a constant bias term

x is the input stimulus

k is the filter estimate

λ is the firing rate given the stimulus and filter

Spike trains can be simulated from this model by drawing spikes from a Poisson distribution whose rate is given by λ

$$y \sim \text{Poisson}(\lambda\Delta t).$$

where

Δt is the binwidth

The LNP modeling framework makes it possible to impose smoothing constraints on the filter \mathbf{k} , yielding more realistic estimates compared to the direct STA approach. The direct STA approach is also known to require large amounts of data to converge (**Chichilnisky, 2001**). These are two major advantages the LNP model has over the STA model.

In conjunction with the above framework, we estimate the linear filter \mathbf{k} using maximum *a posteriori* (MAP) estimation and by maximizing a fitness function which is a sum of the log-likelihood of the data, and a penalization term that favours smooth filters (**Park & Pillow, 2011**). This filter estimation is only based on RGC responses from the unique trials. The fitness function is

$$L = \sum_{t=1}^N (y_t \log(\lambda_t) - (\Delta t)\lambda_t) - \sum_{i,j=1}^K k_i \Sigma_{ij}^{-1} k_j$$

where

y_t denotes the number of spikes in time-bin t .

λ_t is the instantaneous firing rate at time-bin t .

k_i is the i^{th} element of the filter estimate

K is the number of time-bins in the filter

N is the total number of time-bins in a 100 s trial

In the penalization term in the equation above,

$$\Sigma_{ij} = \sigma^2 e^{-\frac{(i-j)^2}{2\tau^2}}$$

where

σ^2 is the variance of the filter values from a zero mean.

τ is the timescale over which the filter is smoothed.

i and j denote the time-bin number in the filter

Σ^{-1} is the inverse of the matrix Σ

Sigma (σ) and tau (τ) are the optimized hyperparameters. The optimization procedure for these hyperparameters is discussed in the following section.

Optimization of hyperparameters

We optimize the hyperparameters sigma (σ) and tau (τ) using grid search with 10-fold cross validation on the log-likelihood fitness function (excluding the penalization term). We first construct a grid of σ and τ values – with both σ and τ ranging from 0.1 to 5. Choosing a value of σ and τ from the grid, we built the covariance matrix. Then, we randomly divided the unique stimulus trials into 10 sets. Using the covariance matrix, we fit the LNP model to 9 sets of data and obtained the estimates for the filter. We calculated the log-likelihood (L without the penalization term) of these estimates on the 10th held-out set of trials. We repeated this with each of the 10 sets of trials held out in turn, to obtain the log-likelihood values averaged across the 10 sets. Once every possible pair of σ and τ from the grid was used in the 10-fold cross-validation, the σ and τ value corresponding to the highest averaged log-likelihood were chosen as the optimized hyperparameters. We used these values to build a covariance matrix and obtain a filter estimate using all the unique stimulus trials.

Comparing LNP and PSTH model performance

We presented 18 interleaved trials each of unique and frozen electrical noise to the retina in order to characterize the degree of linearity and non-stationarity in RGC responses.

We use the linear filter fit k (obtained by fitting the LNP model to the 18 unique stimulus trials) to predict the spiking responses for the 18 frozen trials and then quantify the model predictive performance using the linear correlation coefficient metric (described in the section – ‘Quantifying Model Performance’). Spiking variability not captured by the LNP model is due to a combination of the non-stationarity and nonlinearities in RGC responses.

In the next step, we used the PSTH model to tease apart the nonlinearity from the non-stationarity of the RGC spikes. The PSTH model is a GLM with the same inverse-link function as the LNP model, that directly estimates the parameter controlling the firing rate of the neuron (rather than a stimulus filter). This parameter (z) is time dependent i.e. there is a different value of z for each time-bin.

The equations below describe the PSTH model

$$\lambda = \log(1 + e^z)$$

where

z is the parameter controlling the firing rate for each time-bin

λ is the instantaneous firing rate.

The spike trains can be sampled from this model by generating spikes using a Poisson distribution.

$$y \sim \text{Poisson}(\lambda \Delta t).$$

where Δt is the binwidth

Similar to the LNP, we estimate the PSTH model parameters using maximum *a posteriori* (MAP) estimation - by maximizing a fitness function which is a sum of the log-likelihood of the data, and a penalization term that constrains the log firing rate to be smooth. This parameter estimation is only based on RGC responses from the frozen trials. Given below is the fitness function

$$L = \sum_{t=1}^N (y_t \log(\lambda_t) - (\Delta t) \lambda_t) - \sum_{i,j=1}^N z_i \Sigma_{ij}^{-1} z_j$$

where

y_t denotes the number of spikes in time-bin t .

λ_t is the instantaneous firing rate at time-bin t .

z_i is the parameter controlling the firing rate for the i^{th} time-bin

N is the total number of time-bins in a 100 s trial

$$\Sigma_{ij} = \sigma^2 e^{-\frac{(i-j)^2}{2\tau^2}}$$

where

σ^2 is the variance of \mathbf{z} values from a zero mean.

τ is the timescale over which \mathbf{z} values are smooth.

i and j denote the time-bin number in \mathbf{z}

The PSTH model is designed to highlight stimulus-independent variability in the spiking response by capturing all stimulus-dependent (linear and nonlinear) responses. Hence, it is fit and cross-validated only on the 18 frozen stimulus trials. We use leave-one-out cross-validation to measure the PSTH model performance. First, we obtain the optimized hyperparameters sigma and tau for the PSTH model with a procedure similar to the LNP model. Then, with these optimized hyperparameters, we fit the model to 17 frozen stimulus trials and use the estimated firing rate to calculate the model performance measures on the 18th held-out trial. We repeated this process, with each of the 18 trials being held out in turn and finally average the model performance measures across all 18 trials.

The LNP model captures response variability that is linearly dependent on the stimulus. Since the PSTH model captures any stimulus-dependent variability in RGC response (linear and nonlinear responses), spiking variability not captured by the PSTH, represent stimulus-independent, intrinsic non-stationarity in RGC spiking. Therefore, by comparing the two models (LNP and PSTH) for each cell, we determined the degree of nonlinearity (extent to which PSTH model out performs LNP model) and non-stationarity in RGCs (spiking variability not captured by PSTH model) when encoding for electrical stimulation.

Validation of Frozen:Unique White Noise Ratio

Since the PSTH model requires frozen stimulus trials, and the LNP model requires unique stimulus trials for training, we needed to determine whether 1:1 was an appropriate ratio of frozen to unique stimulus trials to present to the same retina since we already had such **(Sekhar et al., 2017)** recordings.

As mentioned before we used the experiments with only repeating or unique stimuli to validate the 1:1 ratio. For each RGC presented with only unique stimuli, we fit an LNP model using an increasing number of trials (from 2 to 30 in increments of 2) for training. We obtained an upper bound (UB) for model performance by calculating the MPMs on each trial of the training data and averaging across all these trials. We obtained the lower bound (LB) for model performance by calculating the MPMs using leave-one-out cross-validation.

Likewise, for each RGC presented with only frozen stimuli, we fit a PSTH model using an increasing number of trials (from 2 to 30 in steps of 2) for training. We found the upper and lower bound estimates for the MPMs in the same way as for the LNP model.

The upper bound value of the MPM is an estimate of the model performance on the training data. Since the model will overfit to some degree on the training data, the upper bound overestimates the model performance. The lower bound value of the MPM, on the other hand, is an estimate of the model performance on test data. Since the model overfits to the training data and not to the test data, the lower bound underestimates the model performance. The actual value of model performance will lie somewhere in between the upper and lower bound.

Next, we paired together the MPMs, averaged across all cells for each condition (such as lower bound LNP, upper bound PSTH etc), for the PSTH and LNP model such that the number of trials they were trained on summed to 32, and then identified the ratios for which the MPM for both the LNP and PSTH model was optimal. For example, the MPMs for an LNP model trained on 2,4, 6,8,...,30 trials were combined with a PSTH model trained on 30, 28, ... ,2 trials respectively. This procedure led us to validate the 1:1 ratio, as a suitable ratio of unique and frozen trials.

Quantifying model performance

We used linear correlation coefficient to quantify model performance.

This MPM measures the degree of linear relationship between the experimental and predicted response **(Theis et al., 2016)**. The linear correlation coefficient ranges between -1 and 1 (best performance).

$$z = \frac{y - \hat{y}}{\sigma(y)}$$

where

y is the experimentally observed spike train.

\bar{y} is the mean of the experimentally observed spike train.

$\sigma(y)$ is the standard deviation of the experimentally observed spike train.

$$z^{est} = \frac{\lambda - \bar{\lambda}}{\sigma(\lambda)}$$

λ is the estimated firing rate from the model.

$\bar{\lambda}$ is the mean of the estimated firing rate from the model.

$\sigma(\lambda)$ is the standard deviation of the estimated firing rate from the model.

$$\text{Correlation coefficient} = \frac{1}{N} \sum_{t=1}^N z_t * z_t^{est}$$

where

N is the total number of time-bins in a 100 s trial

Results

We recorded from 53 RGCs in total, with 27 RGCs being shown 54 trials of unique electrical noise, 6 RGCs shown 36 trials of frozen electrical noise and 20 RGCs shown 18 trials of frozen and 18 trials of unique stimuli in an interleaved fashion. As mentioned earlier, the experiments with only unique or only repeated stimuli validated the 1:1 ratio of frozen to unique stimuli. This is important since there is a limited time-window for the experiments.

We fit a PSTH model (described in the methods section) for our 6 cells to an increasing number of trials of frozen stimuli. We then estimated upper and lower bound MPMs for the PSTH model. To estimate an upper bound MPM the PSTH model was first fit to the averaged spike trains of k randomly chosen trials. Following this, we evaluated the upper bound predictive power of the PSTH model on each of the k trials individually, using the linear correlation coefficient MPM discussed in the methods section. We repeated this process for $k=2,4,6,\dots,30$ trials (Figure 1a, blue curve).

We used leave-one-out cross validation to calculate the PSTH model's lower bound estimate (Figure 1a, green curve) for the spike rate prediction. Given k randomly chosen trials, we fit the PSTH model to $k-1$ trials. We then used the MPM to evaluate the predictive power of this fit on the held-out k th trial and then repeated this process by holding out each of the k trials in turn and then averaging the MPM across all k trials. We then calculated the MPMs for different values of k ranging from 2 to 30.

In order to estimate the number of unique trials to use, we analyzed 27 cells that were shown 54 unique trials of electrical white noise. The LNP model is trained and tested on k randomly chosen trials. We carried out this process, as with the PSTH model, for k ranging from the first 2 to first 30 trials in increments of 2. Also similar to the PSTH model we estimated an upper and lower bound estimate of the LNP model performance. The upper and lower bound for the LNP are shown in the red and black curve respectively of figure 1a. The error bars in figure 1a

represent the standard error of mean calculated by dividing the standard deviation of the averaged MPM for all the cells given a particular stimulus protocol (unique or frozen) at a certain number of training trials k by the square root of the number of cells.

Following this, scatter plots of the MPM for LNP and PSTH models is made by pairing together upper and lower bound MPMs for PSTH models using 2,4, ... 30 repeated trials with upper and lower bound MPMs for LNP models using 30, 26, 2 unique trials respectively for all 4 combinations (UB PSTH- UB LNP, UB PSTH-LB LNP, LB PSTH- UB LNP, LB PSTH – LB LNP). The points further away from the origin (0,0), in the scatter (Figure 1b), were considered as good combinations of frozen and unique trials. Given these criteria, the 1:1 ratio of frozen and unique trials was validated as a good compromise between all 4 combinations. Some of the points in figure 1b are marked with their corresponding frozen: unique trial ratios.

We obtained 20 cells with the 1:1 ratio of frozen and unique white noise (18 trials each). Of these 20 cells 11, 3 and 6 are ON, OFF and ON-OFF cells respectively. In figure 2a, we show the raster plot of an example cell to 18 trials of frozen white noise. In figure 2b, we show the corresponding raster plot to 18 trials of unique stimuli for the same cell. In figure 2c, we show the recovered STA from these 18 unique trials.

As mentioned in the methods section we used a grid search to obtain the optimized sigma and tau values, used in the penalizing term for MAP estimation. This optimization process consisted of calculating log-likelihood with 10-fold cross validation for different combinations of sigma and tau. That is, for a given value of sigma and tau, we built the corresponding squared exponential kernel. We divided the trials corresponding to a given model into 10 sets. We fit the model on 9 sets and calculated the log-likelihood on the held-out set 10th set. We then repeated this process for each of the 10 sets held out in turn and then averaged the log-likelihood across the 10 sets. In figure 3a, we present the heatmaps displaying the log-likelihood for each of the sigma-tau combinations for the LNP model of an example cell. Figure 3b, shows this heatmap for the PSTH model of another example cell. The fits to the STAs and PSTHs for another two example cells with the optimized sigma-tau values, using the 10-fold cross validation is shown in figure 4a & 4b respectively. The sigma-tau values obtained through this process provide a close fit to the underlying STA or PSTH. We also compared the log-likelihood of these fits to the log-likelihood of the fits obtained with manual hand-tuned estimates of the optimal sigma and tau. The fits using grid search and manual selection were found to be comparable.

In order to compare LNP and PSTH model performance for the cell population from the 1:1 frozen:unique stimulus recordings, the repeating stimulus trials and the non-repeating stimulus trials (18 each) for each cell were separated. The LNP model was fit to all the non-repeating stimulus trials, and the resulting MAP estimates of the model parameters were used to calculate the model performance measures on all the repeating stimulus trials. The model performance measures for the PSTH model were calculated using leave-one-out cross validation on the repeating stimulus trials. We then average the 2 MPMs for each cell across the total population.

In figure 5, we present a comparison between the MPM of the LNP and PSTH model for the entire population of ON (Figure 5a), OFF (Figure 5b) and ON-OFF (Figure 5c) cells, collected

with the 1:1 ratio of interleaved trials. For all 3 cell types, the PSTH model tends to outperform the LNP model. These results show that there is nonlinearity in RGC responses to prosthetic stimulation, that a simple STA based model cannot capture. A comparison of the LNP and PSTH model performances across all 3 cell types is provided in figure 6a and figure 6b respectively.

Discussion

The main aim of this study was to characterize how different classes of RGCs encode for electrical stimulation. Though there have been in recent years a number of papers, which study differences in RGC responses to an electrical stimulus (**Twyford & Fried, 2016**) there was to date no systematic study characterizing these responses. In this paper, we use a GLM framework to tease apart the extent of linearity/nonlinearity and the variability that RGCs display when electrically stimulated. This study is a follow-up to a previous paper that showed that the ON and OFF class of RGCs in the mouse retina have different electrical STAs (**Sekhar et al., 2017**).

In this study, it was found that the PSTH model performed outperformed the LNP model for ON, OFF & ON-OFF cells. This suggests that the coding scheme of all these 3 cell types to prosthetic stimulation has a strong nonlinear component. Therefore, to fully capture the response properties of these cells to electrical stimulation, more sophisticated nonlinear models would have to be developed. In addition to the nonlinear response properties, all 3 cell types also displayed high stimulus-independent variability in their encoding of electrical stimulation. One major reason for this could be desensitization. It has been shown that when RGCs are electrically stimulated at a constant amplitude and frequency, their response rates tend to drop off (**Jensen & Rizzo, 2007**). Though in this study, we presented gaussian white noise modulated voltage pulses, it is conceivable that some of the variability in our responses could be due to adaptation effects to the prolonged high-frequency stimulation. Another cause for the relatively high variability could be the site of stimulation. It has been shown that thresholds for network stimulation are lower in the subretinal space (**Boinagrov et al., 2014**). However, in these experiments we targeted the network from the RGC side. This increase in distance between the stimulating electrode and the intended target of stimulation could lead to higher thresholds and hence higher spiking variability. With a more optimal experimental design in which we stimulate the network from the subretinal space, it would be possible to lower the overall variability. However, for the purposes of this study (to characterize how linearly/nonlinearly ON and OFF cells encoded for electrical stimulation) the present site of stimulation is sufficient. In the future, if one wishes to more thoroughly characterize the stimulus-independent spiking variability itself, it could help to stimulate the network subretinally. Finally, our stimuli were chosen to be deliberately weak in order to avoid single pulse activation. It could be possible to reduce our response variability and increase our signal strength by increasing the mean of our stimulus distribution. This would require several pilot experiments where we study if increasing the mean of the stimulus distribution reduces stimulus-independent spiking variability while still keeping single pulse activation to a minimum. In conclusion, while a simple linear model can capture some of the spiking dynamics of RGCs to electrical stimulation, more sophisticated nonlinear models should also be explored. This deeper understanding could, in turn, have many practical implications for the

design of future implants, by shedding light on which cell types can be controlled by simple STA-based waveforms and which cell types would require more elaborate stimulus design.

Citations

Boinagrov, D., Pangratz-Fuehrer, S., Goetz, G., & Palanker, D. (2014). Selectivity of direct and network-mediated stimulation of the retinal ganglion cells with epi-, sub- and intraretinal electrodes. *Journal of Neural Engineering*, *11*(2), 26008.

Chichilnisky, E. J. (2001). A simple white noise analysis of neuronal light responses. *Network: Computation in Neural Systems*, *12*(2), 199–213.

Czanner, G., Sarma, S.V., Ba, D., Eden, U.T., Wu, W., Eskandar, E., Lim, H.H., Temereanca, S., Suzuki, W.A., Brown, E.N. (2015). Measuring the signal-to-noise ratio of a neuron. *Proceedings of the National Academy of Sciences*, *112*(23), 7141–7146.

Hastie, T. (1987). A Closer Look at the Deviance. *The American Statistician*, *41*(1), 16–20.

Humayun, M. S., Dorn, J. D., da Cruz, L., Dagnelie, G., Sahel, J.A., Stanga, P. E., Cideciyan, A.V., Duncan, J.L., Elliott, D., Filley, E., Ho, A.C., Santos, A., Safran, A.B., Arditi, A., Del Priore, L.V., Greenberg, R. J. Argus II Study Group. (2012). Interim Results from the International Trial of Second Sight's Visual Prosthesis. *Ophthalmology*, *119*(4), 779–788.

Jensen, R. J., & Rizzo, J. F. III (2007). Responses of ganglion cells to repetitive electrical stimulation of the retina. *Journal of Neural Engineering*, *4*(1), S1–S6

Lorach, H., Marre, O., Sahel, J. A., Benosman, R., & Picaud, S. (2013). Neural stimulation for visual rehabilitation: Advances and challenges. *Journal of Physiology Paris*, *107*(5), 421–431.

Theis, L., Berens, P., Froudarakis, E., Reimer, J., Román Rosón, M., Baden, T., Euler, T., Tolias, A.S., Bethge, M. (2016). Benchmarking Spike Rate Inference in Population Calcium Imaging. *Neuron*. *4*;90(3):471-82.

Nelder, J. A., & Wedderburn, R. W. M. (1972). Generalized Linear Models. *Journal of the Royal Statistical Society. Series A (General)*, *135*(3), 370-384.

Paninski, L. (2004). Maximum likelihood estimation of cascade point-process neural encoding models. *Network: Computation in Neural Systems*, *15*(4), 243–262.

Paninski, L., Pillow, J., & Lewi, J. (2007). Statistical models for neural encoding, decoding, and

optimal stimulus design. In *Progress in Brain Research*. 165, 493–507.

Park, M., & Pillow, J. (2011). Bayesian Spike-Triggered Covariance Analysis. *Advances in Neural Information Processing Systems*, 24, 1692–1700.

Pillow, J. (2006). Likelihood-Based Approaches to Modeling the Neural Code. *Bayesian Brain*. 70, 53–70. The MIT Press.

Pillow, J. W., Shlens, J., Paninski, L., Sher, A., Litke, A. M., Chichilnisky, E. J., & Simoncelli, E. P. (2008). Spatio-temporal correlations and visual signalling in a complete neuronal population. *Nature*, 454(7207), 995–999.

Sekhar, S., Jalligampala, A., Zrenner, E., & Rathbun, D. L. (2016). Tickling the retina: integration of subthreshold electrical pulses can activate retinal neurons. *Journal of Neural Engineering*, 13(4), 46004.

Sekhar, S., Jalligampala, A., Zrenner, E., & Rathbun, D. L. (2017). Correspondence between visual and electrical input filters of ON and OFF mouse retinal ganglion cells. *Journal of Neural Engineering*, 14(4), 46017.

Stingl, K., Bartz-Schmidt, K. U., Besch, D., Chee, C. K., Cottrill, C. L., Gekeler, F., Groppe, M., Jackson, T.L., MacLaren, R.E., Koitschev, A., Kusnyerik, A., Neffendorf, J., Nemeth, J., Naeem, M.A., Peters, T., Ramsden, J.D., Sachs, H., Simpson, A., Singh, M.S., Wilhelm, B., Wong, D., Zrenner, E. (2015). Subretinal Visual Implant Alpha IMS – Clinical trial interim report. *Vision Research*, 111, 149–160.

Guo, T., Lovell, N. H., Tsai, D., Twyford, P., Fried, S., Morley, J. W., Suaning, G.J., Dokos, S. (2014). Selective activation of ON and OFF retinal ganglion cells to high-frequency electrical stimulation: A computational modeling study. 36th Annual International Conference of the IEEE Engineering in Medicine and Biology Society, Milan, Italy (pp. 6108–6111). IEEE.

Twyford, P., Cai, C., & Fried, S. (2014). Differential responses to high-frequency electrical stimulation in ON and OFF retinal ganglion cells. *Journal of Neural Engineering*, 11(2), 25001.

Twyford, P., & Fried, S. (2016). The Retinal Response to Sinusoidal Electrical Stimulation. *IEEE Transactions on Neural Systems and Rehabilitation Engineering*, 24(4), 413–423.

Zrenner, E. (2002). Will Retinal Implants Restore Vision? *Science*, 295(5557), 1022–1025.

Zrenner, E. (2013). Fighting Blindness with Microelectronics. *Science Translational Medicine*, 5(210), 210ps16.

Zrenner, E., Bartz-Schmidt, K. U., Benav, H., Besch, D., Bruckmann, A., Gabel, V.P., Gekeler, F., Greppmaier, U., Harscher, A., Kibbel, S., Koch, J., Kusnyerik, A., Peters, T., Stingl, K., Sachs, H., Stett, A., Szurman, P., Wilhelm, B., Wilke, R. (2011). Subretinal electronic chips allow blind patients to read letters and combine them to words. *Proceedings of the Royal Society B: Biological Sciences*, 278(1711), 1489–1497.

Figure 1a

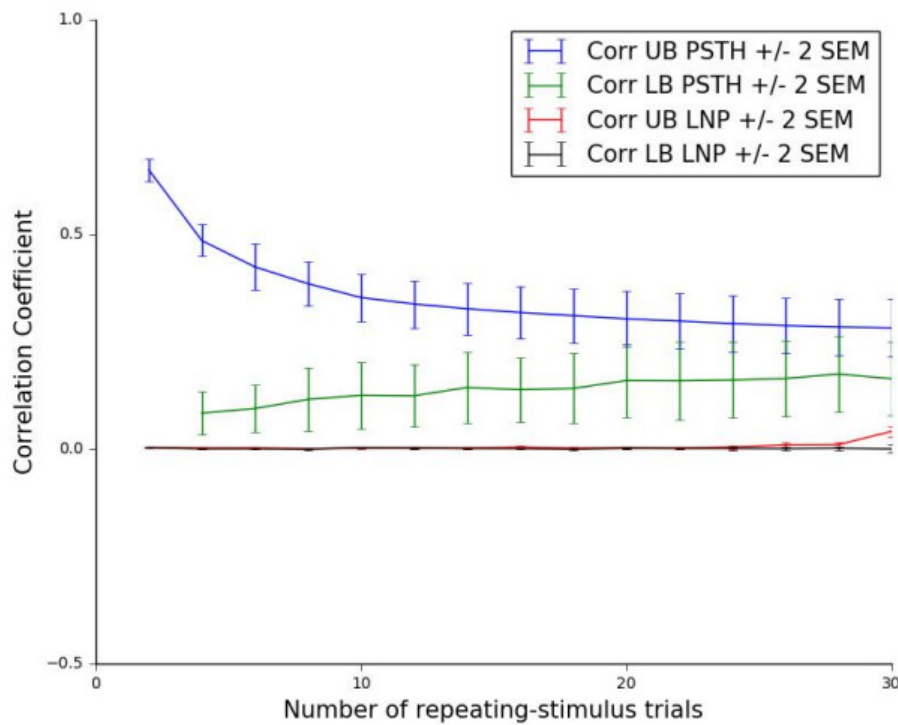


Figure 1b

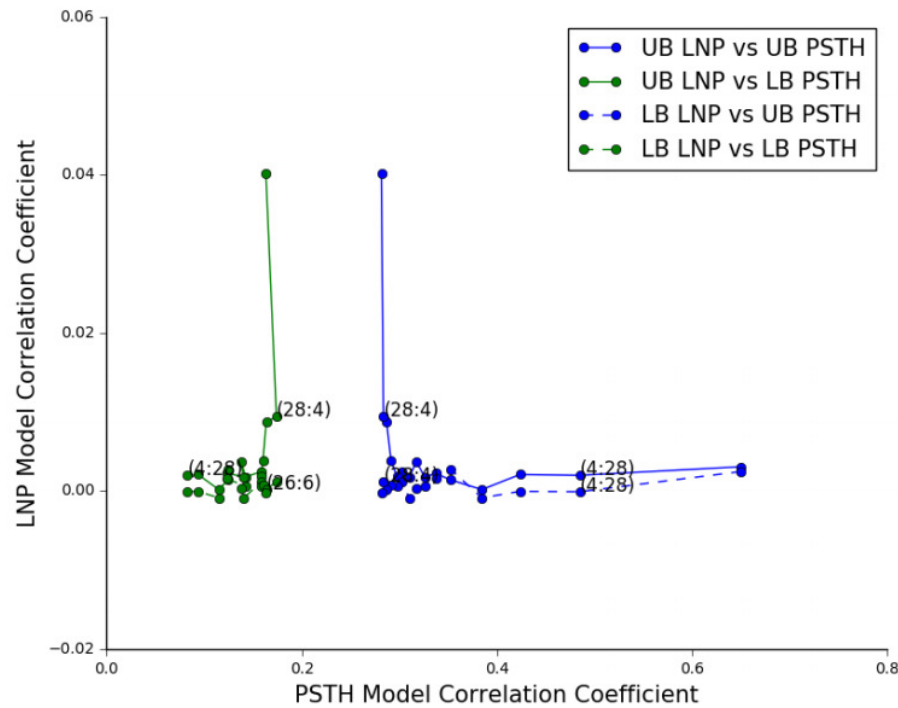


Figure 1 Evaluating optimal ratios of repeating to unique stimuli. a) Model performance measure of Upper Bound PSTH model (blue), Lower Bound PSTH model (green), Upper Bound LNP model (red) and Lower Bound LNP model (black) plotted against the number of

repeated trials used for training the PSTH model. The number of unique trials used to train the LNP model can be inferred by subtracting the number of repeated trials (plotted on x-axis) from 32 b) Scatter plot of paired MPMs for LNP and PSTH models using different ratios of repeated and unique trials. Some of the ratio values are mentioned alongside their respective scatter points, for reference.

Figure 2a

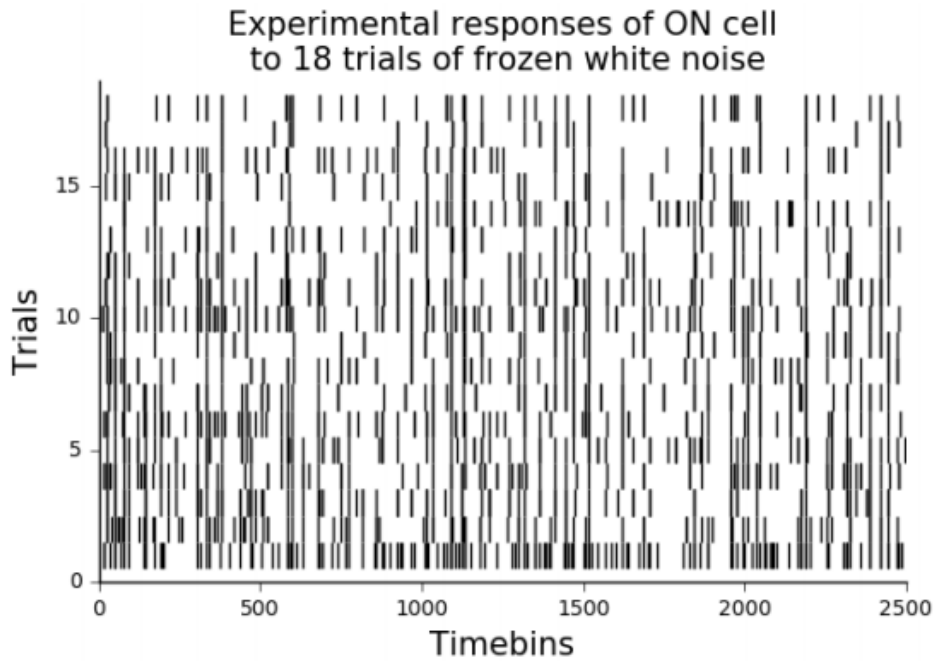


Figure 2b

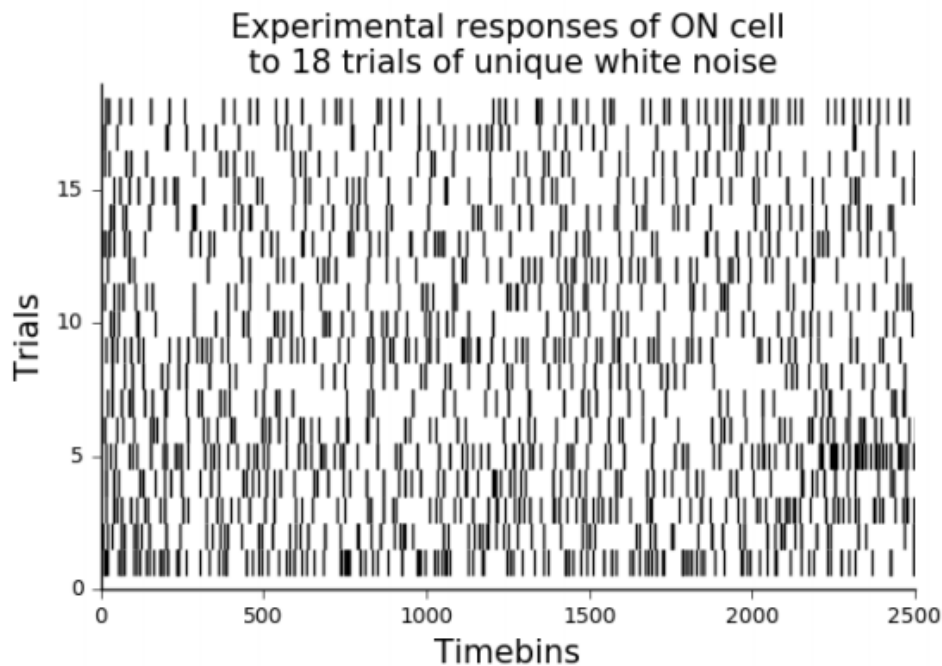


Figure 2c

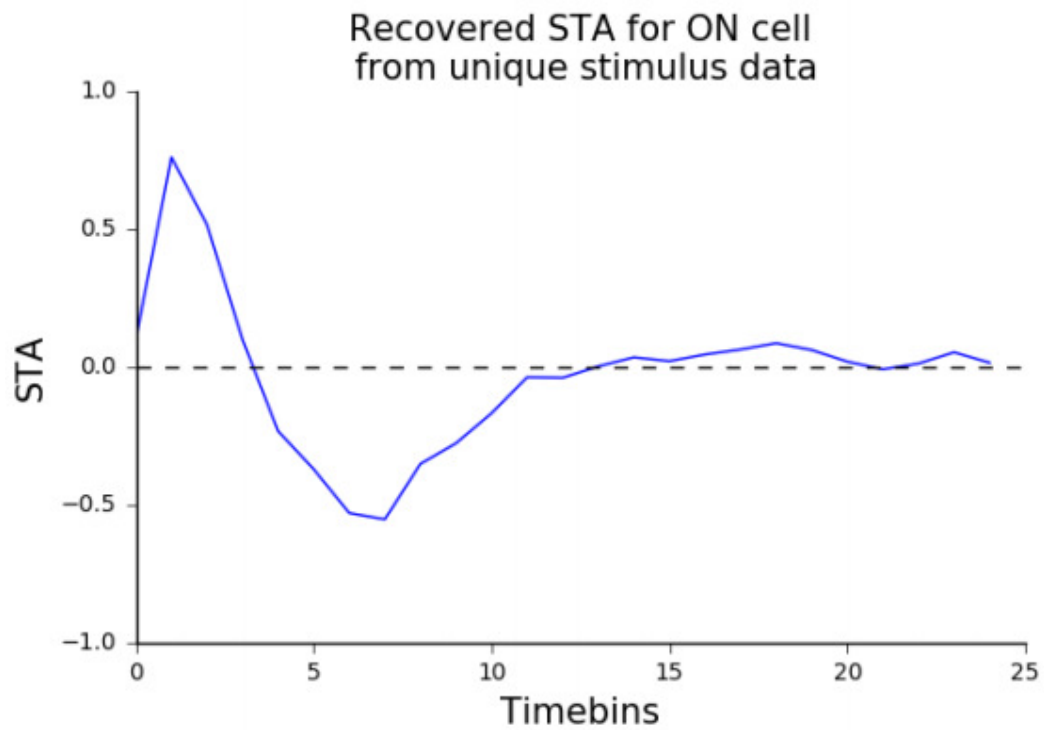


Figure 2. Rasters and STA of an example cell shown multiple interleaved trials of repeated and unique electrical white noise. a) Raster plot of cell to 18 trials of repeated/frozen stimuli. b) Raster plot of cell to 18 trials of unique/non-repeating stimuli c) Electrical STA recovered from 18 trials of unique stimuli

Figure 3a

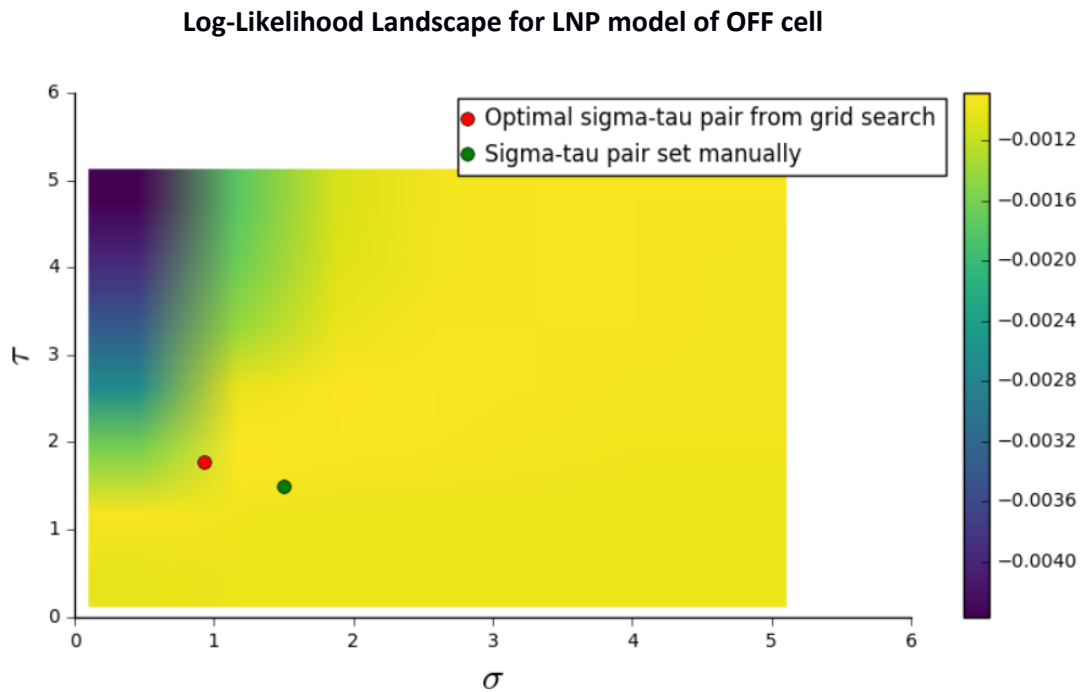


Figure 3b

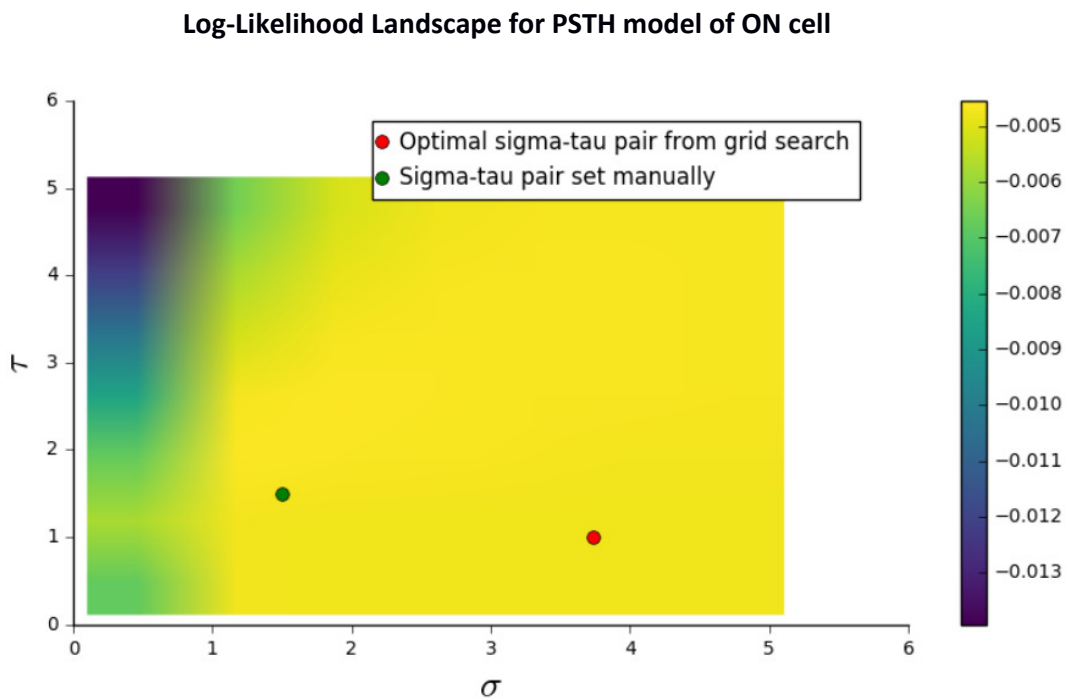


Figure 3 Log-Likelihood landscape plotted for GLM fits using different sigma-tau combinations for a) LNP model b) PSTH model. Plots show both the grid-search estimate, and manual hand-tuned estimates.

Figure 4a

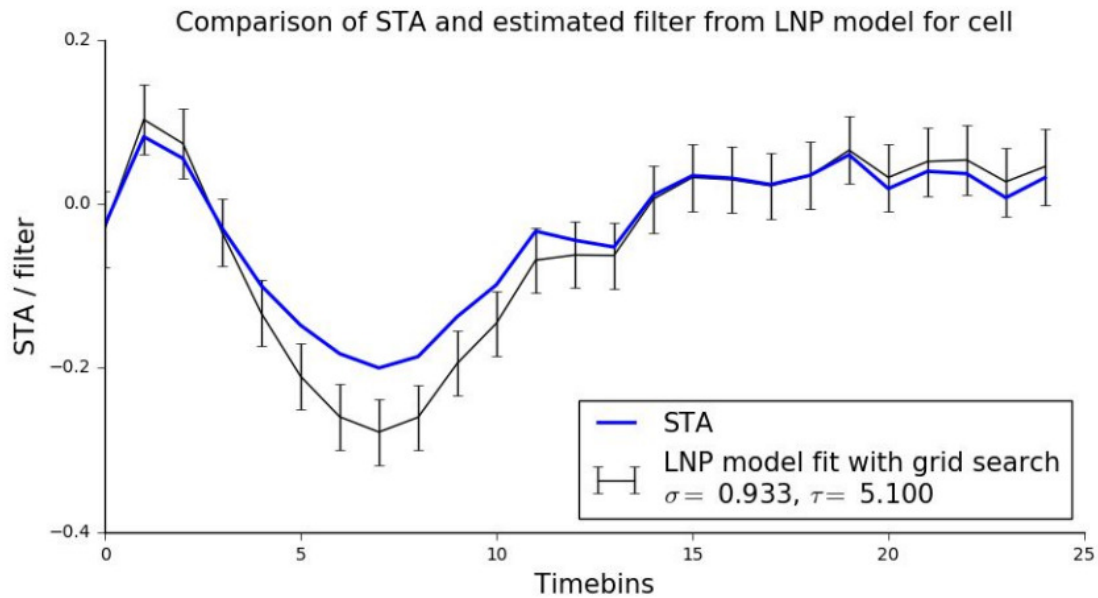


Figure 4b

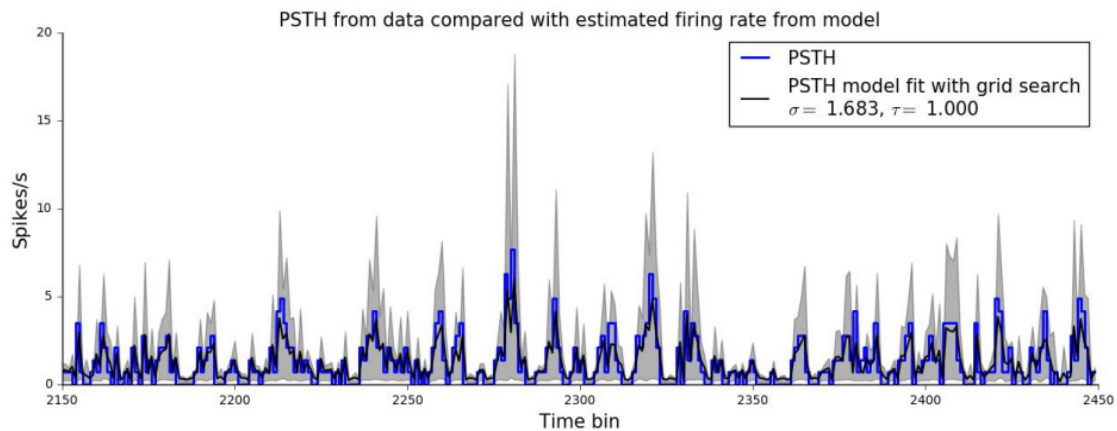


Figure 4. a) GLM fits to STA of a cell using the grid-search based optimized hyperparameters. b) GLM fits to PSTH of a cell using the grid-search based optimized hyperparameters. The standard error of mean and standard deviation for the LNP and PSTH fits respectively are also provided.

Figure 5

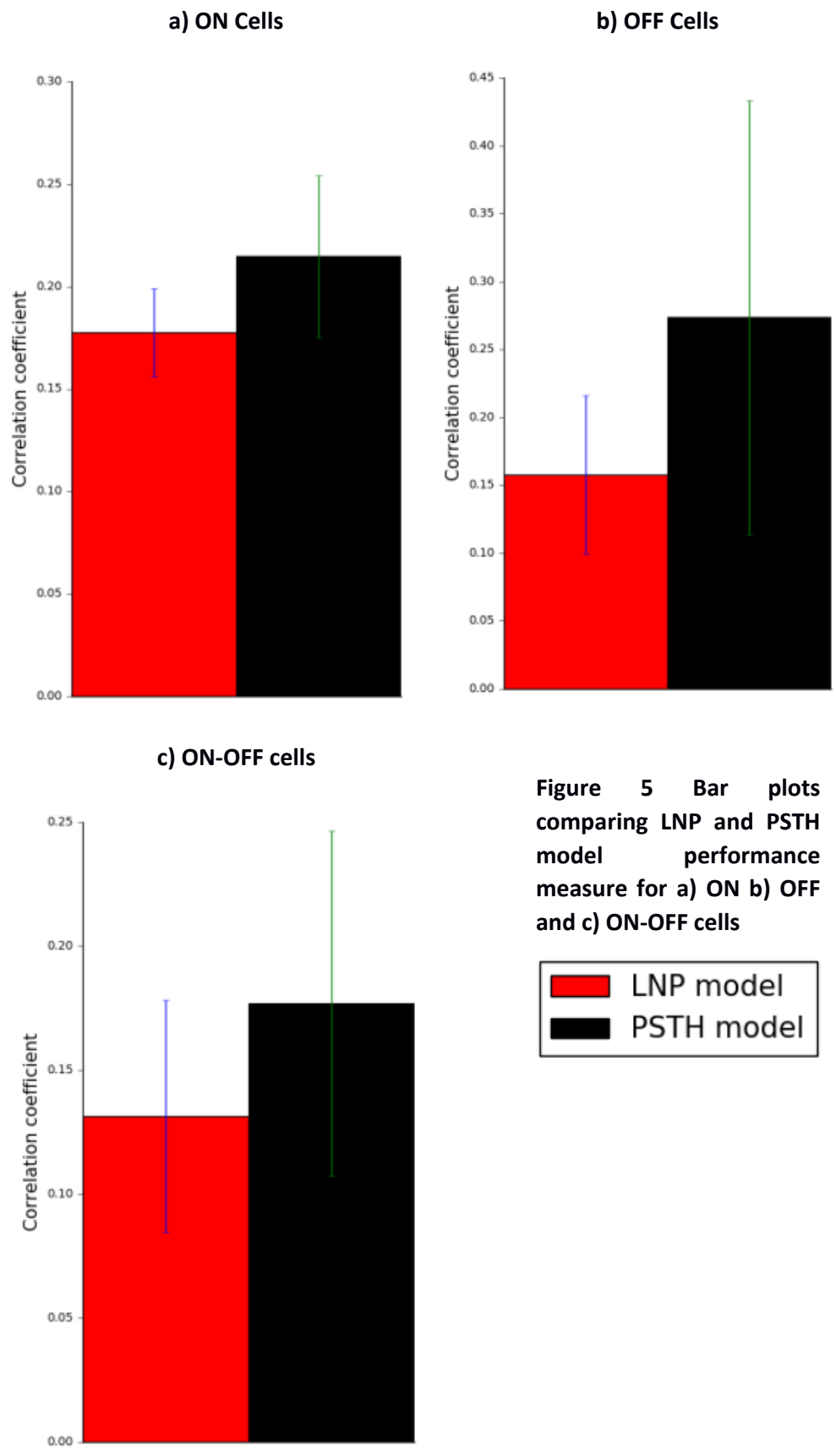


Figure 5 Bar plots comparing LNP and PSTH model performance measure for a) ON b) OFF and c) ON-OFF cells

Figure 6

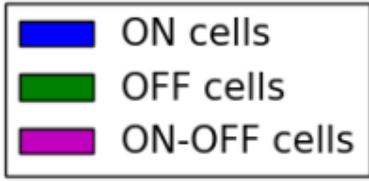
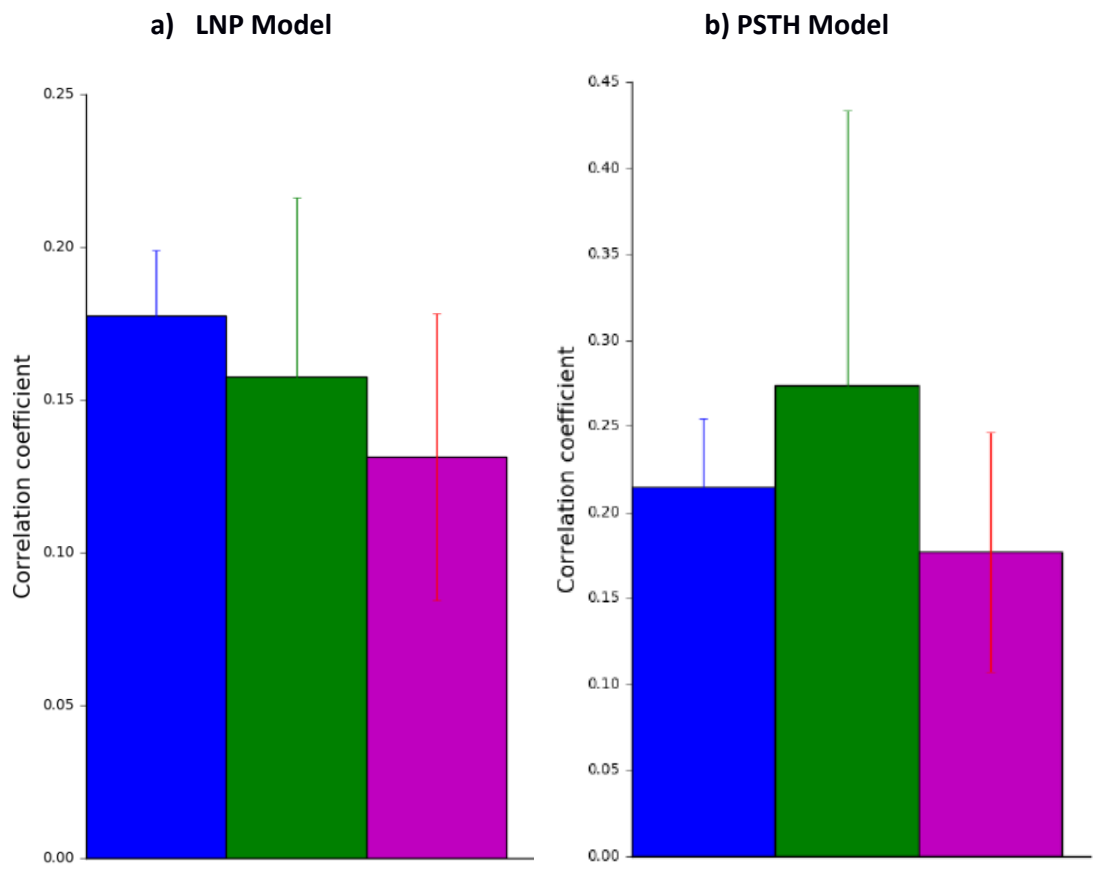


Figure 6 Bar plots comparing model performances between ON, OFF & ON-OFF cells using a) LNP model b) PSTH model

Summary

The aim of this thesis was to lay the groundwork for tackling some of the field's most challenging questions in a more systematic manner. Over the past few years, there have been many excellent new studies trying to answer the question of selective stimulation and desensitization. However, despite this, there was still a significant gap between the raw data and a more theoretical, systems-level interpretation of the experimental findings. It was, therefore, our belief that, by applying tools from the world of systems engineering to retinal prosthetics research, we could bring a fresh new perspective to these still unanswered questions. White noise analysis helped make major strides in our understanding of classical visual physiology. The results of this thesis suggest that the white noise approach could have an equally prominent impact in the field of prosthetic retinal stimulation. Moreover, this thesis has also highlighted several promising avenues of research that should be explored in order to fully understand retinal responses during electrical activation. Only with such a deeper understanding brought about by a multi-pronged approach, can we hope to improve the quality of vision restored to patients suffering from retinitis pigmentosa or age-related macular degeneration. Our findings suggest that we have only scratched the surface of what promises to be a difficult but fruitful endeavour.

Curriculum Vitae

Name: Sudarshan Sekhar

Current Status: Intern at the Max Planck Institute for Intelligent Systems, Tuebingen

Affiliations: Institute for Ophthalmic Research, Graduate School of Neural Information Processing, IMPRS (International Max Planck Research School), University of Tuebingen.

Education History

1. Bachelors. Electrical Engineering from Anna University, Chennai, India with 74% (First Class) 2007-2011.
2. Masters. Neural & Behavioural Sciences from University of Tuebingen (IMPRS), Tuebingen, Germany with a final grade of 1.8/1 (2011-2013).
3. 6th G-Node Winter Course on Neural Data Analysis, Munich, Feb 24 - 28, 2014
4. Ph.D. (2014 January – 2017 October) in the lab of Professor Dr. Eberhart Zrenner at Institute for Ophthalmic Research, University of Tuebingen.

Awards/Scholarships

1. Winner of the Max Planck Scholarship for international students of €650/month from October 2011- March 2013.
2. Recipient of a competitive travel grant (€1000) from PRO-RETINA Foundation.

PhD Summary

Used microelectrode arrays (MEAs), to study if different electrical waveforms can be used to preferentially stimulate various classes of murine retinal ganglion cells (RGCs). Have shown that in addition to traditionally-used large amplitude voltage pulses, the retina can also be activated by the integration of a stream of much smaller pulses [Sekhar et al., 2016]. Furthermore, found that electrical spike-triggered averages (STAs) of RGCs strongly correspond with their visual cell type [Sekhar et al., 2017]. Presently, using generalized linear models (GLMs), to analyze how appropriate STAs are at approximating a cell's electrical filter.

Research Experience

Machine Learning, Signal Processing, Statistical Modeling, Information theory, Microelectrode Array Recordings, Neural Data Analysis, Experimental Design, Spike Sorting, Systems Biology.

Publications

1. Sekhar S, Jalligampala A, Zrenner E, Rathbun DL. Tickling the retina: integration of subthreshold electrical pulses can activate retinal neurons. *J Neural Eng.* 2016 Aug;13(4):046004. doi: 10.1088/1741-2560/13/4/046004. Epub 2016 May 17. PubMed PMID: 27187623.
2. Sekhar S, Jalligampala A, Zrenner E, Rathbun DL. Correspondence between visual and electrical input filters of ON and OFF mouse retinal ganglion cells. *J Neural Eng.* 2017 May 10;14(4):046017. doi: 10.1088/1741-2552/aa722c. [Epub ahead of print] PubMed PMID: 28489020.
3. Jalligampala A, Sekhar S, Zrenner E, Rathbun DL. Optimal voltage stimulation parameters for network-mediated responses in wild type and rd10 mouse retinal ganglion cells. *J Neural Eng.* 2017 Apr;14(2):026004. doi: 10.1088/1741-2552/14/2/026004. Epub 2017 Feb 3. PubMed PMID: 28155848.

Posters

1. Neurowissenschaftliche Nachwuchskonferenz (NeNa), Schramberg, Germany 2012. Optimization of Electrical Stimulation of Retina to Generate Naturalistic Visual Responses. Sekhar S, Rathbun D.L, Zrenner E.
2. PRO RETINA 2014. Potsdam Germany Optimization of Subretinal Electrical Stimulation Parameters. Sekhar S, Jalligampala A, Zrenner E, Rathbun D.L.
3. Bernstein Conference for Computational Neuroscience (BCCN) 2014. Göttingen, Germany, The Importance to Retinal Prostheses of Considering RGC Diversity. Rathbun D.L, Jalligampala A, Sekhar S, Zrenner E.
4. Artificial Vision 2015. Aachen, Germany Linear Input Filters in Retinal Prosthetics: Rathbun D.L, Sekhar S, Jalligampala A, Zrenner E.
5. ARVO 2016. Seattle WA, Electrical and Visual STA Types Correlate in Mouse Retina: Sekhar S, Jalligampala A, Zrenner E, Rathbun D.L.
6. ARVO 2016. Seattle WA, Spatial aspects of electrical desensitization in mouse retina. Jalligampala A, Sekhar S, Zrenner E, Rathbun D.L.
7. Sekhar S, Jalligampala A, Zrenner E, Rathbun D. "A Systematic Approach to Finding Electrical Stimuli that Preferentially Stimulate the ON and OFF Pathways in Mouse Retina." Medical Bionics, Brisbane Australia, Nov. 2016 (chosen for a feature seminar)
8. Jalligampala A, Sekhar S, Zrenner E, Rathbun DL. "Spatio-temporal aspects of electrical desensitization in healthy mouse retina." The Eye and the Chip 10th world congress on artificial vision, Detroit Michigan, USA Sept. 2017.

Acknowledgments

There are several people I feel indebted to for the successful completion of my thesis. Some of them have been actively involved in helping me complete my PhD, while others have been well-wishers who have always taken a keen interest in my progress. Chronologically I would like to start by thanking my school teachers Jashoda Mam, Sundari Mam & Rammurthy Sir. They are educators in the truest sense of the word, never judging a student based on their grades, but only on their willingness to make an effort, and actively helping and encouraging their students to achieve their best. I would like to thank my college professors Parvathy Mam and Aruna Rajan Mam for their great lectures and for providing me with a congenial atmosphere to pursue my interests in neuroscience, in parallel with my college coursework. I would like to thank professor Venkateswaran (or Waran Sir as his students affectionately call him), for introducing me to the world of research, and for showing WARFTians how much can be done with a decent Laptop and a great idea. My 4 years at WARFT were some of my most fun & memorable. I would like to thank the Graduate Training Centre in Tübingen for the great organization and supportive atmosphere they provide to the Masters and PhD students, year after year. In particular, I would like to thank prof Horst Herbert, Dr. Katja Thieltges and Dr. Tina Lampe. I would like to thank prof. Thomas Euler, Dr. Tom Baden, Dr. Timm Schubert and Dr. Thomas Münch for their great lectures on the retina. I would like to thank my Doktorvater prof. Eberhart Zrenner, for giving me the opportunity to work in his lab. Prof. Zrenner's drive/eagerness to always learn something new, try out a new idea, never ceases to amaze me. I would like to thank him for his constant support and guidance, approachability and reassuring manner, that was instrumental in me finishing up my doctoral work, even when things got really overwhelming. His ability to focus on the details of multiple projects at once, while still keeping the big picture in mind is something I wish to acquire. I would like to thank my co-supervisor Dr. Daniel Rathbun for his mentorship, support, guidance, encouragement of a healthy work-life balance, and for our many interesting conversations on politics/history. Daniel always supported my continual improvement either through summer schools or attending various international conferences. Both prof Zrenner & Dr. Rathbun were instrumental in training me to think independently and critically about my work. I would like to thank Torsten Strasser, our unofficial IT guy for always helping out with any software/computer issues and for in general the great work atmosphere at Frondsbergstrasse.

I would like to thank my labmate/friend Archana Jalligampala for actively helping me out with my experiments and for her efforts with respect to my manuscripts. Her critical feedback and advice was invaluable. I would also like to thank her for our many fun and lively conversations over coffee. I wish to thank prof. Jakob Macke, Giacomo Bassetto & Poornima Ramesh for their efforts in helping me complete my thesis work and for introducing me to the amazing world of statistical modeling. Finally, I wish to thank my friends and family for their constant encouragement and support, without which this thesis would not have been possible. I would like to thank Ashish kaul Sahib & Joana Loureiro for the many movie nights and our many awesome trips all over Europe. In particular, I would like to thank Joana for showing me around Lisbon and Ashish for his badminton ‘coaching’ and our marathon Sunday matches. I always looked forward to this after a week of experiments. I would like to thank Hanna Napieczynska for inviting me to Poland and showing me around Warsaw and Krakow. I would like to thank the ‘Sunday Brunch’ group namely Andre Maia Chagas, Samyra Salek & Pooja Viswanathan for our many lively discussions over beers, fries and burgers. In particular, I would like to thank Andre and Samyra for inviting me to Brazil, in what was for me the trip of a lifetime. Finally, I wish to thank my family. In particular, I wish to thank my Thatha, Paati, brother, father and mother. Delhi Paati’s zest for life, and constant curiosity is something I really admire. I am still amazed that despite her arthritis she would insist on joining my brother and I, for our cricket games. I will always remember fondly her rendition of ‘Yengum Nirandayo’. I wish to thank Delhi Thatha for his words of encouragement and blessings. His stoicism, ‘In those days’ stories, and attempts to resolve any problem with banana chips are greatly missed. I am greatly indebted to the both of them for the many great memories and fun times we had when we lived with them in R.A Puram. Finally, I would like to thank my father and mother. I will never be able to repay them for their constant love, support and encouragement, and for always putting our interests ahead of theirs. I wish to thank my father for showing me by example how to always persevere, and to never give up, to always look calmly for a solution, and for his motivational talks whenever I was feeling overwhelmed by work or life. Many of his stories, such as the ‘Butterfly’ story have left a lasting impression. Last but not least I wish to thank my mother. Whether it was driving me to chess classes or tennis classes, or just listening to the mundane details of my day, my mother’s constant love, support, encouragement, and belief in me was one of my biggest sources of strength. Ma you are my best friend and I could not have done this without you. Thanks Ma.